UNIVERSITEIT GENT

Connecting the dynamics of financial markets to the dynamics of non-equilibrium fluids

Simon Standaert

Promotor: Prof. Dr. Jan Ryckebusch

Faculteit Wetenschappen

Fysica en Sterrenkunde

Ghent University
Faculty of Sciences
Department of Physics and Astronomy

Proefschrift ingediend tot het behalen van de academische graad van Doctor in de Wetenschappen: Fysica
Academiejaar 2010-2011

Connecting the dynamics of financial markets to the dynamics of non-equilibrium fluids

Simon Standaert

Promotor: Prof. Dr. Jan Ryckebusch

Universiteit Gent
Faculteit Wetenschappen

Vakgroep Fysica en Sterrenkunde
Proeftuinstraat 86, B-9000 Gent, België

Tel.: +32 9 264.65.28

Ghent University
Faculty of sciences
Department of physics and astronomy

Proefschrift tot het bekomen van de
academische graad van
Doctor in de Wetenschappen:
Fysica
Academiejaar 2010-2011

Dankwoord

Men heeft mij altijd verteld dat het schrijven van een dankwoord iets is dat je pas kan doen als de rest van je thesis reeds op papier staat. Wat ze (de oude garde) er dan niet bij vertellen is dat het enige dat je op dat moment nog kan bedenken 'oef' is. Een worsteling van vier jaar met artikels, je pc, je programma, je Engels, maar vooral met jezelf ten einde, en toch verwacht men nog een laatste reflectie op de voorbije tijd. Hoewel een doctoraatsthesis het eindpunt is van de 'wetenschappelijke ontplooiing van een individu', zijn er toch veel mensen die ik wens te bedanken voor hun steun tijdens deze rit.

Eerst en vooral wil ik Jan bedanken, die lang geleden, ter ere van het Einstein-jaar, mijn interesse in Econofysica heeft opgewekt en die gedurende vier jaar (en een beetje) heeft weten vast te houden.

Een band met een thesisstudent is ook altijd speciaal, vooral als deze dan nog eens blijft plakken. Daarom wil ik Lesley ook bedanken, die samen met mij de eerste stappen in moleculaire dynamica en anomale diffusie heeft gezet. Zij maakte ook deel uit van een groepje INW'ers die steevast hun boterhammetjes op het werk opaten. Ik heb altijd met veel plezier brood, thee, honing, kaas, verhalen over Brugse processies, ... met jullie gedeeld.

Aan de mensen die met mij een bureau hebben gedeeld zal ik niet té veel woorden vuil maken, maar wel natuurlijk net genoeg zodat zij weten waarover het gaat: Sinterklaas-turf, motor-broek.

Verder zijn er nog wel een aantal groepjes mensen waar ik, al dan niet tijdelijk of slechts sporadisch, deel van heb uitgemaakt. Zo is er de pita-groep, die ik ten dele mede verantwoordelijk acht voor het fusioneren van onze vakgroepen. De koffie-groep, die ik mede verantwoordelijk acht voor het naar beneden halen van mijn humor-niveau. Aangezien Pieter een speciale vermelding wou, is die hier misschien wel op zijn plaats.

Dus bij deze, Pieter, bedankt om voor humor op het werk te zorgen. De minivoetbalgroep, die nergens voor verantwoordelijk kan gesteld worden, aangezien ikzelf mijn tenen gebroken heb. De UZ-groep, waar ik altijd met tegenzin lid van was, acht ik mede verantwoordelijk voor het ontwikkelen van mijn smaakzin. Aan al de rest van het INW, bedankt om mijn over-en-weer geloop van de laatste maanden te tolereren.

Pietje, Ewoud, Bart, Willy, Benoît (en eega's), bedankt om af en toe en pint met mij te gaan drinken en om voor ontspanning en vriendschap in mijn leven te zorgen. Ook alle mensen van Diggie en de gentseeuh verdienen eenzelfde bedanking. Dankjewel om mij soms meer student dan werknemer te doen voelen.

Er wordt altijd verwacht dat ook de ouders en familie een bedankje krijgen, maar ik voel dit zeker niet aan als een verplicht nummer. Moeke en papa, bedankt om mij keuzes te laten maken en mij te steunen bij al wat ik doe.

Marie, ook al maak ik het niet altijd direct heel duidelijk, ik waardeer je steun, ik geniet heel hard van je aanwezigheid, en ik denk dat we alletwee weten dat ik je nodig heb.

Contents

Chapter 1

Introduction

It is a good thing for an uneducated man to read books of quotations.
Sir Winston Churchill

The desire of human beings to comprehend and explain what occurs in the world around them has lead to many great discoveries and a deeper understanding of nature. Physicists have developed an accurate description for many events observed in the physical world. For example, lightning, freezing, planetary movement, blue skies, etc. are phenomena that can be perfectly explained by physics. Human behaviour, on the other hand, cannot be understood, modelled, or predicted up-to the same level of accuracy. Social sciences have explored some facets of human behaviour, with varying degrees of success. Economics is a social science that adopts an empirical approach more akin to the physical science in order to understand certain aspects of human behaviour.

A vast amount of economic data is available in the modern world. Statistical tools are necessary to grasp the trends, and draw appropriate conclusions. It comes therefore as no surprise that statistical physics and economics cross each other's path at some point in time. Econophysics is born! Econophysics is a term coined by E. Stanley in 1995, and it describes the interdisciplinary research field that uses methods and theories from physics (mostly statistical physics) in the domain of economics. The aim of econophysics is to develop mathematical models that provide an accurate description of the observed dynamical physical properties of financial markets.

Short history of economics

The operation of the current world economy is dominated by a non-physical quantity, "money". With regard to the duration of human history, money has been around for

only a small fraction of time. The evolution of the concept of money is strongly related to evolution in general. The driving force in evolution is the necessity to survive and reproduce, which leads to the concepts of natural selection and genetic drift that produce the so-called "survival of the fittest". At a certain point in history, humans were able to convert their lifestyle from hunter-gatherers to sedentary societies based on agriculture, thus controlling their environment and improving their chances of survival. Further evolution gave rise to complex (religion-based) societies, in which trading played an essential role. This allowed less "physically fit" humans to thrive, because those who had money, had a bigger chance of survival. In this way, a battle for food became a battle for money [PCB98, Far02, DS06].

The desire of humans to comprehend the world around them, also contains the understanding of their own behaviour. As money-related processes became more and more dominant, the desire to understand and manage these processes grew. This evolution eventually led to scientific activities that we now denote as economics. The term economics comes from *oikonomia*, Greek for *management of a household*. Modern economies have a wide perspective and deal with topics as broad as the actions of a single agent (this can be an investor but also the man in the street) as well as the operation of a global economy.

Short history of econophysics

An overlap between economics and physics (or bèta sciences in general) has existed for a long time. As early as the beginning of the nineteenth century, some individuals started to cross the boundary between social sciences and the physical sciences. In these days, the boundaries between disciplines were less strict, which enabled gifted people to contribute to vastly different fields. Here we present some examples of people who made early contributions to both the social and the bèta sciences.

Adolphe Quetelet, a mathematician of education (at Ghent University), was very influential in introducing statistical methods in social sciences. He had a broad range of interests, as he was involved in research in meteorology, astronomy, mathematics, statistics, demography, sociology, criminology and the history of science. His introduction of statistics, *Sur l'homme et le développement de ses facultés. Essai d'une physique sociale* [Que35], involved the introduction of an *average man* in the science of physical characteristics (like the height of people, life expectancy, ...), where mean values of measured variables follow a normal distribution. This approach is very similar in vein to what is known as the mean-field approach to complex many-body systems in physics.

Louis Bachelier was a mathematician who derived and solved a random walk equation for the evolution of stock prices. In his doctoral thesis *Théorie de la Spéculation* [Bac00], he tried to model prices of the French stock exchange. His work was seminal in establishing a link between the random walk, Brownian motion and normal diffusion. In Chapter 2 we will elaborate on Bachelier's work.

Vilfredo Pareto, an economist, introduced the power law into the world of statistics [Par16]. He studied income and wealth distributions in Italy and came to the conclusion that 80% of the land was owned by 20% of the population. Nowadays, this principle of unequal partition of wealth is known as the Pareto principle. Income distributions continue to interest scientists from different scientific fields [YRJ09].

Benoît Mandelbrot, a mathematician, is famous for his self-similar fractals [Man82]. In [Man63, Man60] he proposed to use a Lévy stable distribution (Appendix A), as opposed to the Gaussian distribution of Bachelier's work, for the modelling of option prices.

Some time after the contributions from the above mentioned individuals, econophysics became an accepted interdisciplinary research field [SAC+99, GKLO06, McC06, GI01, Bal06, JJH03, Das05, Vas04], with contributions from various fields of physics. Percolation theory, self-organized criticality, spin glasses, path integrals and critical transitions were an essential part of early contributions to econophysics [BP03, Man04, MS99, Baa04, McC04, Roe05a, Sch78, Sor03b, PB00, LCX06]. Most contributions of physicists to economics occur in the field of finance, which is the science of funds management, and econometrics, which combines economic theory with statistics to analyse and test economic relationships.

Motivation and outline

Motivation

As the global economies experience another financial crisis, correct pricing of derivatives, such as options, is as important as ever. The human race and its inventiveness create ever more complex financial instruments, thus constructing the seeds of a possible financial downfall for those that cannot fully understand the risks that these new instruments incorporate (which can even include the inventors of the financial instrument). The contribution of econophysics is to be found in the possible simplification of theories and the possible identification of universal dynamics in the operation of complex systems like financial markets. Complex building blocks can be divided into simpler parts that are more understandable. Crude models (such as Ising systems or

percolation) can provide insights into the dynamics that drive these complex systems.

Molecular dynamics (MD) is one of those powerful models from physics that calculates the time evolution of a complex system. In MD, the complex system consists of a large collection of interacting units (molecules) and the system evolves in accordance with the Newtonian equations of motion. In this way, MD is a technique very similar in vein to the Monte-Carlo technique, but it has the advantage that it creates realistic time sequences for the evolution of the system. In this way, not only the spatial but also the temporal correlations in the dynamic microscopic and macroscopic variables of a large amount of interacting units can be calculated.

A prime example of the power of MD can be found in the modelling of liquids. Various aspects, such as self-diffusion, phase diagrams, absorption of particles and viscosity of liquids can be simulated with MD. The complexity in the observed macroscopic features of a liquid can be attributed to the short-range interactions between the molecules and some macroscopic parameters like density, pressure, and temperature.

Fluids have been the standard example of a system in which normal diffusion occurs. In this work it is investigated whether MD can also be used to model the time evolution of assets in financial markets. There are a number of striking analogies between fluids and financial markets.

- Both systems consist of a large number of units that interact with each other on a microscopic scale. In financial markets this can represent the interactions of investors with each other, and in MD this represents the interactions of the molecules with each other. Both systems have, on the other hand, also a macroscopic interaction typified by a so-called “mean-field” variable. In MD this variable could be the density or the temperature, in a financial system this could be the current price of the asset or the interest rate.

- In both systems, emergent collective behaviour is observed. In fluids, this is represented by the different phases of the system (gas, liquid, solid) and the sudden abrupt phase transitions between them. A good example of emergent behaviour in financial markets are herding, bubbles, and crashes. During these periods, the financial agents act in a coherent fashion which makes the market prone to crashes.

- In both systems one observes temporal and spatial correlations in the observables. In MD these are represented by the radial distribution function, the velocity autocorrelation function or the diffusion coefficient. Their analogues in financial markets are the return autocorrelation, volatility autocorrelation or the volatility distribution.

- Both liquids and markets can be considered as multi-scale systems. In markets this reflects itself in correlation times of the order of minutes for the returns of financial assets, whereas the correlation time in the corresponding volatility is of the order of hours. Liquids, in their turn, are characterized by rather brief correlation times for the molecular velocities, whereas the diffusion coefficient remains constant (infinite correlation time).

These analogies represent our interest in MD as a simulation tool for financial markets. However, normal MD simulations do not reproduce the characteristics of financial markets and will have to be modified to simulate financial time series in a more realistic manner. Thereby, the major challenge lies in identifying the physical mechanisms that lead to non-Gaussian diffusion.

Outline

Chapter 2 focuses on the question why diffusion takes centre stage in the description of financial markets. The first mathematical description of a random walk by Bachelier leads to a normal distribution for the observed variations in stock prices. Geometric Brownian motion (GBM) is a model, based on Bachelier's derivation, that focuses on returns (a relative measure) and not absolute price changes for the evolution of a financial asset.

One of the building blocks of option pricing is the Black-Scholes formula, which calculates a fair price for options of stocks. The derivation of this equation is based on the GBM equation that governs the price dynamics of the option for changing values of the underlying stock. Many, more complex and contemporary, option pricing models use alternative stochastic differential equations (SDE) to describe the evolution of the stock price. Usually, the SDE can be related to some sort of diffusion process.

All of these models are carefully tuned so as to reproduce as closely as possible the characteristic statistical features of the financial asset under investigation. Some of these features are unique in the sense that they only occur for a specific financial market. Some features, on the other hand, are universal in the sense that they are observed for a wide range of financial assets and over long time periods. Based on an analysis of the time series of a characteristic index, the S&P 500, these generic features will be identified and discussed.

Chapter 3 introduces the MD technique and the properties of a reference MD simulation. We focus on the properties that are useful in a financial context and in particular on the self-diffusion properties of the molecules in a liquid. We examine both the mean

squared displacement and the single time step displacement distribution in a reference MD simulation. In the reference MD simulation, an intermolecular interaction of the Lennard-Jones type is used. The hard core of that interaction poses real difficulties when attempting to generate conditions of non-Gaussian self-diffusion in the MD simulation system. Some sort of the hard-core part is indispensable. To that end, we study liquids with molecules that interact via the soft-core potential proposed in Ref. [Fra07]. The behaviour of the various observables of MD is examined with this soft-core potential to make sure that it does not alter the dynamics of a reference MD simulation.

Our non-equilibrium molecular dynamics set-up is presented in Chapter 4. Driving the system out-of-equilibrium is an essential step in simulating non-Gaussian diffusion in MD. It is also a very natural step given that we wish to emulate a financial system which cannot be considered as residing in equilibrium.

The main aspects of the non-equilibrium set-up are shown, which explain the internal dynamics that lead to the non-Gaussian self-diffusion. Driving the system out-of-equilibrium is achieved by modifying the interaction parameters so as to mimic a change in the radius of the particles in MD. The robustness of the self-diffusion properties with regard to the model parameters is established, which supports the use of this set-up as a model for simulating the generic features of financial markets.

The resulting behaviour of the generic features for this non-equilibrium MD model as compared to those of financial markets is examined in Chapter 5. Linking the MD model to financial markets implies linking two major variables of stock markets, price and time, to variables associated with the molecules. Once this is achieved, a full mapping of a non-equilibrium MD simulation onto a financial time series can be given. Some improvements are suggested that can make the model more realistic and that can clarify the meaning of some thermodynamical variables in a financial context.

Some concluding remarks and an outlook for further research are discussed in Chapter 6. Some technical aspects of the presented research are presented in the appendices. Appendix A focuses on the description of diffusion in physics. Appendix B describes the usage of Ito's lemma for stochastic differential equations. The derivation of the Black-Scholes formula is discussed in Appendix C.

Chapter 2

Diffusion in Economics

In economics there is a long history of attempting to model financial time series as a diffusion process. We mention the work of Bachelier [Bac00] and Mandelbrot [Man63], the Black-Scholes equation [BS73] and all of the derivations thereupon.

In this chapter, we will present both historic and modern work in economics in modelling financial time series. This is not meant as a review at all, but rather as a discussion of examples of models that relate diffusion processes to the dynamics of markets.

One of the ways to assess the value of a model is to compare the statistical properties of the time series that it produces with those of real markets. We will therefore restate some of the generic properties that are present in time series of stock market indices. Any realistic model for the dynamics of markets should reproduce those properties.

2.1 Bachelier

Bachelier was the first person to link a random walk with the normal distribution and with stock prices. In his doctoral thesis (Bachelier was a mathematician and was supervised by H. Poincaré), *Théorie de la Spéculation* [Bac00], he tried to model the price changes in the French stock market. In his work he makes some assumptions regarding the behaviour of the prices of the traded products. His first assumption is that regardless of the current price, the expectation for the next price change is zero. This translates into saying that there is no memory in the market and that price changes are unpredictable. Another assumption is that the probability distribution of the price steps is independent of the time and current value of the price. This translates into a continuous Markov process, homogeneous in time and space. Using this, Bachelier linked the price evolution with Brownian motion and the parabolic diffusion equation. He also

found a (not unique) solution to the diffusion equation in the form of the Gaussian distribution. The link between diffusion and Brownian motion is established in detail in Appendix A.

Bachelier's work was a first step in the direction of modelling the pricing of financial products [DE06, CKB+00], but is also essential in the derivation of stochastic calculus. Based on Bachelier's work, it is straightforward to make a *reference model*, that uses geometric Brownian motion to model the price changes of a financial product.

2.2 Geometric Brownian Motion

In Bachelier's derivation of the random-walk model for financial products, he assumed symmetric price changes. This implies, for instance, that prices could become negative! It is therefore favourable to use a random walk for the relative price changes, not the price changes themselves. This is essentially the concept of geometric Brownian motion.

In GBM one describes the time evolution of some variable $S(t)$. In many physical problems, the time evolution of some quantity S is determined by a differential equation. We mention the well-known harmonic oscillator

$$\frac{d^2S}{dt^2} + \omega^2 S = 0 \,, \tag{2.1}$$

that results in a predictable periodic motion of S with a period of $\frac{2\pi}{\omega}$. In contrast, the time evolution of S in GBM is determined by an equation that belongs to the class of stochastic differential equations (SDE). SDEs combine standard differential equations with a stochastic process. This stochastic process is often *white noise*, which can be thought of as the differential steps of Brownian motion: the stochastic steps are normally distributed.

Starting from the basic SDE

$$dS(t) = \mu S(t)dt + \sigma S(t)dz(t) \,, \tag{2.2}$$

a model for GBM can be constructed. In this SDE, $S(t)$ is the time evolution of the variable under study (for example the index price) dt is a normal differential (very small steps in t), z describes the stochastic process and $\mu,\ \sigma$ are constants. This basic SDE can be expanded to include more involved processes by adding extra terms or by making $\mu,\ \sigma$ time dependent: $\mu(t),\ \sigma(t)$. Some of these extensions are reviewed in section 2.3.4.

If z is a white noise process, one can use $(dz2(t))^2 \sim dt$, which only states that the variation of the Gaussian process is proportional to the time t. Using Ito's lemma (section B.2) for $f(S) = \ln(S)$ one obtains from Eq. 2.2

$$d\ln(S) = \left(\frac{1}{S}\cdot \mu S + \frac{1}{2}\cdot\frac{-1}{S^2}\cdot(\sigma S)^2\right)dt + \frac{1}{S}\cdot\sigma S dz(t) \ . \tag{2.3}$$

This results in the unexpected (because for a non-stochastic differential equation one would expect $dS/S = d\ln(S)$) but elegant

$$d\ln(S) = (\mu - \frac{\sigma^2}{2})dt + \sigma dz(t) \ . \tag{2.4}$$

Integration over $[0, t]$ results in

$$\ln S(t) - \ln S(t=0) = (\mu - \frac{\sigma^2}{2})t + \sigma z(t) \ . \tag{2.5}$$

The solution to geometric Brownian motion is

$$S(t) = \exp\left[(\mu - \frac{\sigma^2}{2})t + \sigma z(t)\right] S(t=0) \ . \tag{2.6}$$

Accordingly, geometric Brownian motion is a log-normal process when $z(t)$ is normally distributed. In logarithmic coordinates, $\ln(S(t))$, it is governed by a drift of $(\mu - \frac{\sigma^2}{2})$ and volatility σ.

Examples of GBM are shown in Fig. 2.2 for different values of μ and σ. Comparing the time evolution of $S(t)$ for different values of σ and a fixed value of μ reveals which influence σ has on the fluctuations of $S(t)$. For fixed σ, changing μ results in a different long term trend of $S(t)$. Notice that negative values for $S(t)$ do not occur in this time series, as opposed to Bachelier's model.

The most important variable in stock markets is the return traders get on their investments. Two definitions of returns exist. One is the logarithmic return, G:

$$G = \ln V_f - \ln V_i \ , \tag{2.7}$$

with V_f the final value of an asset and V_i the initial value of this asset. The other definition uses an arithmetic return G_a

$$G_a = \frac{V_f - V_i}{V_i} \ . \tag{2.8}$$

The logarithmic return has the advantage that subsequent returns of $+50\%$ and -50% cancel each other out and results in an cumulative return of 0%. The same process with

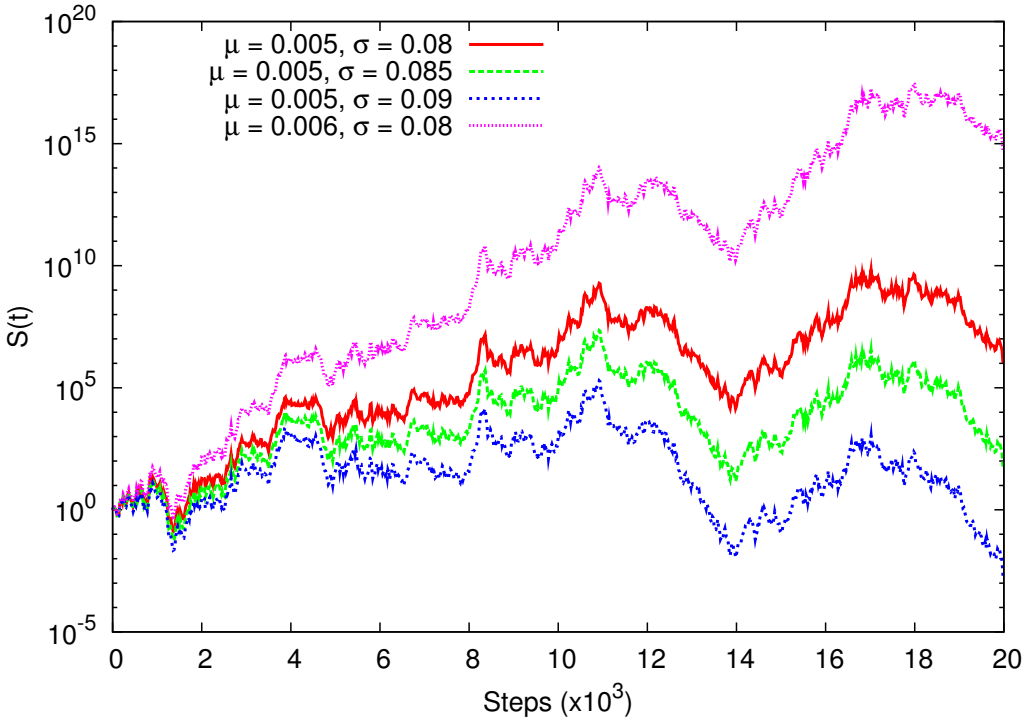

Figure 2.1 Evolution of geometric Brownian motion $S(t)$ for different values of μ and σ. On this logarithmic scale, a trend of $(\mu - \frac{\sigma^2}{2})$ is visible, while the difference in σ is too small to be perceptible in the fluctuations.

an arithmetic return results in an overall return of -25%, because $+50\% - 50\% \neq 0\%$ for G_a.

For small differences in initial and final value the different returns converge to the same value:

$$G = \ln \frac{V_f}{V_i} = \ln \frac{V_f - V_i + V_i}{V_i} = \ln \left(1 + \frac{V_f - V_i}{V_i}\right) \approx \frac{V_f - V_i}{V_i} = G_a \ , \tag{2.9}$$

with $\ln(1+x) \approx x - \frac{x^2}{2} + \ldots$. For the smallest time steps both definitions of the returns are commonly used.

If we use the definition of the logarithmic returns, the returns of geometric Brownian motion are

$$G(t) = \ln S(t + \Delta t) - \ln S(t) = \Delta \ln S(t) = (\mu - \frac{\sigma^2}{2})\Delta t + \sigma \Delta z(t) \ . \tag{2.10}$$

It is essential to stress the difference between both returns in the GBM model, since the value of the trend of the returns depends on the definition of the return: μ for G_a and $(\mu - \frac{\sigma^2}{2})$ for G. From now on we will use G unless otherwise stated.

The time series produced in a GBM model are a zero-th order approximation to those of assets in real financial markets. A close look at the returns in this model, Fig. 2.2,

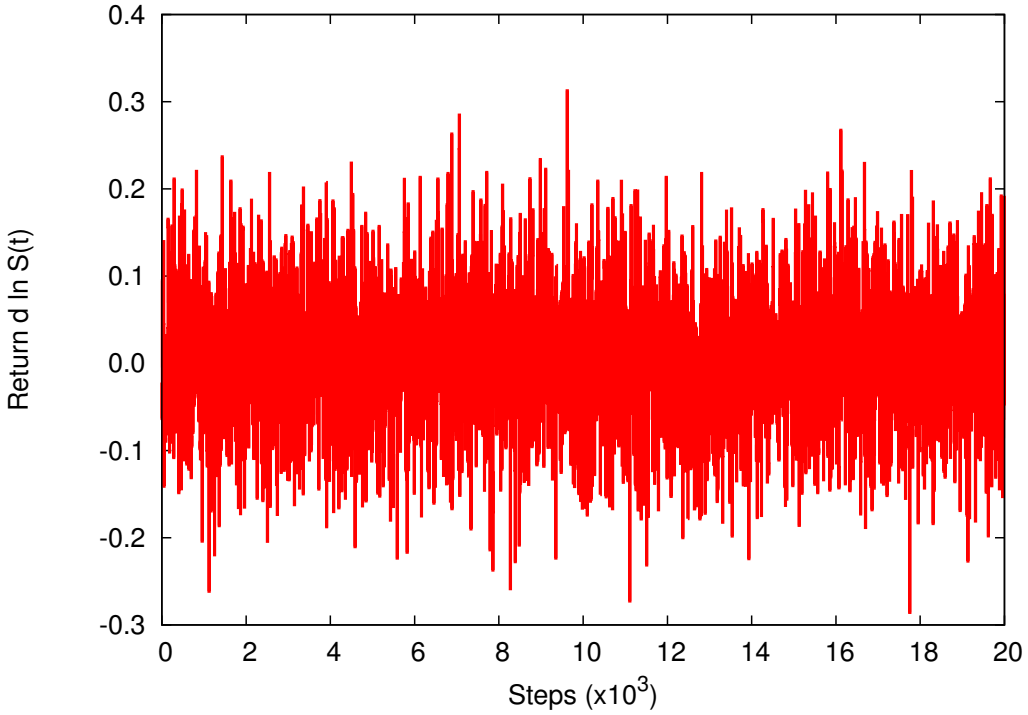

Figure 2.2 Evolution of the returns $d \ln S(t)$ for geometric Brownian motion, with $\mu = 0.005$ and $\sigma = 0.008$.

reveals the underlying Gaussian white noise stochastic process. As will be pointed out in section 2.4, normally distributed returns are only an approximation of the real financial return. This doesn't exclude the random walk as a tool for modelling financial time series [Bou05]. We will specify the main differences between the GBM time series and financial time series in chapter 5. Here, we will compare the generic properties of section 2.4 to the generic features of the GBM model. We will then investigate in how far non-equilibrium molecular dynamics can serve as an improved model for financial time series. Thereby, GBM will serve as a benchmark tool.

2.3 Option pricing

Stock pricing models are based on a variety of underlying distributions for the returns of assets, such as Lévy distributions, truncated Lévy flights, student t-distributions, log-normal distributions, etc. Option pricing, however, can often be reduced to a single underlying model, the Black-Scholes formula, on which a multitude of other models are based. In this section we will derive the Black-Scholes equation and comment on its strengths and its weaknesses. Other models of option pricing are also mentioned.

2.3.1 What is an option?

An option is essentially a derivative financial product, for which the price depends on another (more basic) underlying financial product. Other derivatives include forward contracts, futures and swaps.

There are essentially two different types of options, put options and call options.

1. A put option provides the buyer with the right, but not the obligation, to sell the underlying financial product at a certain pre-arranged price and date. The seller of the option is obliged to buy the underlying financial product (if the buyer wishes to exercise his option) at this pre-arranged price and date.

2. A call option gives the buyer the right, but not the obligation, to buy the underlying financial product at a certain pre-arranged price and time instance. The seller is again obliged to sell at this date and price.

The value of the option depends on the pre-arranged price, K, the strike price or exercise price, but also on the expiration date T, also called the date of maturity. Put and call options enable one to speculate on the variations of the underlying financial product. If one expects that prices will rise over time, a call option can be bought. If the price of the underlying $S(t)$ does rise above the strike price K, a profit of $S(T) - K$ can be made by the buyer. The total profit is thus determined by $[\max(S(T) - K, 0) - c(S, 0)]$, where $c(S, t)$ is the value of the option at time t (also called premium).

In Fig. 2.3 the total pay-off of a put and call option are shown, for the buyer and the seller of the option. It is clear that these pay-offs are asymmetric functions, and that the buyer of an option is always limited in his losses ($c(S, 0)$), but not in his gains ($S(T) - K - c(S, 0)$). A seller, on the other hand, has only limited gains but could face unlimited losses.

The options described in the above section are known as European call and put options. There are many different styles of options, because the only limitation for selling an option is that there needs to be another party who buys this option. Options exist that can be exercised at any date before expiration (American options), or that can only be exercised if the underlying asset passes a certain barrier during the lifetime of the option (Barrier options). Apart from these, many other exotic types of options have been developed in international markets.

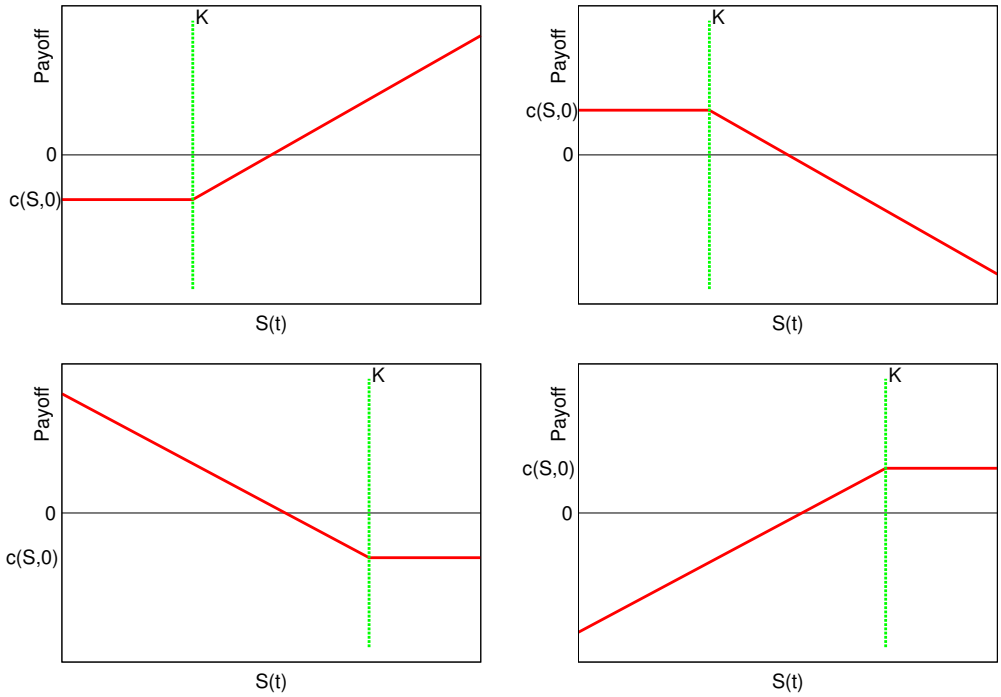

Figure 2.3 Pay-off of a call option for the buyer (left top) and for the seller (right top) of the option, for a strike price K, stock price $S(t)$ and option price $c(S,0)$. Pay-off of a put option for the buyer (left bottom) and for the seller (right bottom) of the option, for a strike price K, stock price $S(t)$ and option price $c(S,0)$.

2.3.2 Derivation of the Black-Scholes equation

The price of the option is the price that the two parties (buyer and seller) can agree upon. When attempting to determine the value of an option, models can be used to give an estimate for a fair and rational price $c(S,t)$. The first reliable formula for option pricing was proposed by Black and Scholes in 1973 [BS73].

To derive the B-S equation, some assumptions are made:

- The stock price follows the geometric Brownian motion of Eq. 2.2.
- There are no transaction costs.
- There are no dividends during the lifetime of the derivative.
- There are no arbitrage opportunities (there is no free lunch).
- The risk-free interest rate, r, is constant over the lifetime of the derivative.
- The trading is continuous.

It is now possible to assemble a portfolio that behaves exactly like the price of the derivative. This portfolio will contain bonds, stocks or the derivative itself. The assumption of the risk-free interest rate leads to a bond, $B(t)$, which earns this rate r:

$$dB = rBdt \ . \tag{2.11}$$

The stock price, $S(t)$, is assumed to follow the SDE of geometric Brownian motion, Eq. 2.2:

$$dS = \mu S dt + \sigma S dz \ . \tag{2.12}$$

With Ito's lemma, the price increments of the $c(S,t)$ are determined by:

$$dc = \left(c_t + \mu S c_S + \frac{\sigma^2 S^2}{2} c_{SS} \right) dt + \sigma S c_S dz \ . \tag{2.13}$$

Making a portfolio, $G(t)$, out of bonds and stocks can make the portfolio behave as $c(S,t)$:

$$G = xS + yB \ , \tag{2.14}$$

where x is the number of shares of stock S and y the amount of bonds B in the portfolio. The investor is trying to find the correct ratio of $\frac{x}{y}$ for which this portfolio mimics the behaviour of the option price.

If we do not add or withdraw any money from this portfolio, the gain or loss due to changes in the market (using Eqs. 2.11-2.12) is

$$\begin{aligned} dG &= xdS + ydB \\ &= x\left(\mu S dt + \sigma S dz\right) + yrBdt \\ &= \left(x\mu S + yrB\right) dt + x\sigma S dz \ . \end{aligned} \tag{2.15}$$

Since the price of the portfolio $G(t)$ and the derivative $c(S,t)$ are equivalent, the equations $G = c$ and $dG = dc$ should hold at all times. Since dt and dz are independent, the coefficients of dt in Eqs. 2.13 and 2.15 need to be the equal. The same holds for the coefficients of dz. This results in three equations that establish relations between S, B and c:

$$xS + yB = c \ , \tag{2.16}$$

$$x\mu S + yrB = c_t + \mu S c_S + \frac{\sigma^2 S^2}{2} c_{SS} \ , \tag{2.17}$$

$$x\sigma S = \sigma S c_S \ . \tag{2.18}$$

Eq. 2.18 readily reduces to $x = c_S$, which can be inserted in Eq. 2.16:

$$y = \frac{1}{B}(c - Sc_S) \ . \tag{2.19}$$

The B-S equation is found upon inserting this result in Eq. 2.17:

$$c_t + rSc_S + \frac{\sigma^2 S^2}{2} c_{SS} = rc \ , \tag{2.20}$$

where the price dynamics of the option depends on r, σ and $S(t)$. Note that is does not depend on μ.

2.3.3 Black-Scholes option pricing

A solution to the B-S equation gives the price of the derivative, without knowing the exact time series of the underlying stock price. The boundary conditions differ according to the type of option under study. In Appendix B the derivation of the B-S formula for a European call option is shown. The B-S formula for a European call option is

$$c(S, 0) = S_0 N(d_1) - K \exp[-rT] N(d_2) \ , \tag{2.21}$$

with

$$d_1 = \frac{1}{\sigma\sqrt{T}} \left(\ln \left[\frac{S_0}{K} \right] + \left[r + \frac{\sigma^2}{2} \right] T \right) \ , \ d_2 = d_1 - \sigma\sqrt{T} \ . \tag{2.22}$$

Since the B-S equation is based on some assumptions, real prices of options differ from the prices based on the B-S formula. We present the assumptions underlying the B-S equation together with their shortcomings.

- *The stock price follows the geometric Brownian motion of Eq. 2.2*:

  As we will explain in section 2.4, stock prices are not log-normally distributed and deviations from geometric Brownian motion should be included in the price of the underlying stock. The variance σ of Eq. 2.2 cannot be considered a constant and this is remedied for example in GARCH models.

- *There are no transaction costs*:

  This is not true in any market. Indeed, upon using the B-S formula to delta hedge in a very volatile market, one has to trade many times thus accumulating transaction costs. Delta hedging is a technique derived from the B-S formula that minimizes the risk of a portfolio (expressed as delta δ), by including the desired ratio of options and underlying stocks. The value of δ expresses the sensitivity of

the option price to a change in the value of the underlying. If the investor buys an amount of the underlying corresponding to this delta value, the delta value of the portfolio can be made to sum up to zero.

- *The risk-free interest rate, r, is constant over the lifetime of the derivative*:

  The risk-free interest rate is never known for the whole time window of the option, and for large time windows it is not safe to assume it will remain at its initial value.

- *The trading is continuous*:

  Trading on real markets is not continuous and it is therefore not always possible to buy or to sell stocks, bonds or options at any given time. This can lead to less-than-optimal hedging and increases the risk of the portfolio.

2.3.4 Option pricing models

The Black-Scholes formula is not the end-of-the-road for mathematical economists, but only a starting point. The shortcomings of the B-S formula are an incentive to find models that incorporate these non-Gaussian distributions, non-constant volatility, volatility clustering, varying risk-free interest rates, etc. A short summary of a selection of these models is presented here.

GARCH models

GARCH (generalized autoregressive conditional heteroskedasticity) models [Bol86] are based on a varying volatility in the geometric Brownian motion. In particular, the GARCH(1,1) model has a volatility that depends on the variance of the model up-to that time, a random factor and the squared value of past returns:

$$\begin{aligned} \frac{dS(t_i)}{S(t_i)} &= \mu dt_i + \sigma(t_i) dz(t_i) \\ \sigma(t_i)^2 &= \omega \overline{\sigma}^2 \alpha \sigma(t_{i-1}) + \beta \epsilon(t_{i-1}) \\ \epsilon(t_i)^2 &= \left(\sigma(t_i) dz(t_i)\right)^2 . \end{aligned} \tag{2.23}$$

The variance in this model is an autoregressive process around the long-term average variance $\overline{\sigma}$. This model can be generalized to a GARCH(p,q) model in which p previous terms of the volatility and q previous random terms determine the current volatility. The result of this non-constant volatility is that the return distribution is non-Gaussian and it can also exhibit volatility clustering.

The GARCH model can be further enhanced and this results in exponential GARCH (EGARCH) models, threshold GARCH (TGARCH) models, quadratic GARCH (QGARCH) models, etc., that incorporate more terms in the determination of the volatility than the GARCH model.

Jump diffusion models

Jump diffusion models are used to model the non-Gaussian tails of return distributions. The introduction of additional Poisson jumps makes the return distribution leptokurtic. The corresponding SDE for these models reads

$$\begin{aligned} dS(t) &= \mu S(t)dt + \sigma S(t)dz(t) + S(t)dJ(t) \\ dJ(t) &= (Y_{N(t)} - 1)dN(t)\ , \end{aligned} \tag{2.24}$$

with $N(t)$ a homogeneous Poisson process with intensity λ and Y_j is the size of the j-th jump, which are log-normally distributed. A Poisson process is a stochastic process where events occur continuously and independently of each other. $N(t)$ measures the number of events or jumps that have taken place up-to time t. The waiting time between jumps is an exponential distribution.

A homogeneous Poisson process with intensity λ is a process such that the number of events in a timespan $[t, t+T]$ follows a Poisson distribution with parameter λT:

$$P[(N(t+T) - N(t)) = k] = \frac{e^{-\lambda T}(\lambda T)^k}{k!} \qquad k = 0, 1, \dots\ . \tag{2.25}$$

Using this definition for $N(t)$, the equation for the logarithm of the price is:

$$d\log S(t) = \left(\mu - \frac{\sigma^2}{2}\right) dt + \sigma dz(t) + \log(Y_{N(t)})dN(t), \tag{2.26}$$

and the solution for this SDE is

$$S(T) = S(0)\exp\left[\left(\mu - \frac{\sigma^2}{2}\right)T + \sigma z(T)\right] \prod_{j=1}^{N(T)} Y_j\ . \tag{2.27}$$

In this process, up-to time T, $N(T)$ Poisson jumps have occurred. The parameters of this system can be calibrated so as to match a real stock price time series [CT04]. This model has the desired non-Gaussian, fat-tailed, return distributions but doesn't display the volatility fluctuations encountered in financial time series, see section 2.4.

Variance gamma models

Instead of changing the probability of large events (as in the jump diffusion model) or modifying the volatility (GARCH), one can play with the concept of time and introduce *time changing*. Time changing makes a random process of the time through a new process, a so-called subordinator. This philosophy can be supported by the interpretation that real time and financial time are not equivalent, because market activity is not constant over time.

The SDE of the variance gamma model for the log-returns is

$$d\log S(t) = \mu dt + \theta dg(t) + \sigma dz(g(t)) \ . \tag{2.28}$$

In this model, $g(t)$ characterizes the market time and it follows the constraints:

$$\mathrm{E}[g(t) - g(u)] = t - u \text{ and } g(u) - g(t) > 0 \text{ for } u \geq t \geq 0 \ , \tag{2.29}$$

where E is defined as the expectation value.

These conditions express that the market time is an increasing random process, but, on average, the market time and physical time are equivalent. This model is a suitable option for currency exchange rates time series.

Defaultable Bonds

In this model some sort of bankruptcy is taken into account. A bankruptcy is a sudden event and modelling these events is ideally based on the discontinuous Poisson process π. There are two important factors in this model, the interest rate r and the default factor. These are modelled as

$$\begin{aligned} dr &= adt + bdz \\ dN &= d\pi(\alpha) \ . \end{aligned} \tag{2.30}$$

The SDE for a default free bond $B(T)$ is:

$$dB(T) = (B_t(T) + aB_r(T) + \frac{1}{2}b^2 B_{rr}(T))dt + bB_r(T)dz \ . \tag{2.31}$$

Then, the SDE for the default-able bond price becomes:

$$dB(N) = \mathcal{L}B(N)dt + bB_r(N)dz + (B(N+1) - B(N)(d\pi(\alpha) - \alpha dt)) \ , \tag{2.32}$$

with,

$$\mathcal{L}B(N) = \left(B_t(N) + aB_r(N) + \frac{1}{2}b^2 B_{rr}(N) + \alpha(B(N) - B(N+1)) \right) \ . \tag{2.33}$$

This model can be incorporated into the above models to make them more realistic.

2.4 Generic features of stock markets

In the previous sections we have noticed that attempts to describe various features of financial markets in a mathematical way, date back to the early 1900s [Bac00]. We have described the evolution from simple Brownian motion, over geometric Brownian motion and the Black-Scholes equation, to rather complex and involved models for option pricing. The complexity of these models obscures the intrinsic dynamics of the system. For a physicist the internal dynamics, that drives the evolution of financial markets, is of great interest and importance.

In this work, we wish to develop a simulation system that can reproduce the robust and generic features of a financial market. In this way, we hope to learn more about the dynamics of financial markets. We stress that we focus on the big picture and will point out in Chapter 5 how refinements in the model can be implemented.

2.4.1 S&P 500 time series

We wish to illustrate the generic features of financial time series by making an analysis of a well-known index, the S&P500. We adopt the view that generic features do not require extensive data but can be distilled from data that are freely available on the web. The data have been downloaded from `finance.yahoo.com`. The S&P500 is a large and weighted index of 500 actively traded stocks of the United States of America. During the lifespan of this index, the exact composition of the S&P 500 has been regularly changed, so as to make the index match the evolution of the American economy. The data from `finance.yahoo.com` spans the period from January 3, 1950 up to the present. The data that entered our analysis end at September 28, 2009, and thus span over 59 years of financial activity. The data from `finance.yahoo.com` are free of cost, and are limited to intraday data. For every trading day, the opening and closing prices, as well as the highest and lowest point of the day are given.

In Fig. 2.4 the S&P 500 daily closing prices are shown ($Z(t)$), together with the absolute daily returns ($|G(t)|$) and the volatility ($V_T(t)$) over a period ($T = n\Delta t$) of 100 days. Here, we define the volatility at t as in [LGS99]:

$$V_T(t) = \frac{1}{n} \sum_{t'=t}^{t'=t+n\Delta t} |G(t')| \ . \tag{2.34}$$

This definition of volatility is not a unique definition. The concept of volatility tries to capture the amount of fluctuations during a certain time window T of the time series. This time window can be as small as a single time step, where the volatility becomes

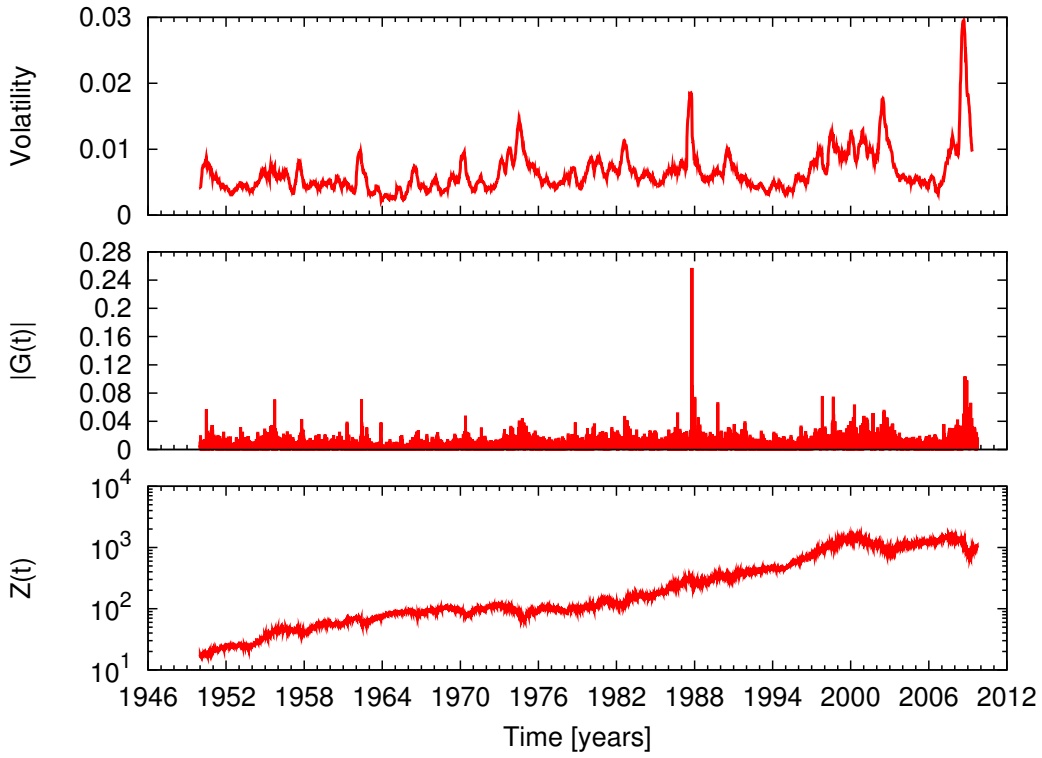

Figure 2.4 S&P 500 closing prices, $Z(t)$, from 01/03/1950 to 09/28/2009 (bottom panel). S&P 500 absolute daily returns, $|G(t)|$, from 01/03/1950 to 09/28/2009 (middle panel). S&P 500 volatility , $V_T(t)$, with $T = 100$ days, from 01/03/1950 to 09/28/2009 (top panel).

the absolute return, upto an indefinite length. Smaller time windows focus on the more instantaneous fluctuations and larger time windows capture the average amount of fluctuations.

Another generalized definition uses higher or lower order values of $|G(t)|$:

$$V_{T,\gamma}(t) = \frac{1}{n} \sum_{t'=t}^{t'=t+n\Delta t} |G(t)|^{\gamma} \ . \tag{2.35}$$

Using $\gamma > 1$ gives more weight to large values of $|G(t)|$ and $0 < \gamma < 1$ enlarges the weight of smaller values.

Another definition of volatility uses the standard deviation of the returns over a certain time window as precursor for the amount of fluctuations in this time window:

$$V_{T,s}(t) = \frac{1}{n} \sum_{t'=t}^{t'=t+n\Delta t} \left(G(t') - \overline{G(t')} \right)^2 \ , \tag{2.36}$$

where $\overline{G(t')}$ denotes the average return in this time window. These definitions can be used interchangeably because the generic features of the volatility remain present

independent of the mathematical formula. We will use the first definition throughout this work to maintain the simplicity of our approach.

A first observation of Fig. 2.4 is that there is an obvious long-term growth of the index $Z(t)$ and that the index $Z(t)$ wildly fluctuates around this long-term trend. More information can be obtained by studying the intraday returns during the timespan of over a half-century. The returns of Fig. 2.4 are predominantly small ($0 \leq |G(t)| \leq 0.04$), but some very large returns are also observed. This contrast is typical for non-Gaussian processes. Compare for example the returns of the geometric Brownian motion of Fig. 2.2 and the returns of real financial time series of Fig. 2.4. We can show the returns of both processes by fitting μ and σ of the GBM model to the returns of the S&P 500 time series. The resulting values, $\mu = 0.00032$ and $\sigma = 0.0097$, are then used in a GBM simulation for which the returns are calculated.

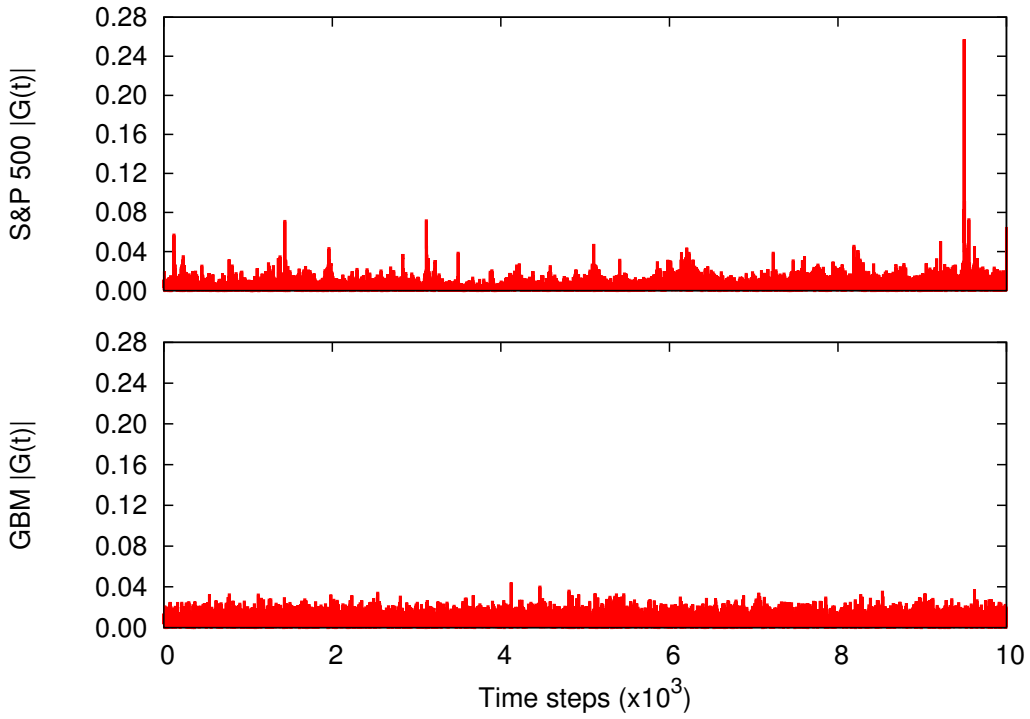

Figure 2.5 S&P 500 absolute returns, $|G(t)|$, for the first 10000 time steps of the data set (top panel), GBM model absolute returns, $|G(t)|$, with $\mu = 0.00032$ and $\sigma = 0.0097$ for 10000 simulation steps (bottom panel).

A comparison of the absolute returns of the S&P 500 and the GBM model with this constants is shown in Fig. 2.5 for the first 10000 time steps of both time series. It is clear that the GBM returns are confined to a certain scale < 0.04, whereas the returns of the S&P 500 have much larger extreme values.

The third observable is the volatility, which gives information about the fluctuations

of the index during a time interval of 100 time steps. The volatility clearly has periods where large fluctuations are present, for example in the periods around crashes. A more detailed analysis of the volatility will be performed in the following sections and in Chapter 5.

2.4.2 Heavy tailed return distributions

It has been pointed out that the returns of financial markets behave as non-Gaussian processes. The returns of the middle panel of Fig. 2.4 clearly demonstrate that there are more large events than one would expect for a Gaussian process. In Fig. 2.6 the distribution of the normalised (divided by the standard deviation σ of the distribution) returns is shown for the S&P 500 data considered here. There are clearly more events with $|G(t)| > \sigma$ than could be expected for a Gaussian distribution. The extreme event of 'Black Monday' in 1987 falls beyond the adopted scales as it is a clear outlier of this distribution because $|G(\text{"Black Monday"})| \approx 22\sigma$.

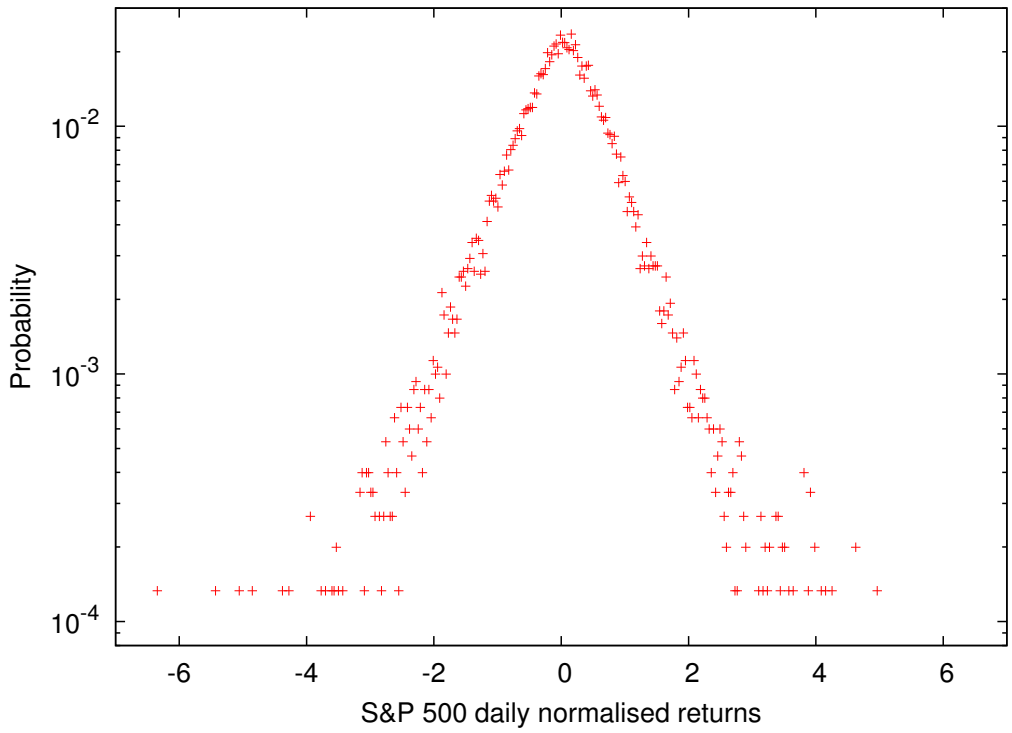

Figure 2.6 Distribution of the normalised (divided by the standard deviation σ of the distribution) daily returns of the S&P 500 data from 01/03/1950 to 09/28/2009.

This characteristic of markets is also expressed in Fig. 2.5. The returns in the GBM model have a definite scale to which 98% of the returns are confined, but no such scale exists for the S&P 500 data.

It is clear that a realistic simulation of a financial market should result in heavy-tailed distributions that do not display the Gaussian behaviour of the early economic models [Bac00, BS73].

2.4.3 Short memory of the returns

It is established that the distribution of the returns is highly non-Gaussian, but this could result from different origins. One of the possibilities is that the *intra-minute* returns are correlated in time, thus resulting in larger than Gaussian daily returns. This possibility cannot be verified using the dataset that we consider here. We will use the study of [LGS99] to verify this conjecture.

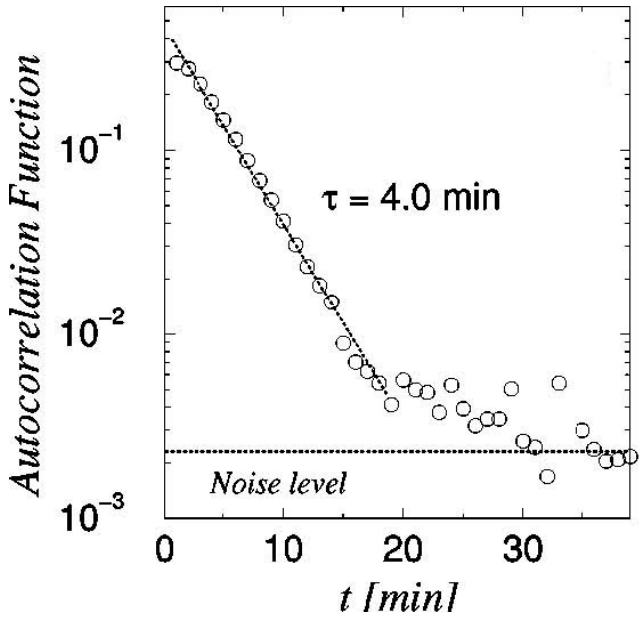

Figure 2.7 Autocorrelation function of $G(t)$ of the S&P 500 intra-minute data on a log-linear scale. Taken from [LGS99]. A fit with an exponential distribution results in a decay time of 4 min.

In Fig. 2.7 the autocorrelation of the returns is shown, with the same dataset as ours, but with intra-minute data. We see that after ≈ 30 min, the autocorrelation function is at the noise level, and the decay of the autocorrelation function can be approximated by an exponential, with decay time of 4.0 min.

Free minute-by-minute data is available on-line for a limited amount of indices and assets. We have analysed such a dataset from `http://www.livecharts.co.uk`, with 2000 events during the interval 06/24/2010-02/07/2010. The calculated return autocorrelation function is displayed in Fig. 2.8.

This autocorrelation function clearly displays the generic feature of a very short

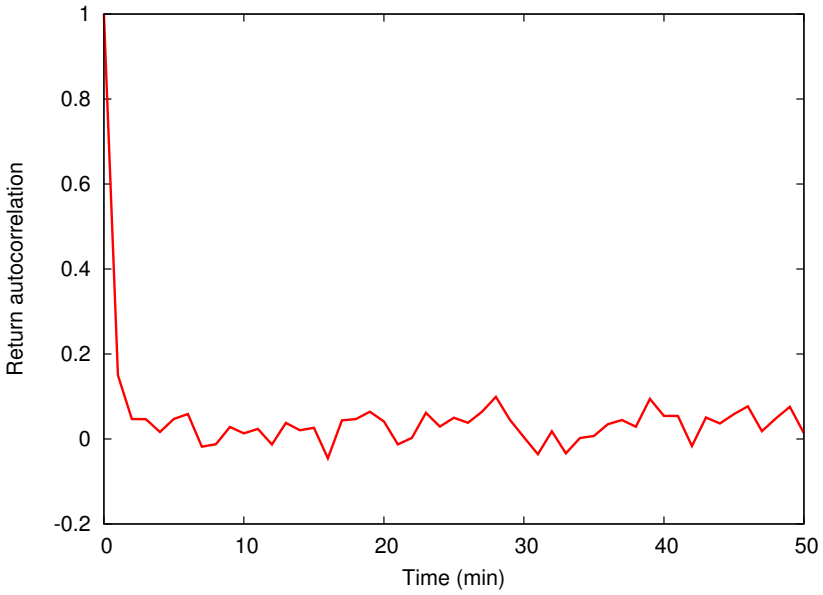

Figure 2.8 Autocorrelation function for the intraminute returns $G(t)$ of the S&P 500 for the timespan 06/24/2010-02/07/2010. The data cover 2000 minutes of market time and are obtained from http://www.livecharts.co.uk

memory for the returns. We see that after 5 min the autocorrelation function is at the noise level and the information generated by the trades at $t = 0$ has dissipated in the market.

This behaviour of the autocorrelation function is what we expect from the no arbitrage argument (there is no free lunch!). If the returns would be highly correlated in time, one could predict with a high degree of accuracy the returns of the future. The effect of using this information would result in the opposite effect, where the correlation between returns vanishes, and thus the arbitrage opportunity is destroyed. In practice, the decay time is so small that arbitrage is practically impossible. Indeed, exploitation of the short correlation time leads to transaction costs that are higher than the profit that could be made.

Another example of the unpredictability of the prices of stocks is shown in Fig. 2.9. The figure displays the autocorrelation of price changes in the exchange rate of the USD/Yen on the level of ticks. Ticks are the smallest increments by which the price of stocks or other exchange-traded instruments can move. The time in the system is changed from physical time to tick time, where every trade makes the tick time move one unit. The autocorrelation function of Fig. 2.9 indicates that time correlations become negligible after 5 ticks (or trades)!

This behaviour of the returns is a very general and commonly accepted characteristic of financial markets, see [BG90, MS99, Man63]. The no-arbitrage argument ensures

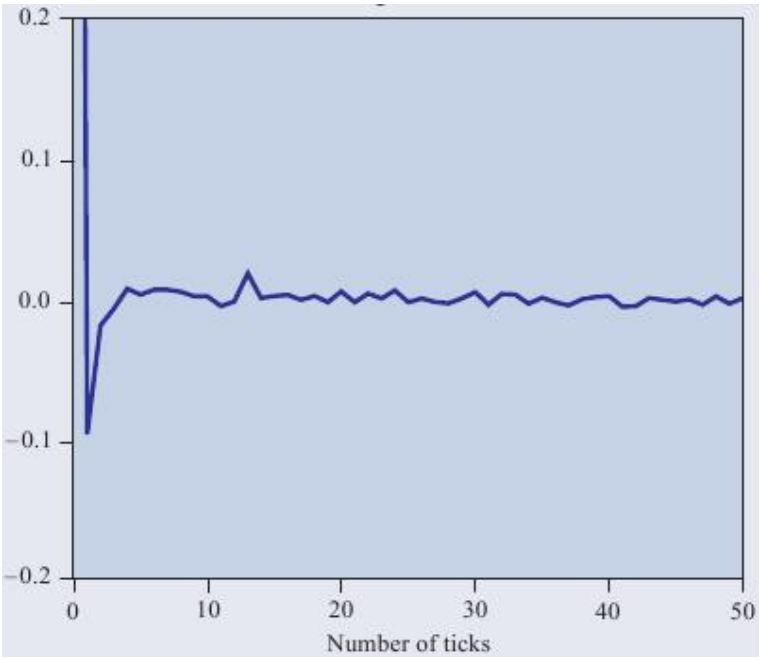

Figure 2.9 Autocorrelation function of price changes in the USD/Yen exchange rate as a function of the number of ticks. The data refer to the period 1992-1994. The figure is taken from [Con01].

that the memory of the returns will be very short across all markets. This makes that this generic feature is definitely a universal generic feature.

2.4.4 Long memory of the volatility

Another generic feature of financial markets is the behaviour of the volatility. As can be observed in Fig. 2.4, the time intervals with a very large volatility are clustered, and there are also very large periods in which the volatility, and thus the fluctuations, are very small. The autocorrelation function of the volatility will mimic this behaviour and will not decay exponentially as did the autocorrelation function of the returns.

In Fig. 2.10 the autocorrelation of the volatility is shown. We have chosen $T = 1$ which is the highest resolution possible with the dataset of the intraday S&P 500 index contained in Fig. 2.4. This is equivalent to calculating the autocorrelation function of the absolute daily returns $|G(t)|$. It is clear that there are higher order correlations in this function and we have fitted a power law to this function, $C(t) \sim t^{-\gamma}$, with $\gamma \approx 0.26$. The slow decay of the volatility autocorrelation function indicates that bursts of activity are grouped together and calm periods, without much fluctuations, occur intermittently. This generic feature is called volatility clustering or long memory of the volatility.

This generic property of financial markets is well-known in the financial literature,

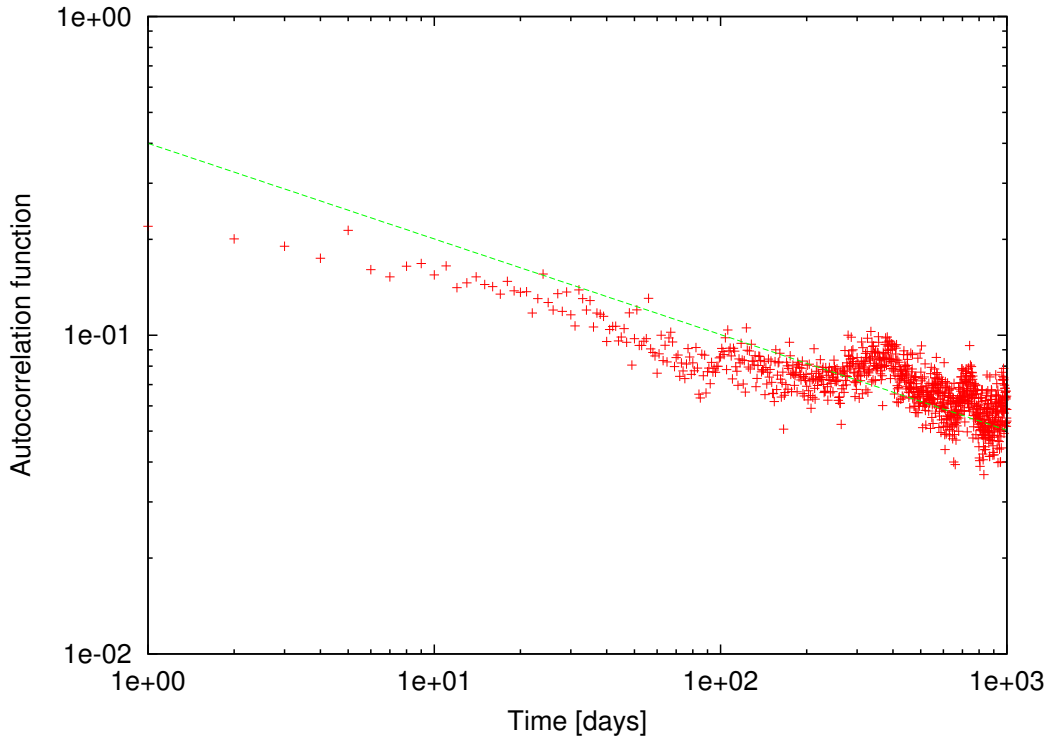

Figure 2.10 Autocorrelation function $C(t)$ of the absolute daily returns $|G(t)|$ of the S&P 500 dataset on a logarithmic scale. Fitted with a power law: $f(x) = 0.4x^{-0.26}$.

and is very important for the Black-Scholes calculations, since the volatility has to be estimated for the lifetime of the option. There are multiple ways in which to model this long-term behaviour, such as ARCH (autoregressive conditional heteroskedasticity) and GARCH (generalized autoregressive conditional heteroskedasticity) models.

2.4.5 Universality

The generic features of the S&P 500, as described in the previous sections, are also present in other indices and asset prices. The above mentioned analysis of the S&P 500 can be repeated for other financial indexes, such as the DAX, the Deutscher Aktien IndeX, that comprises 30 major German companies traded on the Frankfurt Stock Exchange. A complete analysis of the available data on `finance.yahoo.com`, from 11/26/1990 to 05/07/2010, results in the same generic features as observed in the S&P 500. A visual comparison of the time evolution of the essential variables of the S&P 500, Fig. 2.4, and the DAX, Fig. 2.11, leads to equivalent observations.

From Fig. 2.11 it is clear that the DAX has non-Gaussian distributions for the returns. During the latest stock market crisis, 2008-2009, particularly large returns (either positive or negative) occur.

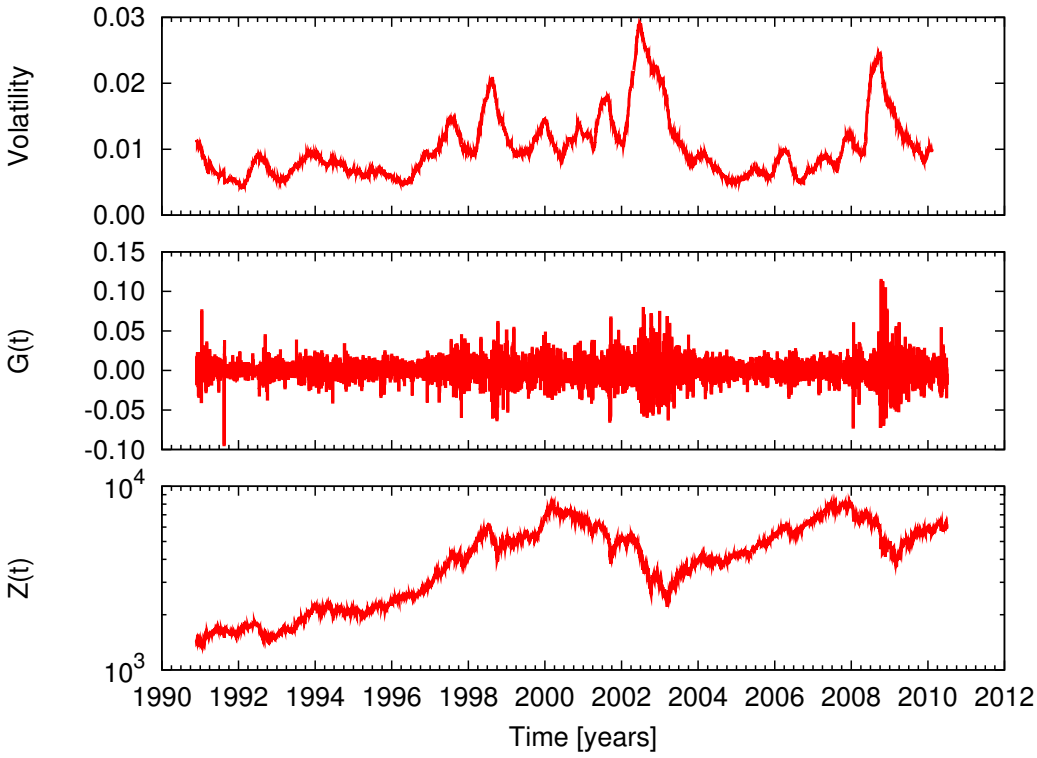

Figure 2.11 DAX intraday closing prices, $Z(t)$, from 11/26/1990 to 05/07/2010 (bottom panel). DAX absolute daily returns, $G(t)$, for the same timespan (middle panel). DAX volatility, $V_T(t)$, with $T = 100$ days, for this time span (top panel). Data from finance.yahoo.com.

The DAX returns are equally unpredictable as any other index. Indeed, the time series of the returns shows no apparent correlation in the returns, positive returns are equally likely followed by negative returns as by positive returns.

The third generic feature, the long memory of the volatility, can be detected in the time series of the volatility of the DAX. The long persistence of the peaks in the volatility is a clear signal that the autocorrelation function of the volatility will have long time tails. The magnitude of the volatility of the DAX is of the same order as the one observed for the S&P 500.

A third index shown here is the Nikkei 225, Fig. 2.12, which is a stock market index for the Tokyo Stock Exchange. It calculates a weighted average of 225 stocks of companies across all Japanese industries.

The same generic features as in the S&P 500 and the DAX are present in this index. The heavy tails of the return distributions, the short memory of the returns and the long memory of the volatility can all be distinguished from Fig. 2.12. It is clear that the long-term behaviour has no apparent effect on these generic features. Whereas the S&P 500 and DAX time series show a long-term growth, no such trend is observed in the Nikkei 225 time series. One can also observe that trends in indices are not permanent

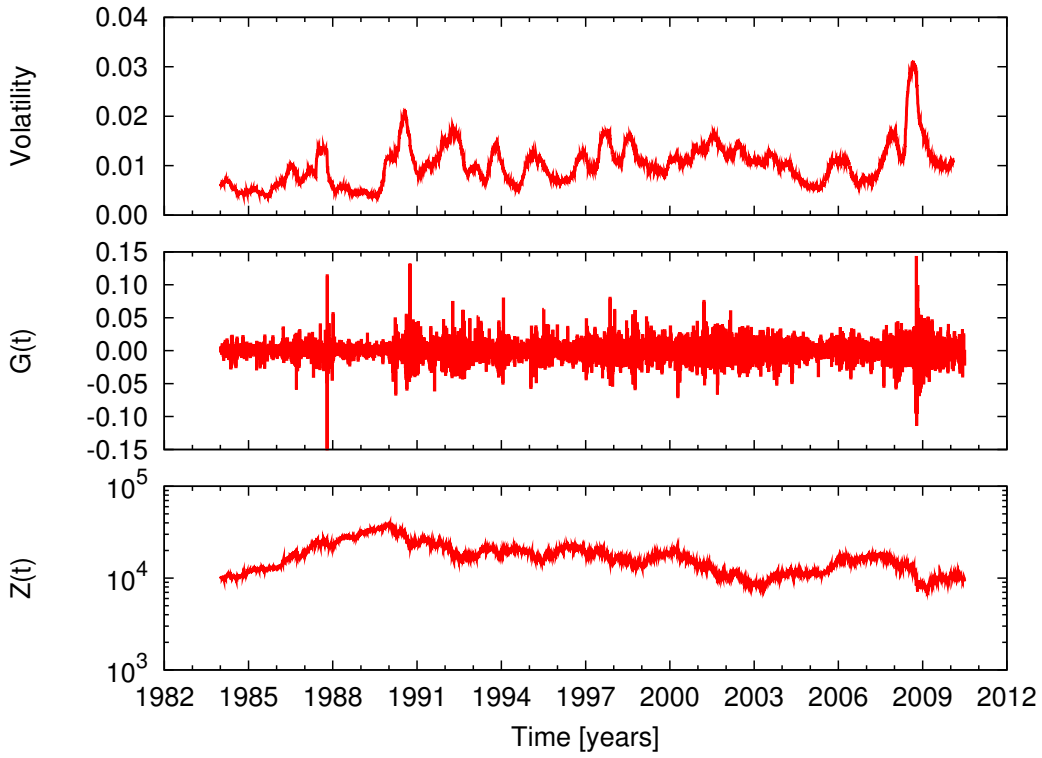

Figure 2.12 Nikkei 225 intraday closing prices, $Z(t)$, from 01/04/1984 to 05/07/2010 (bottom panel). Nikkei absolute daily returns, $G(t)$, for the same timespan (middle panel). Nikkei 225 volatility, $V_T(t)$, with $T = 100$ days, for this time span (top panel). Data from `finance.yahoo.com`.

and trend-switching occurs in the time series of the three indices.

The universality of these generic features is confirmed by comparing the three different indexes presented here, see also [Con01, MS95]. These indexes represent different economies from different parts of the world, with different taxes, costs and governments, but they share these three robust features, which shows that these features are truly generic features that are universally present in stock markets.

2.4.6 Crash dynamics

Bubbles and crashes are well-known manifestations of financial market dynamics. Despite the fact that their rate of incidence is relatively low, they are a perpetual source of stress for traders and investors. Crashes represent a major source of instability and are of great concern to societies as they may have a severe impact on the lives of many people. Not only the traders and investors are affected, but economies as a whole suffer from market crashes. We simply have to mention the crash of the housing bubble in the USA to exemplify this.

In the context of standard economic theories the origin of a crash has to be sought

in the sudden revelation of a dramatic piece of information. Examples are sudden outbreaks of war, terrorist attacks, natural disasters like earthquakes, sudden and unexpected drops in revenues of firms, ...

Crashes have also attracted the attention of the econophysics community. In particular, one has tried to establish connections between the physics of phase transitions and crashes. As an example we mention the work of D. Sornette and collaborators [JSL99, Sor98a, JLS00, SJ01, Sor03a, JZS+10]. They claim to discern universal behaviour in the time series of assets that are prone to a crash. It is conjectured that crashes are not the result of a sudden influx of information but should be considered as the end points of bubbles that are linked to cooperative behaviour of players in the market over a rather long period of time (months or even years). The cooperativity reflects itself in time series that can be described by log periodic power laws (LPPL) that are reminiscent for the discrete scale invariance of the players in the market.

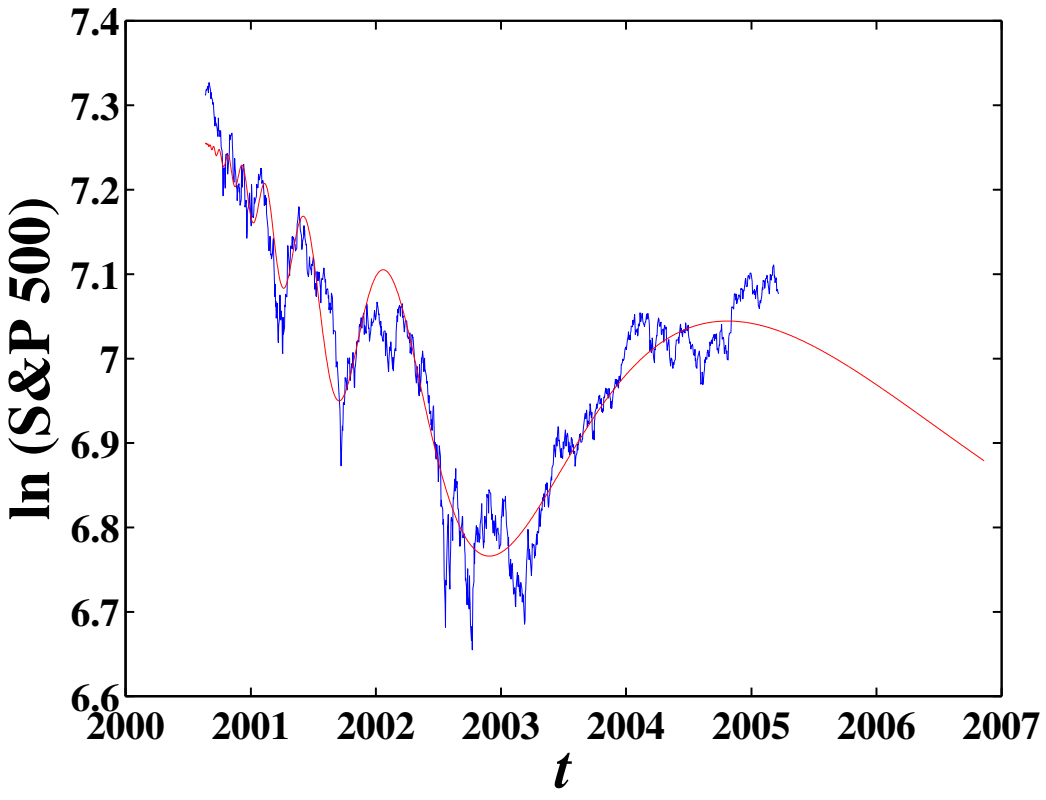

Figure 2.13 S&P 500 from 2000/08/21 to 2005/03/21. Fit with Eq. 2.37, with parameters: $t_c = 2000/08/17$, $m = 1.32$, $\omega = 13.72$, $\psi = 1.31$, $\Delta_t = 545$, $\Delta_\omega = -10.28$, $A = 7.26$, $B = -9.505 \times 10^{-5}$, and $C = -4.224 \times 10^{-5}$. Taken from [ZS06].

Fig. 2.13 shows a typical LPPL evolution of the S&P 500, which in this case describes

an anti-bubble. The LPPL function that is fitted to it is described by (with $\tau = t_c - t$):

$$I(t) = A + \frac{B\tau^m + C\tau^m \cos\left\{\omega \ln\tau + \frac{\Delta_\omega}{2m}\ln\left[1 + \left(\frac{\tau}{\Delta_t}\right)^{2m}\right] + \psi\right\}}{\sqrt{1 + \left(\frac{\tau}{\Delta_t}\right)^{2m}}}\ , \tag{2.37}$$

for which 9 parameters need to be determined. This large number of parameters partly explains the universal occurrence of this formula, since a wide range of time series can be described by a formula with this many parameters.

Scale invariance is a generic feature of phase transitions in physics and is reflected in observables that are power laws as a function of a control variable [LA02]. More evidence for the scale invariant behaviour of markets near crashes is provided by the analysis of the Tokyo group [KSY06]. This group has performed a multiscale analyses of the S&P 500 time series and they analyse 'non-crash' and 'crash' data in an attempt to distinguish the difference between the dynamics of a non-crash operation of the market and the crash dynamics.

Their analysis focuses on the fluctuations of stock prices and they therefore use detrended data. The detrending is performed by dividing the time series $\big(\{x(t)\},\, x(t) \equiv \ln Z(t)\big)$ into boxes of size s. In each interval $[1 + s(k-1), s(k+1)]$ of length $2s$ they fit $x(t)$ to a linear function. The variable $x^*(t) = x(t) - x_{fit}(t)$ represents the data with the removal of the exponential trend of the original time window. For every time scale s the detrended log returns read

$$\Delta_s Z(t) = x^*(t+s) - x^*(t), \qquad 1 + s(k-1) \le t \le 1 + sk\ . \tag{2.38}$$

They then use a random multiplicative process to model the non-Gaussian distributions for these returns. Suppose the increments are described by the following form

$$\Delta_s Z(t) = \xi_s(t)\exp[\omega_s(t)]\ , \tag{2.39}$$

where ξ_s and ω_s are both Gaussian variables with zero mean and variance σ_s^2 and λ_s^2, respectively, and they are independent of each other. This leads to a probability density function (PDF) of $\Delta_s Z(t)$ that is described by Castaing's equation [CGH90]:

$$P_s(\Delta_s Z) = \int F_s(\frac{\Delta_s Z}{\sigma})\frac{1}{\sigma}G_s(\ln\sigma)d(\ln\sigma)\ . \tag{2.40}$$

The Gaussian distributions are represented by F_s and G_s, which have zero mean and variance σ_s^2 and λ_s^2, respectively. The PDF $P_s(\Delta_s Z/\sigma_s)$ converges to a Gaussian distribution for $\lambda_s \to 0$.

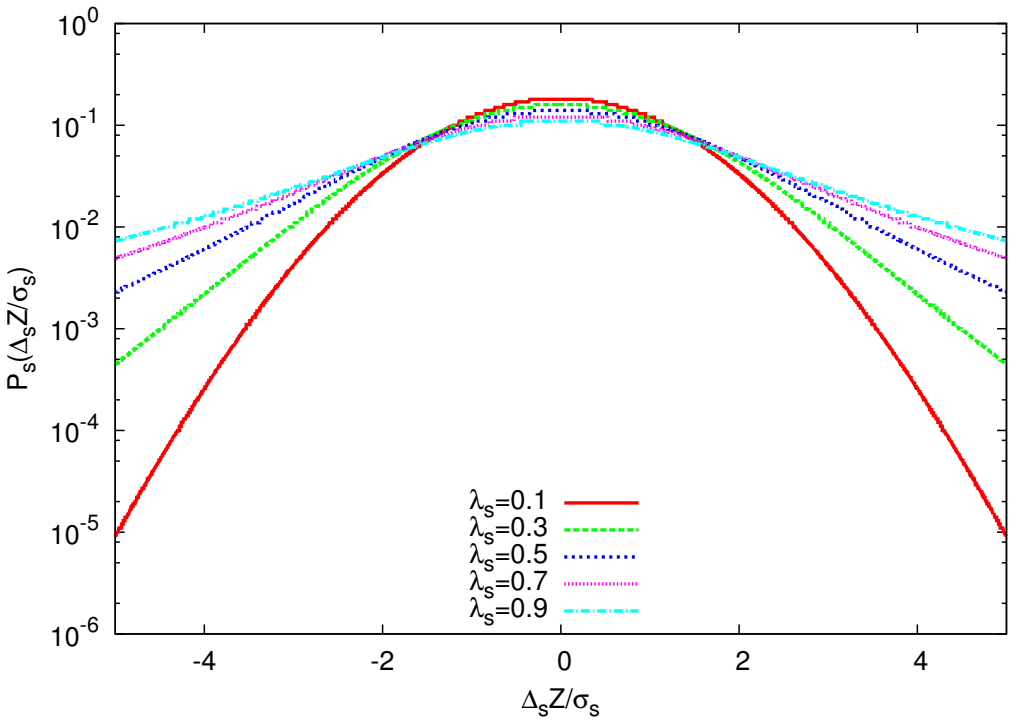

Figure 2.14 Evolution of Castaing's equation for normalized variables $\frac{\Delta_s Z}{\sigma_s}$ for different parameters λ_s.

In using normalized variables $\frac{\Delta_s Z}{\sigma_s}$ one can study the dependence of $P_s(\Delta_s Z/\sigma_s)$ on the value of λ_s. Fig. 2.14 shows the function $P_s(\Delta_s Z/\sigma_s)$ for a range of values λ_s. One readily observes large deviations from the Gaussian distribution for large values of λ_s and the convergence to a Gaussian distribution for λ_s.

The S&P 500 under non-crash market conditions

The Tokyo group has used the variable λ_s to quantify the non-Gaussian tails of distributions at different time scales. In Figs. 2.15 and 2.16, the core results of their analysis is shown. In Fig. 2.15 they show the PDFs of $\frac{\Delta_s Z}{\sigma_s}$ of the S&P 500 intra-minute data for different time scales $s = 8,\ 16,\ 32,\ 64,\ 128,\ 256,\ 512,\ 1024,\ 2048$ min, for the time interval 1984-1995, but excluding the data from 1987, 1988, 1990 and 1991 identified as crash periods: 1987 and 1988 includes *Black Monday* and the Gulf War also resulted in crashes (1990-1991).

In these time periods without a crash, Fig. 2.15, returns at short time scales have large, non-Gaussian tails, as opposed to the long time scales, where the returns are almost Gaussian. The non-crash dynamics leads to values of λ_s that decrease with increasing time window s.

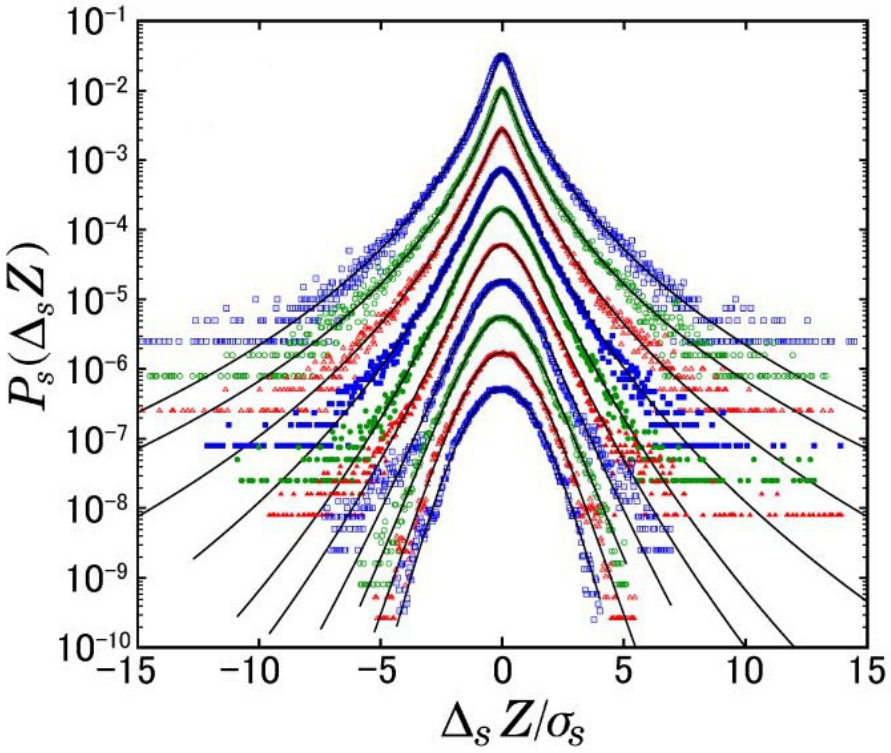

Figure 2.15 $P(\Delta_s Z/\sigma_s)$ of the S&P 500 from 1984 to 1995 for different time scales $s = 8,\ 16,\ 32,\ 64,\ 128,\ 256,\ 512,\ 1024,\ 2048,\ 4096$ min from top to bottom, but without data from 1987, 1988, 1990 and 1991. Taken from [KSY06].

This is a very interesting feature because it means that during normal operation of financial markets, the central limit theorem prevails because the non-Gaussian tails are limited with a finite standard deviation and there are not enough time correlations to sustain these tails.

The S&P 500 under crash conditions

In Fig. 2.16 the PDFs of the returns at different time scales are shown for financial data of a quarter of the year which includes the 1987 stock market crash. One can clearly see that the non-Gaussian tails of the return distributions do not vanish for long time scales. The values of λ_s are large at every time scale s.

This generic feature must stem from large time correlations during the stock market crash. During normal operation of the stock market, these time correlations seem to be small enough to be overridden by the central limit theorem. But, during the crash timespan, the time correlations seem to be large enough to generate non-Gaussian distributions at all time scales, thus evading the central limit theorem. This scale invariant behaviour is typical of a phase transition and a crash could be considered to be a critical

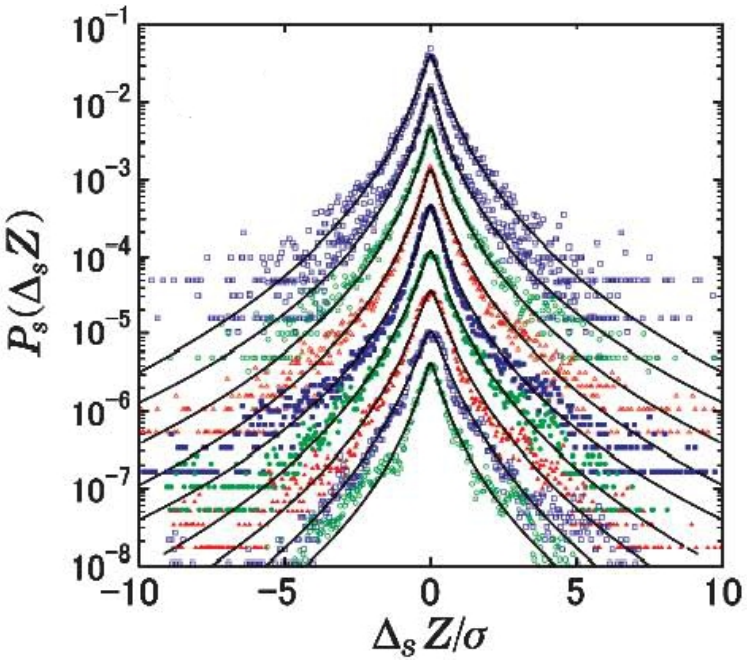

Figure 2.16 $P(\Delta_s Z/\sigma_s)$ of the S&P 500 for different time scales $s = 8,\ 16,\ 32,\ 64,\ 128,\ 256,\ 512,\ 1024,\ 2048$ min from top to bottom, during a quarter of the year which includes Black Monday. Taken from [KSY06].

phenomenon.

The dynamics present in Figs. 2.15-2.16 are very useful to evaluate the presence of crashes in a model. Instead of defining crashes as outliers on a return distribution [JLS00], or as draw-downs over several days [Sor03b], one is able to look at the time evolution of the returns distributions and decide if a market model possesses the ability to reproduce the dynamics that are present in real financial markets crashes.

Chapter 3

Diffusion in Molecular Dynamics

Ever since Einstein made geometric Brownian motion famous [Ein05], a liquid has been the prime example of a system in which normal diffusion occurs. We will attempt to recreate the properties of financial markets encountered in the previous chapter, where anomalous non-Gaussian distributions are ever-present. Many models use interacting agents to simulate the behaviour of markets, [BPS97, Lux05, CMZ05, Coo05, ACPZ08]. Interacting agents (molecules) are also present in a liquid and is therefore a candidate whereupon a model can be based. We will use a powerful and widely used method in physics to simulate the interacting agents of a liquid.

3.1 Molecular Dynamics

Simulations of thermodynamic properties of physical systems have centered around two different methods: Molecular Dynamics (MD) and Monte Carlo (MC). MD and MC are both methods that determine physical quantities by averaging over a finite set of configurations of the system under study. By using the ergodic principle one can justify this approach. The ergodic principle states that all accessible configurations of a system are equiprobable over a long period of time. As a result, one can relate the average over the configurations to the time average in a real system.

In the MD and MC method, the configurations are generated one after the other and are not independent. MD and MC differ essentially in the way this succession of configurations is calculated.

The MC simulation method is fully based on the underlying (Boltzmann) statistics of the system under observation. In this way, a new configuration is accepted at random but the random probability is based on the statistical probability of this new configuration. Since MC methods have no inherent time, the new configuration is not linked in

time with the previous one, it is difficult to simulate diffusion and time correlations in a liquid with MC.

MD on the other hand relies, *nomen est omen*, on calculating the dynamics of a (molecular) system based on solving the equations of motion via a specific algorithm. This method has an indigenous time that links the next configuration to the previous one via Newton's equations (or the natural time evolution). As a consequence, a MD simulation allows one to investigate many aspects of liquids and other systems such as self-diffusion, phase diagrams, absorption of particles and viscosity [AW70, KH93, MG97, CRH+01, TO96].

3.1.1 Standard MD

The MD technique solves the equations of motion for a number of particles (N) embedded in a certain volume V:

$$\frac{d^2\vec{r}_i(t)}{dt^2} = \frac{\vec{F}_i}{m_i} , \qquad \forall i = 1 \ldots N . \tag{3.1}$$

With $\vec{r}_i$ the position of particle i in the volume, m_i the mass of this particle and $\vec{F}_i$ the force acting on this particle. This force is determined by calculating the sum of interactions of one particle with all the other particles in the system:

$$\vec{F}_i = \sum_{j=1(j\neq i)}^{N} F(|\vec{r}_i - \vec{r}_j|)\vec{e}_{ij} , \tag{3.2}$$

with $\vec{e}_{ij}$ the unit vector along $\vec{r}_{ij}$.

The solution to these equations describes the time evolution of a real system for a given set of boundary conditions. There are of course some difficulties embedded in this method.

- The computational cost of this simulation scales as N^2. This means that it is impossible to simulate real systems, which have $N \sim 10^{23}$. In this way, only a very small part of real systems can be calculated. This does not discredit the results. Indeed, as long as the correlation length is smaller than the system size, the produced statistical results are representative for the real results.

  The effect of using only a small number of particles (up to 10000) manifests itself by the presence of a boundary. This physical boundary results in a high percentage of particles on the surface of the simulation system. In a $10\times10\times10$ lattice, not less than 488 particles are situated on the surface (the outer two layers). The solution

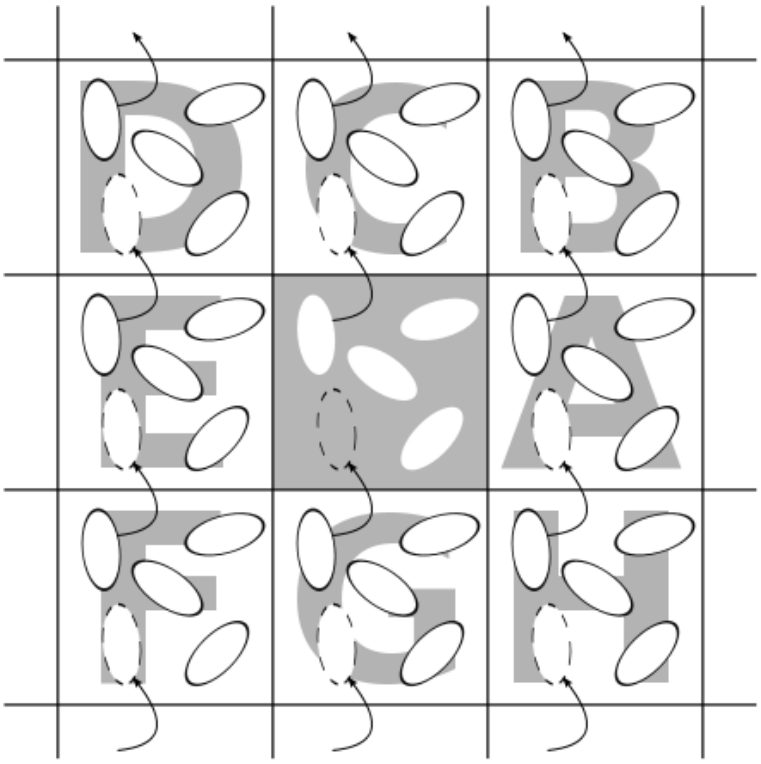

Figure 3.1 Periodic boundary conditions for a two-dimensional system.

that is commonly adopted is to use periodic boundary conditions (PBC). In Fig. 3.1 these conditions are represented in the two-dimensional case. By using PBC, the simulation system is surrounded by an infinite amount of equivalent systems and 0% of the particles are situated at the surface, because a particle leaving the box enters the simulation at the opposite part of the box. The interaction between two particles can be evaluated as the force between the first particle and the copy of the second particle that is closest to the first one (minimum image convention).

- Another factor that limits the capabilities of a MD simulation is the use of a realistic force between two particles. The forces adopted in simulations are usually a parametric simplification of real systems. In simulations for ideal liquids the Lennard-Jones potential (section 3.1.4) is widely used. The forces between particles can incorporate quantum mechanical effects, but the interactions are described in a classical way. The classical description can be justified in commonly used systems such as galaxies and liquid Argon [Thi99].

- The equations of motion can only be solved at finite time steps. This is a source of deviations between the ”real” and ”computed” dynamic evolution. The effect this

has on the physical quantities is small because the configurations that are visited will still average out into an approximation of the real system by using the ergodic hypothesis.

For a typical classical liquid, the finite time step is usually equal to about 10^{-14} seconds, which is only a small fraction of the real time over which a system is studied. To avoid artefacts of this small time step, the temporal correlations in the system should be smaller than the time over which the simulation is run. To a certain extent, this can be resolved by using a larger time step, but this leads to a greater inaccuracy in the time evolution of the system.

Integration algorithm

A very widely used algorithm to solve differential equations is the Verlet algorithm and we will use a variant of this algorithm, the velocity Verlet algorithm or the leapfrog method.

Based on the Taylor expansions of the position of a particle:

$$\vec{r}_i(t+\Delta t) = \vec{r}_i(t) + \vec{v}_i(t)\Delta t + \frac{\vec{a}_i(t)(\Delta t)^2}{2} + \frac{\vec{b}_i(t)(\Delta t)^3}{6} + \mathcal{O}(\Delta t^4) \ , \tag{3.3}$$

and the equivalent expansion of the velocity of a particle, the velocity Verlet algorithm reads:

$$\begin{aligned} \vec{r}_i(t+\Delta t) &\approx \vec{r}_i(t) + (\Delta t)\vec{v}_i(t) + (\Delta t)^2\frac{\vec{F}_i(t)}{2} \ , \\ \vec{v}_i(t+\Delta t) &\approx \vec{v}_i(t) + \frac{\Delta t}{2}[\vec{F}_i(t+\Delta t) + \vec{F}_i(t)] \ , \end{aligned} \tag{3.4}$$

where the acceleration $\vec{a}_i$ is replaced by $\vec{F}_i$, for $m_i = 1$. The advantage of the velocity Verlet algorithm is that both the position and velocity are calculated at the same time. Only the forces need to be evaluated twice to calculate the evolution of the system over one time step.

The cumulative error of the above algorithm is $\mathcal{O}(\Delta t^2)$ and this algorithm is very stable with respect to the total energy of the simulation system. The cumulative error can be obtained by induction and is:

$$\text{error}\,(\vec{r}_i(t+n\Delta t)) = \frac{n(n+1)}{2}\mathcal{O}(\Delta t^4) \ , \tag{3.5}$$

and can be generalized to a time $T = n \times \Delta t$:

$$\text{error}\,(\vec{r}_i(t+T)) = \left(\frac{T^2}{2\Delta t^2} + \frac{T}{2\Delta t}\right)\mathcal{O}(\Delta t^4) \ , \tag{3.6}$$

which results in a global error of $\mathcal{O}(\Delta t^2)$.

System units

To simplify the notation and the computational cost, all physical quantities are expressed in system units. The values of these units are determined by the use of the LJ-potential:

$$U_{LJ}(r) = \epsilon((\frac{r_0}{r})^{12} - 2(\frac{r_0}{r})^6) \ . \tag{3.7}$$

This potential links the energy and radius of the particles to those of the real monoatomic Argon liquid. The system units are therefore referring to a simulation of liquid Argon with a LJ potential.

Setting $r_0 \equiv 1$ and $\epsilon \equiv 1$ with particles that have unit mass, i.e. $m_i \equiv 1$, sets the time and temperature of the simulation. Since energy is expressed in $J = \frac{\mathrm{kg \cdot m^2}}{\mathrm{s^2}}$ and temperature $[T] = k_B[E]$ we can derive the system units:

$$\begin{aligned}
\epsilon_{Ar} &= 1.6537 \times 10^{-21}\mathrm{J} \ , \\
(r_0)_{Ar} &= 3.405 \times 10^{-10}\mathrm{m} \ , \\
m_{Ar} &= 6.63 \times 10^{-26}\mathrm{kg} \ , \\
\tilde{E} &= \frac{E}{\epsilon_{Ar}} \ , \\
\tilde{x} &= \frac{x}{(r_0)_{Ar}} \ , \\
\tilde{\rho} &= \rho \times (r_0)^3_{Ar} \ , \\
\tilde{t} &= t\sqrt{\frac{\epsilon_{Ar}}{m_{Ar}(r_0)^2_{Ar}}} \ , \\
\tilde{T} &= \frac{k_B T}{\epsilon_{Ar}} \ ,
\end{aligned} \tag{3.8}$$

with $k_B = 1$.

Evolution of the system

There are three distinct phases in the simulation:

1. Initialization: The initial positions of the particles are drawn on a grid that is energetically favourable for the molecules in the simulation. In the case of Argon atoms an FCC grid, with four particles per unit cell, is a stable configuration. This grid has $4k^3$ particles to fill a complete cubic simulation systems. Therefore it will be convenient to chose the number of particles so as to fill the grid completely ($N = 8788 = 4 \times 13^3$). Here $k = 13$ is chosen because it results in an amount of

particles for which the simulation is computationally feasible. An initial density and temperature have to be chosen, and in this way the unit cell length (via the density) and the time step of the simulation ($t = \frac{0.001\rho^{-1/3}}{\sqrt{2T}}$) are set. We will use a *reference MD simulation* in this thesis which has initial conditions: $N = 8788,\ T = 0.7,\ \rho = 0.5$. Unless otherwise mentioned, all simulations start with these *reference MD* initial conditions. Given a temperature, the average velocity of the particles is set, via $T = \frac{2}{3}E_{kin}$.

2. Evolution to equilibrium: During this phase of the simulation the equations of motion for the particles are solved using the Verlet algorithm. Since we have randomly chosen velocities for the particles, and have placed them on a grid, there will not yet be thermodynamic equilibrium in the system. Therefore we let the system evolve for a certain time period (longer than the temporal correlations in the system) until it reaches equilibrium. The equilibrium temperature reached by the system can be different from the initial temperature. In order to run simulations at some desired temperature we will rescale the velocities at regular time intervals:

$$\vec{v}_i \rightarrow \vec{v}_i \sqrt{\frac{\frac{3}{2}(N-1)T_{avg}}{E_{kin,avg}}}\ . \tag{3.9}$$

This rescaling ensures that we start the next phase with the initialized conditions.

3. Production: Once the simulation system has reached equilibrium, we reset the time and start the actual data taking. Physical properties from this phase can be meaningfully linked with properties of real systems. The different physical properties that can be evaluated are explained in the next section.

3.1.2 Various ways of reading a simulation

A MD simulation produces step-by-step data of the position and velocity of every particle. To analyse all this, one could rerun the movie of the entire simulation, which is not practically feasible. Data storage is limited, so one has to chose carefully what to save and what not to save. There are several ways to look at the abundance of information stored in one simulation. In the following sections it will be pointed out how one can cope with all this information.

Distributions and moments and cumulants

A basic method to minimize the amount of data to investigate is to monitor the cumulants of the distribution of the steps ($\Delta x_i(t) = x_i(t + \Delta t) - x_i(t)$) and the velocities ($\vec{v}_i(t)$). At certain time steps one can accumulate all the information about the distance travelled, the instantaneous velocities and the positions and use the moments of the distribution to summarize the state of the system at this point. The gathered information consists of the cumulants of the absolute step distribution and the velocity distribution for all dimensions. These cumulants are: the mean, the mean squared displacement (second cumulant), the skewness (third) and the kurtosis (fourth). The derivation of these cumulants can be found in Appendix A.

These cumulants can give one a basic understanding of the time evolution of the system, since for example one can look at the symmetry in the system (first and third cumulant). Another property, the self-diffusion of the system, can be determined by analyzing the second cumulant of the positions, see section 3.1.3.

Another basic method of limiting the amount of data to scrutinize is to focus on one time step. This method enables one to store the temporal data and investigate how the internal dynamics behaves. One can look at potential energy gain or loss of every particle and the movement off all particles. This will be essential when investigating the instantaneous self-diffusion in the system, as will be discussed in sections 3.1.3 and 4.3.

Thermodynamic information

One way of looking at a MD simulation, is to compute the thermodynamic variables of the simulation. An essential variable during the initialization is the temperature, which is calculated by averaging over the kinetic energies:

$$T = \frac{1}{3(N-1)k_B} \sum_{i=1}^{N} m v_i^2 \ . \tag{3.10}$$

Monitoring of this variable provides insight into global variations away from equilibrium of the system. Indeed, during a normal simulation the temperature fluctuates around its equilibrium value.

The potential energy of the system is determined by summing the potential energy of the particle pairs in the system:

$$E_{pot}(t) = \sum_{i<j=1}^{N} U(r_{ij}(t)) \ . \tag{3.11}$$

The sum of these two energetic variables, the total energy, is constant using a Verlet algorithm, and therefore it is very useful to track both these variables (there is only a numerical deviation from the theoretical total energy). As we will see in chapter 4, these variables also offer insight into the dynamics that restore equilibrium in the system.

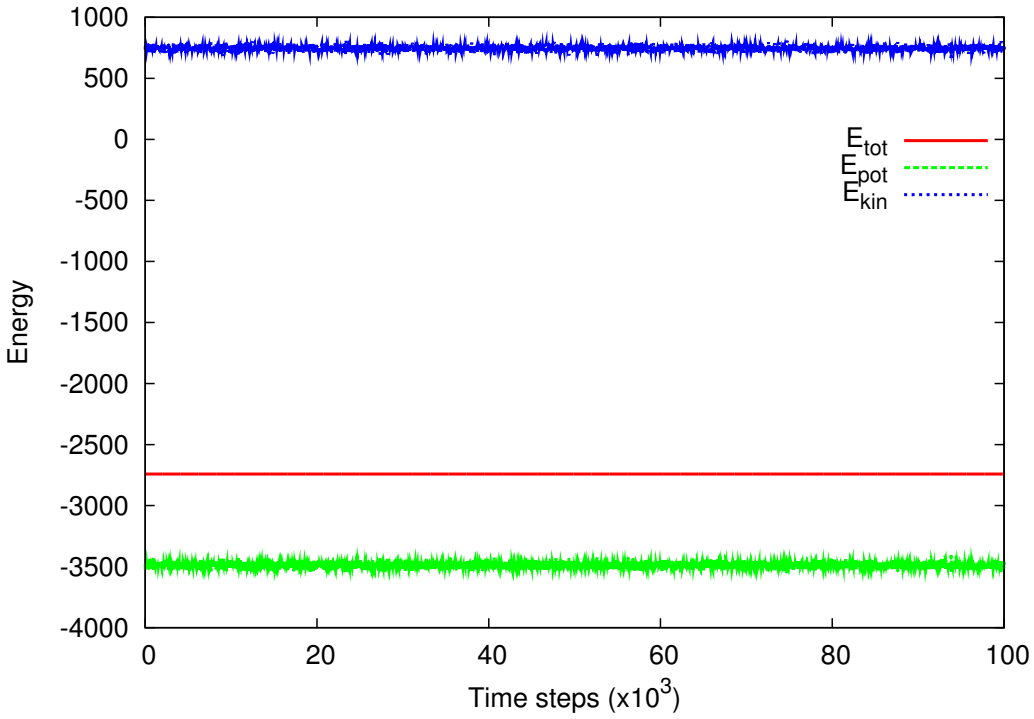

Figure 3.2 The total, potential and kinetic energy in a reference MD simulation for 100000 time steps during the production phase.

In Fig. 3.2 we show a representative example of the time evolution of the total, potential and kinetic energy of a reference MD simulation. The conservation of total energy and the fluctuations of the kinetic energy (and thus also of the temperature) during equilibrium are clearly visible.

Dynamic information

Another way of observing the internal dynamics of the system is by calculating the (spatial and temporal) correlations in the system. The velocity autocorrelation function (VACF) and the radial distribution function (RDF) display the correlations in time and space respectively. The RDF can be calculated at every time step and can be averaged over multiple time steps. Averaging over multiple time steps decreases the statistical

fluctuations of the RDF. The pair correlation function ($g^{(2)}(r_{12})$) is defined as:

$$g^{(2)}(\vec{r}_1,\vec{r}_2) = \left(\frac{V}{N}\right)^2 (N)(N-1) \times \frac{\int d\vec{r}_3 \int d\vec{r}_4 \ldots \int d\vec{r}_N e^{\sum_{i<j} -\beta U(\vec{r}_i,\vec{r}_j)}}{\int d\vec{r}_1 \int d\vec{r}_2 \ldots \int d\vec{r}_N e^{\sum_{i<j} -\beta U(\vec{r}_i,\vec{r}_j)}} \; . \tag{3.12}$$

Since the potential energy only depends on the relative distances between particles ($\vec{r}_{12}$), one commonly writes the RDF as:

$$g(r) = g^{(2)}(r_{12}) = g^{(2)}(\vec{r}_1,\vec{r}_2) \; . \tag{3.13}$$

With the definition of Eq. 3.12, $g(r)$ is related to the probability for finding a particle at a distance r from a reference particle. Integration of $\frac{N}{V} g(r) 4\pi r dr$ over the whole simulation volume provides the total number of particles minus one:

$$\int \frac{N}{V} g(r) 4\pi r dr = N - 1 \; . \tag{3.14}$$

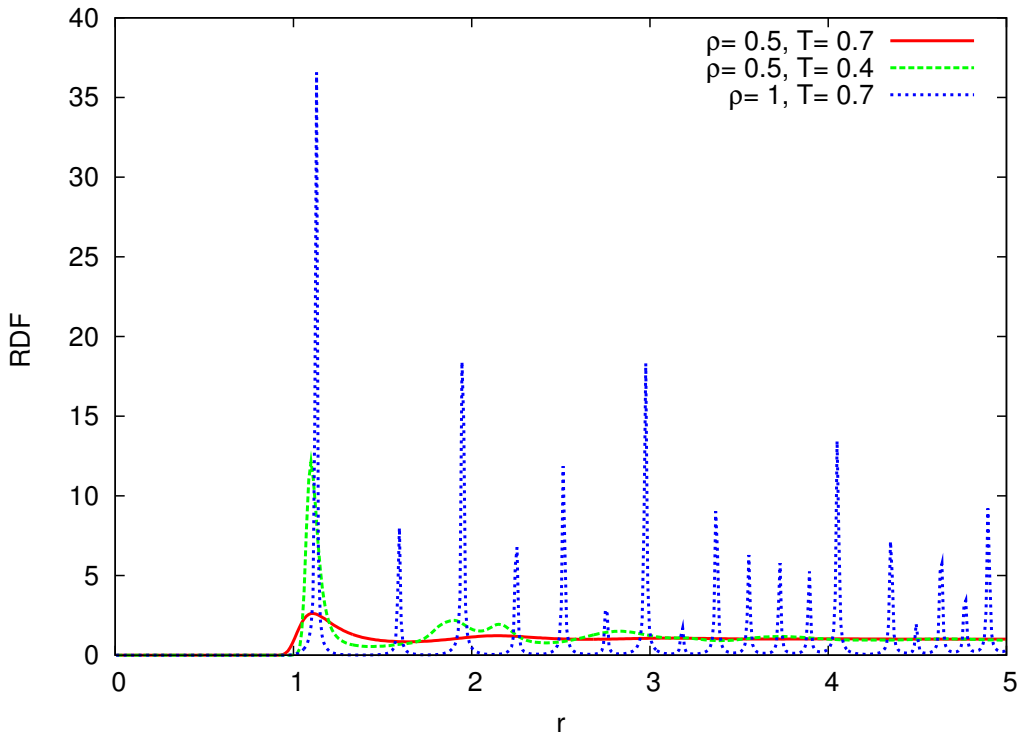

Figure 3.3 RDF in a standard MD simulation of a gaseous, liquid and solid phase. The red line represents a simulation of a gas ($\rho = 0.5, T = 0.7$), with no correlation between particles at large distances, and thus only one peak in the RDF. The blue curve represents the simulation of a solid system ($\rho = 1, T = 0.7$), where particles have fixed positions, which results in clear peaks of the RDF. The green curve is the RDF of liquid system ($\rho = 0.5, T = 0.4$), with intermediate correlations, and an RDF that has several fluctuations.

The method used in MD to calculate the RDF is by using a histogram to count pairs of particles. The maximal distance between particles, which equals half the box size, is divided into P parts $\Delta r = \frac{boxsize}{2\times P}$. At any instance of time the number of pairs (n) with $r < r_{12} < r + \Delta r$ is stored in the histogram. The resulting histogram $n(r)$ doesn't have the correct normalisation since

$$\sum_{r=0}^{\text{box size}/2} n(r) = \frac{N(N-1)}{2} \ , \tag{3.15}$$

the number of pairs in the system and not $N - 1$, as in 3.14. Using 3.15 and 3.14, we compute the RDF with the histogram as,

$$g(r) = \frac{V}{N^2}\frac{2n(r)}{4\pi r} \ . \tag{3.16}$$

As illustrated in Fig. 3.3, in an MD simulation, the RDF can be used to discriminate between the solid, liquid and gaseous phase of the system. In the solid phase there are only a number of fixed positions on the grid, forcing the particles to fluctuate about their equilibrium positions and resulting in a clear peak of the RDF at this distance, with the height of the peak an indication of the number of neighbours at this position. This behaviour is completely opposite to what happens in the gaseous phase, where there is no discernible spacial correlation for lengths $> 1.5\sigma$. In the liquid phase, there is competition between the order created in the solid phase and the freedom present in the gaseous phase. This results in a RDF that has a couple of discernible peaks but also a smooth tail where there is no more information.

A good method of investigating the temporal correlations in the system is by calculating the VACF,

$$\text{VACF}(t_1, t_2) = \frac{1}{N v_0^2}\sum_{i=1}^{N} \langle \vec{v}_i(t_1) \cdot \vec{v}_i(t_2) \rangle \ . \tag{3.17}$$

with $v_0^2 = \frac{1}{N}\sum_{i=1}^{N} \langle \vec{v}_i(t_1) \cdot \vec{v}_i(t_1) \rangle$.

This autocorrelation function tracks the persistence of motion for the moving particles. The VACF behaves differently for the three phases (gas, liquid and solid) and is heavily influenced by the density and the temperature of the system. In Fig. 3.4 the influence of the density on the VACF is clearly visible. The larger the density the more frequent the collisions and the harder it becomes for a particle to preserve its direction of motion and size of its velocity. This results in a VACF that falls off relatively quickly and can even make a particle travel in the opposite direction (= the VACF becomes negative). For small densities the particles retain their velocity for larger time periods, resulting in a VACF that falls at slow pace.

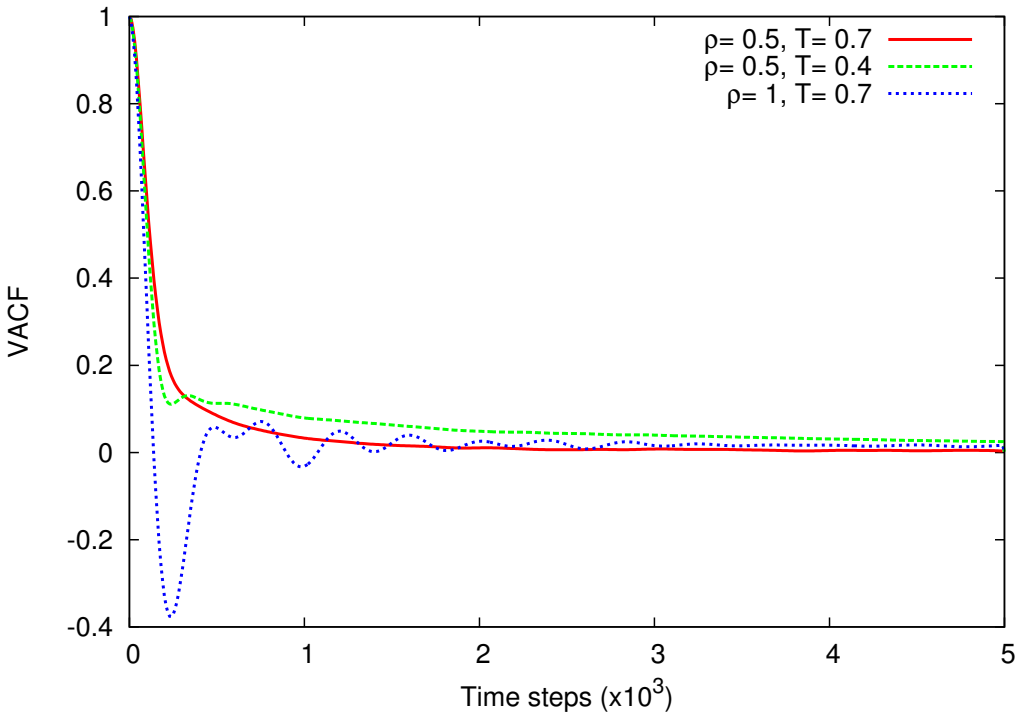

Figure 3.4 VACF in an MD simulation of a gaseous (red solid curve), liquid (green dotted curve) and solid (blue dotted curve) phase.

3.1.3 Diffusion in MD

Since we are interested in the self-diffusion properties of the simulation, we will explain how this underlying property of the simulation can be revealed. There are several ways of looking at the self-diffusion properties of the system. One way is via the mean squared displacement and the subsequent diffusion parameter (D). This is a global and very general method that focuses on the time-averaged behaviour of the system. Another method is by looking at the instantaneous self-diffusion in the system, where the relevant information is gathered for one or a few time steps.

Mean squared displacement

Diffusion in a system can be characterised by the mean squared displacement (MSD). This function tracks how far, on average, a particle has moved from its original starting point. Plotting this distribution as a function of time can determine whether the system has a normal or anomalous (sub- or super-)diffusion regime:

$$\left\langle \Delta r^2(t) \right\rangle \sim t^\gamma \ , \ 0 < \gamma < 2 \ , \tag{3.18}$$

with $\gamma < 1$ the subdiffusion regime, $\gamma > 1$ superdiffusion and $\gamma = 1$, normal diffusion.

An example of the MSD is shown in Fig. 3.5, where we can distinguish two different regimes:

1. A first period where $\langle \Delta r^2(t) \rangle \sim t^2$, $t < 500$, indicating that the particles move freely. This free movement is only an artefact, because the data taking only starts at the beginning of the production phase. The steps of a fraction of the particles, that are not in a collision at the start of the production phase, dominate the MSD for time steps < 200. After this initial period all particles have at least collided with one other particle and are thus not moving freely. This clearly illustrates that the MSD method for observing self-diffusion must be used as a global tool for long time periods, otherwise the artificial (short term) effect of the unhindered movement dominates the initial analysis.

2. A second period in where $\langle \Delta r^2(t) \rangle \sim t^1$. This observation implies that during a normal equilibrium MD simulation the self-diffusion properties are determined by Brownian motion. This normal diffusion is the expected behaviour for liquids (= gas + liquid phase). In the solid phase there is no self-diffusion since the particles are anchored at a certain grid position and $\gamma = 0$.

The MD method allows to determine the diffusion coëfficiënt by calculating the slope of $MSD(t) = \langle \Delta r^2(t) \rangle = 6Dt$, which was first calculated by Einstein [Ein05].

Single time step displacement distribution

As explained, the global self-diffusion behaviour can be determined by studying the time dependence of the MSD. The study of the instantaneous self-diffusion properties requires an alternative technique. Consequently, we will have to search another way of looking at this sort of self-diffusion. The single time step displacement distribution, P(Δx), offers an elegant solution. This distribution gathers the information of the size of the steps of the particles during the last time step. By comparing this distribution to a normal distribution we are able to differentiate between normal and anomalous instantaneous self-diffusion.

In Fig. 3.6 this distribution is shown for the momentary displacements along the three axes during one time step. One can clearly see the Gaussian shape of the normal distribution, and we are able to accurately fit a Gaussian curve to this distribution.

Since the size of the average steps during a simulation is determined by the density and temperature of the system, the absolute displacements differ for different simulations. An elementary method to eliminate the simulation settings from the single time

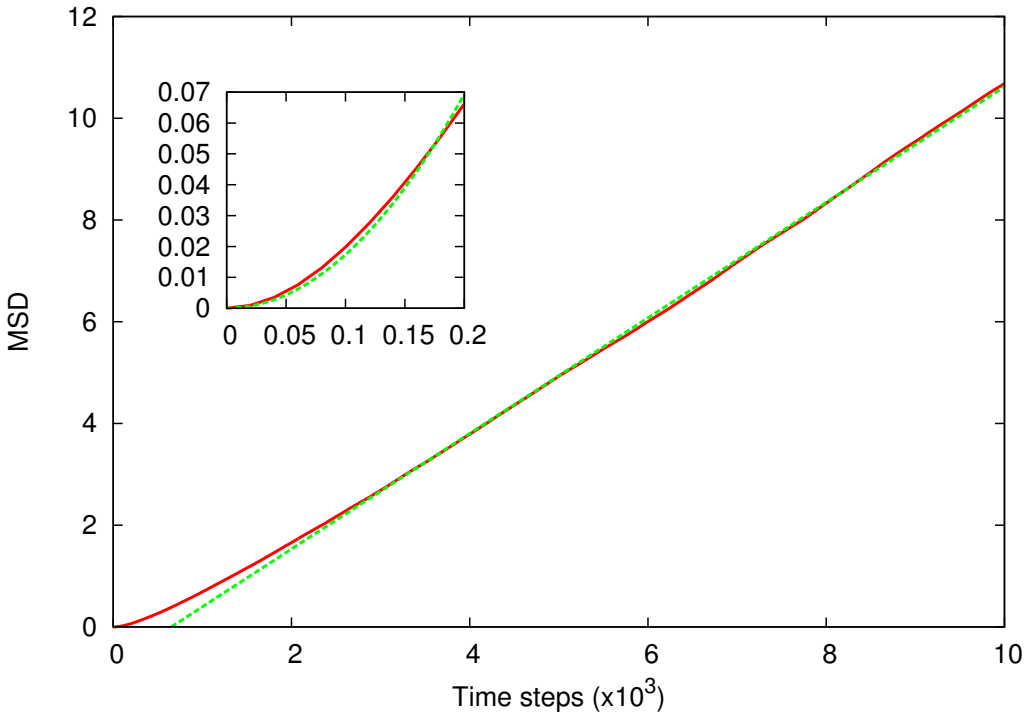

Figure 3.5 MSD $\langle r^2(t)\rangle$ in a reference MD simulation. Fit with $f(x) = ax + b$, $a = 1.136 \pm 0.002$, $b = -0.741 \pm 0.008$ for the normal diffusion after long times (time steps > 3000). Inset: short time quadratic fit, $g(x) = cx^2$, with $c = 1.73 \pm 0.03$ upto time step 200.

step displacement distribution is done by calculating the standard deviation (σ) of every P(Δx) and use this to normalize the distribution. In this way, distributions P($\Delta x/\sigma$) can be compared against each other and against a normal distribution. The above normalization of the P(Δx) of Fig. 3.6 is shown in Fig. 3.7. Remark that steps $\Delta x > 3\sigma$ are very rarely seen.

Normal diffusion

We can conclude from the methods at our disposal that during a standard molecular dynamics simulation of Argon molecules, the self-diffusion properties are those of a normal, Gaussian self-diffusion process. To find distributions that behave like those in 2.4.2, and thus display anomalous self-diffusion, we will need to modify the reference MD simulation methods. A first obstacle in generating conditions of anomalous diffusion are the Lennard-Jones-like potentials.

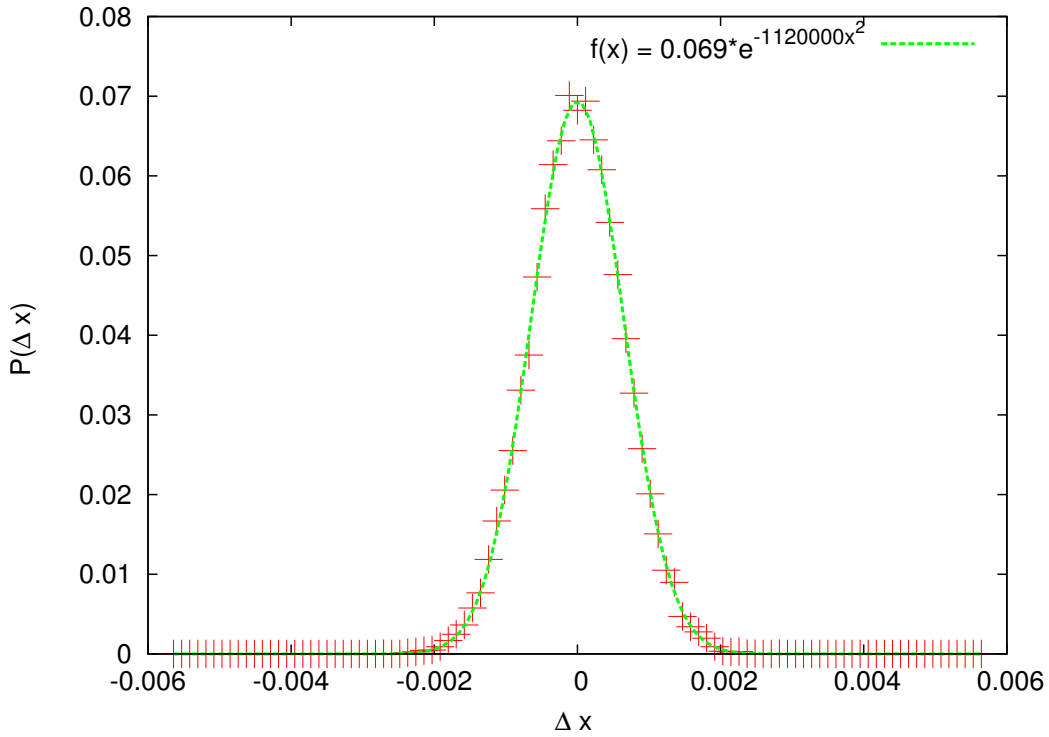

Figure 3.6 Single time step distribution $P(\Delta x)$ of a reference MD simulation step, red points, fitted with a Gaussian distribution $f(x) = a \times \exp(-bx^2)$, with $a = 0.069 \pm 0.001$ and $b = 120 \pm 1 \times 10^4$ (green dotted curve).

3.1.4 Limitations of Lennard-Jones-like potentials

Lennard-Jones potential

The LJ potential of Eq. 3.7 reveals three major characteristics:

- It is of short range. As soon as $r > 5$, the potential vanishes, meaning we only have to take in to consideration the particles that are close to each other. In an MD simulation one usually only computes the forces for particles close to each other by keeping track of which particles are within range, and storing this into a pair list which is only updated after a certain number of steps.

- An attractive part for $r \geq 1$. This part of the potential tries to hold two particles together and is commonly explained as a Van der Waals interaction. The balance between this attractive force and the average kinetic energy of a molecule decides whether the system is in the gaseous, liquid or solid phase.

- A hard core part: the potential approaches infinity as $r \to 0$. This entails that a particle travelling in the direction of another particle encounters a repulsive

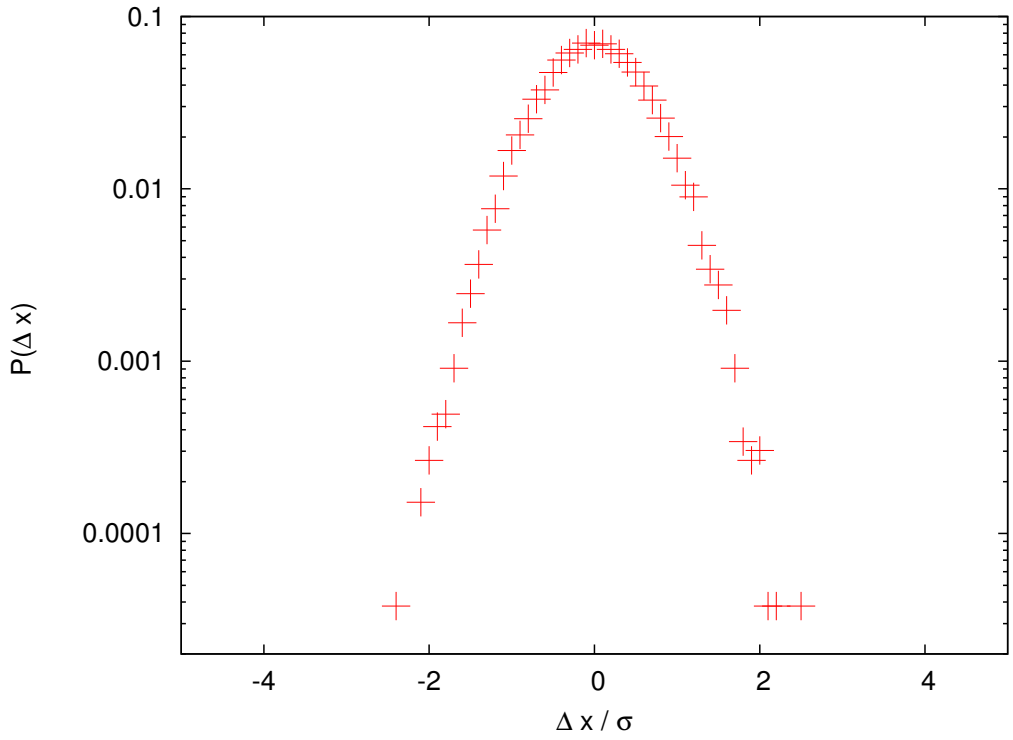

Figure 3.7 Normalized single time step distribution $P(\Delta x/\sigma)$ on a semi-log-scale in a reference MD simulation.

force from $r < 1$, and this force becomes larger the closer the particle gets. This implies that an approaching particle will need an infinitely large kinetic energy to overcome this potential barrier.

This hard core becomes a big obstacle when attempting to generate anomalous self-diffusion. This results from the fact that the integration algorithm is not 100% accurate. The combination of a finite time step and a very steep potential ($U_{LJ}(r)$ for $r < 1$) results in an unstable handling of very fast-moving particles. Collisions involving these fast-moving particles can result in even faster moving particles: a particle with $r_{ij} \approx 1$ that moves towards the other particle with a large velocity, will be able to penetrate the other particle more than would be theoretically possible. At $r_{ij} \approx 1$, there is almost no force acting on the particle, and it will therefore travel a distance $|\Delta\vec{r}(t)| = (\Delta t) \times |\vec{v}_i(t)|$. To remedy this, one would have to update Δt to a smaller value. This would eventually result in a simulation where only one particle moves (the fastest), and the other particles seem to be frozen, due to a very small Δt.

If this rescaling of Δt does not take place, some particles can attain an unphysical amount of potential energy, resulting in an unstable system, where other particles

too are given additional potential energy. In the end, the added kinetic energy results in a temperature gain, which can't be stopped and the simulation becomes uncontrollable. Naturally, this is an unwanted effect and in the next section we will look at a possible method of overcoming this vicious cycle.

3.2 Other potentials in Molecular Dynamics

We are looking for a soft core potential which reproduces most of the dynamics properties obtained with a LJ potential. Under study here are two different candidates, a sinusoïdal potential and a renormalized LJ potential. There are more soft core potentials available, but we will restrict ourselves to these two that both have distinct advantages: the sinusoïdal potential has a mathematically simple description and the continuous potential resembles most the LJ potential shape.

3.2.1 A sinusoïdal potential

The potential that we consider is of the type:

$$U_{sin}(r) = \sin(br) * \exp(-cr) \ , \tag{3.19}$$

with b and c parameters for the distance between peaks and the severity of the damping respectively.

This potential has some of the features of the LJ potential and it can be tuned so as to match the medium-range attractive force of the LJ potential. In Fig. 3.8 one can clearly see the attractive part for $r \approx 1$. It also has the desired long-range cut-off, thanks to the damping factor $\exp(-cr)$. Most importantly, it possesses a finite potential energy at the center $U_{sin}(0) = 0$. However, this also creates a problem, because combining this value with a peak before $r = 1$, creates another attractive part of the potential that is not present in the LJ potential.

Now, we discuss the properties of a simulation system of particles that interact via $U_{sin}(r)$. The thermodynamic and diffusion properties of this simulation are relatively similar to those of a standard Lennard-Jones MD simulation. The correlation functions are representative for the dynamics developed by the system. The RDF is displayed in Fig. 3.9. The short-range attractive part of $U_{sin}(r)$ makes the particles cluster in a very small range. This cluster resembles a gaseous phase, because there are no more peaks in the RDF.

One can use the VACF of Fig.3.9 to discern the phase of the system. We can observe a steady decline in the VACF, implying a gaseous or liquid phase of the system. This

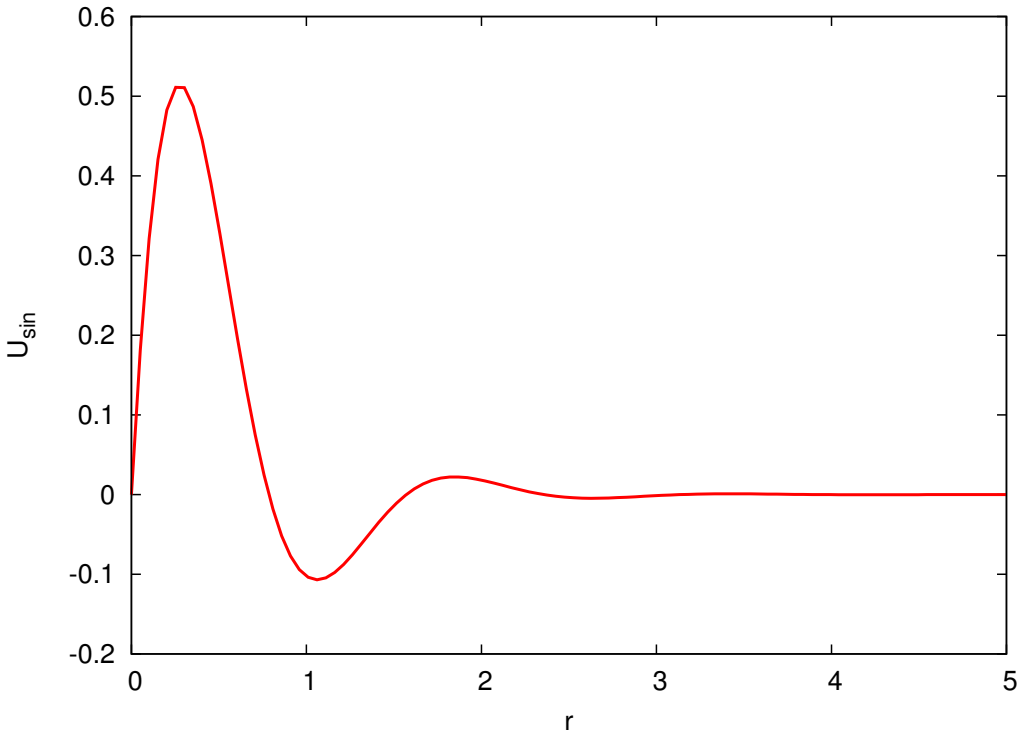

Figure 3.8 Sinusoïdal potential, with $b = 4$ and $c = 2$

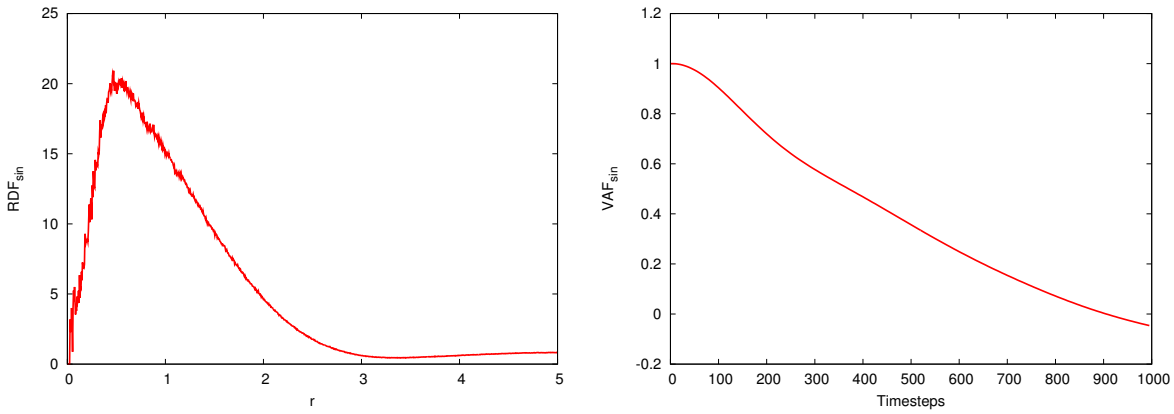

Figure 3.9 RDF of a simulation system with a sinusoïdal potential, $U_{sin}(r)$ (left). VACF of a simulation system with a sinusoïdal potential (right).

behaviour suggests the system is converted to a large gaseous cluster, where the whole dynamics of the system are determined by the location and size of the first peak. This is completely opposite to the behaviour of a simulation with an LJ potential, where the dynamics are determined by the location and size of the first pit.

In Fig. 3.10, the self-diffusion properties are shown for a simulation with a sinusoïdal

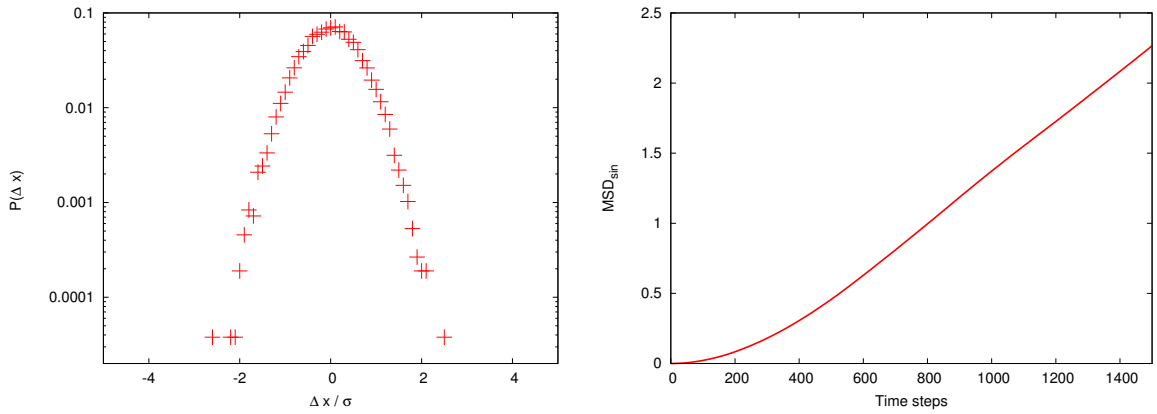

Figure 3.10 Normalized single time step displacement distribution $P(\Delta x/\sigma)$ of a simulation system with a sinusoïdal potential, (left). MSD of a simulation system with a sinusoïdal potential (right).

potential. Both the single time step displacement distribution and the MSD show the normal, Gaussian properties of the self-diffusion of this system.

In conclusion, we have found a potential with the possibility of generating anomalous diffusion via its soft core, but since the overall properties deviate much from the normal MD simulation we will not use this potential in our further studies.

3.2.2 The renormalised LJ potential

A renormalised version of the LJ potential has been proposed in Ref. [Fra07]. This potential has the long and medium range behaviour of the LJ potential and is finite at $r = 0$:

$$U_{SC}(r) = \frac{H}{1 + \exp \Delta \left(r - R_R\right)} - U_A \exp\left[-\frac{\left(r - R_A\right)^2}{2\delta_A^2}\right] . \tag{3.20}$$

A closer look at this potential reveals the role of the different parameters:

- $\frac{H}{1+\exp(\Delta(r-R_R))}$: This is the soft core of the potential. The value of H determines the necessary kinetic energy for a particle to be able to penetrate into the core of another particle. If $H \to \infty$ the core of the potential behaves as a LJ-like potential and it becomes impenetrable.

  The range of the soft core is determined by R_R. Δ modifies the slope of the soft core, the larger Δ the steeper the descent of the slope and the larger the instantaneous force. This parameter will have to rise for a rising H, because a larger soft core implicates a steeper descent to the fixed minimum.

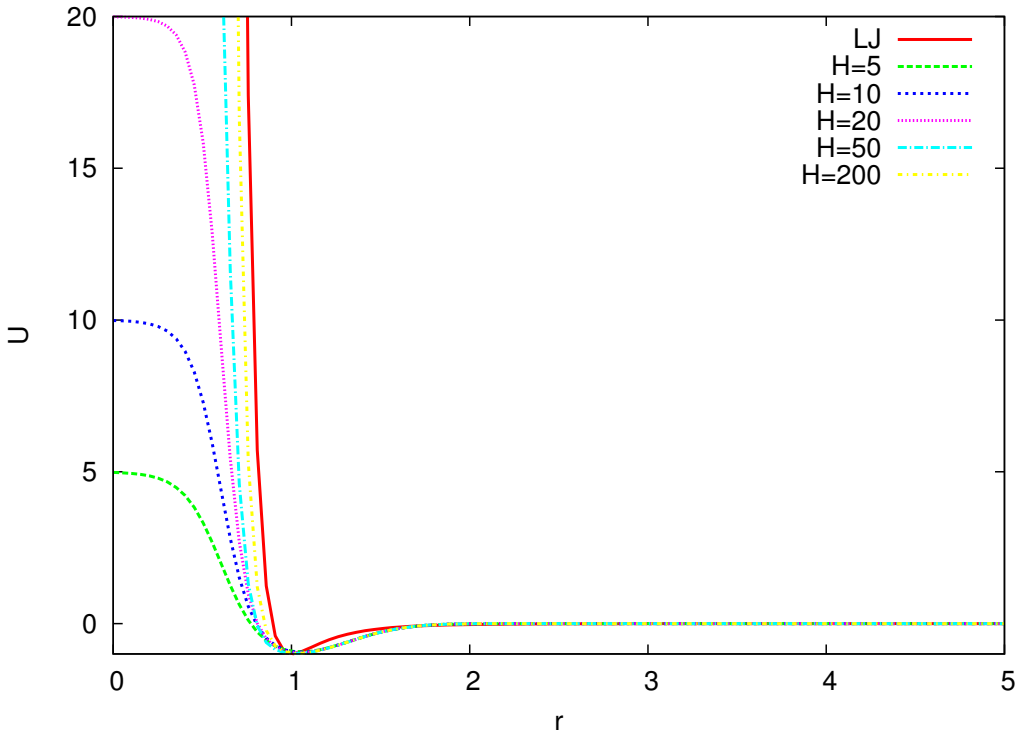

Figure 3.11 Comparison of renormalised potentials with different parameter H and a LJ potential

- $U_A \exp\left[-\frac{(r-R_A)^2}{2\delta_A^2}\right]$ is a Gaussian attractive part that is centred around R_A. The minimum of the potential is however not entirely determined by this parameter, because a slow descent of the soft core can dominate the shape of the Gaussian cavity.

  The width of the Gaussian pit is determined by δ and can be fitted to the LJ slope of the attractive part.

  The parameter U_A is the depth of the potential pit and in order to be able to compare our results to a normal simulation, we will take $U_A \equiv 1$.

Since H determines the height of the potential barrier, this parameter is considered essential for the simulation behaviour and below we will investigate the influence of this parameter. The parameters $\Delta, R_R, R_A, U_A, \delta_A$ were optimized so as to match the medium- and long-range part of $U_{LJ}(r)$ and are listed in table 3.1.

This potential gives us the opportunity to look at different methods of generating anomalous diffusion in a MD simulation without having to worry about the hard core of the LJ that makes the simulation to go out of control.

Table 3.1 Fitted parameters for the soft-core potential for five different values of H.

H (in units U_A)	5	10	20	50	200
Δ (in units R_A^{-1})	36.7	31.9	39.4	26.0	28.3
U_A (in units U_A)	1	1	1	1	1
$2\delta_A^2$ (in units R_A^2)	0.089	0.090	0.062	0.096	0.089
R_A (in units R_A)	1	1	1	1	1
R_R (in units R_A)	0.85	0.82	0.79	0.73	0.70

3.3 MD simulation with softcore potential

First, we wish to discriminate between the dynamical properties of the mono-atomic liquid for $U_{LJ}(r)$ and $U_{SC}(r)$. To this end, the potential $U_{SC}(r)$ of (3.20) is used in an MD simulation program. We investigate the thermodynamic and self-diffusion properties, the velocity auto-correlation function (VACF) and the radial distribution function (RDF).

3.3.1 Thermodynamic properties of softcore simulations

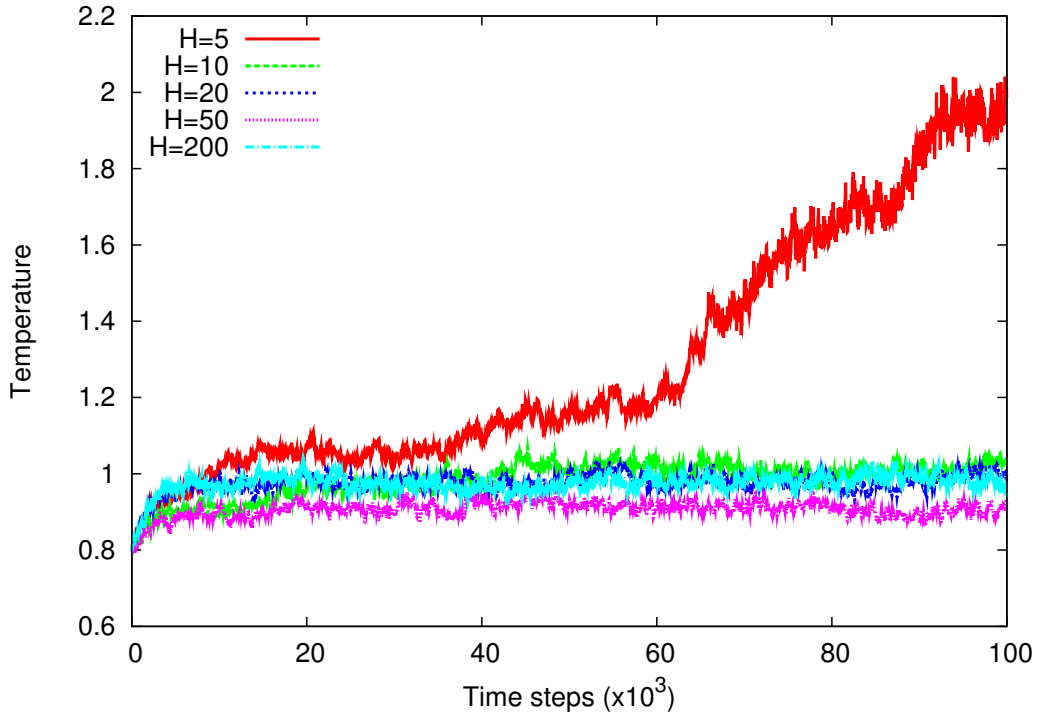

Figure 3.12 Temperature in the production phase for reference MD simulations with different softness parameters H.

In Fig. 3.12 the temperature of the system is shown for simulations with different

heights of the softcore potential, H. As one can see clearly there is a qualitative difference between $H = 5$ and the other simulation results. All the softcore systems tend to have a higher effective temperature than the initial temperature of the initialisation phase. This slightly higher temperature could be a result from the shape of the potential and the soft shoulder of the potential. There is however one big exception, with temperatures that are a factor 5 higher than the initialised temperature, for $H = 5$. This system doesn't reach equilibrium, even in simulations with a large amount of particles over long time periods. In this case, the ratio of the potential barrier to the potential well is 5. Thus, particles with a larger than average kinetic energy will have enough momentum to penetrate another particle, even under normal simulation conditions! This characteristic results in the same unstable system as a LJ potential with fast-moving particles.

The simulations with $H \neq 5$ have the same drift in temperature at the beginning of the simulation (in the production phase!), but the temperature rise stops at a new equilibrium value, without going completely out of control. Another important thermodynamic property is the conservation of energy, which is ensured for every parameter H.

3.3.2 RDF in a softcore simulation

Since the shape of the potential well of the softcore potential and a LJ potential are different, one can expect to see this difference reflected in the RDF. In Fig. 3.13 the RDFs for different softcore parameters H are shown. We can see that all RDFs have the same robust features as a liquid RDF of Fig. 3.3. For example, the RDF knows about the length scale of the molecules which is reflected in the bump of $g(r)$ for $r \approx 1$. The height of the first peak depends on the softcore parameter H, which is easily explained, since the wells of the softer potentials are broader than those with a higher H-value. For $H \leq 20$, we notice that the RDF doesn't vanish for $r \to 0$. This indicates that the softcore can be penetrated even under those conditions. For $H \geq 20$ there are no qualitative differences with the RDF of a LJ simulation.

The case of $H = 5$ is not shown in Fig. 3.13 because for this small value of H the RDF is almost completely dominated by a peak at $r < 1$. This behaviour results again from the low peak-to-well ratio of this potential, which results in a significant number of particles that are almost situated on top of each other.

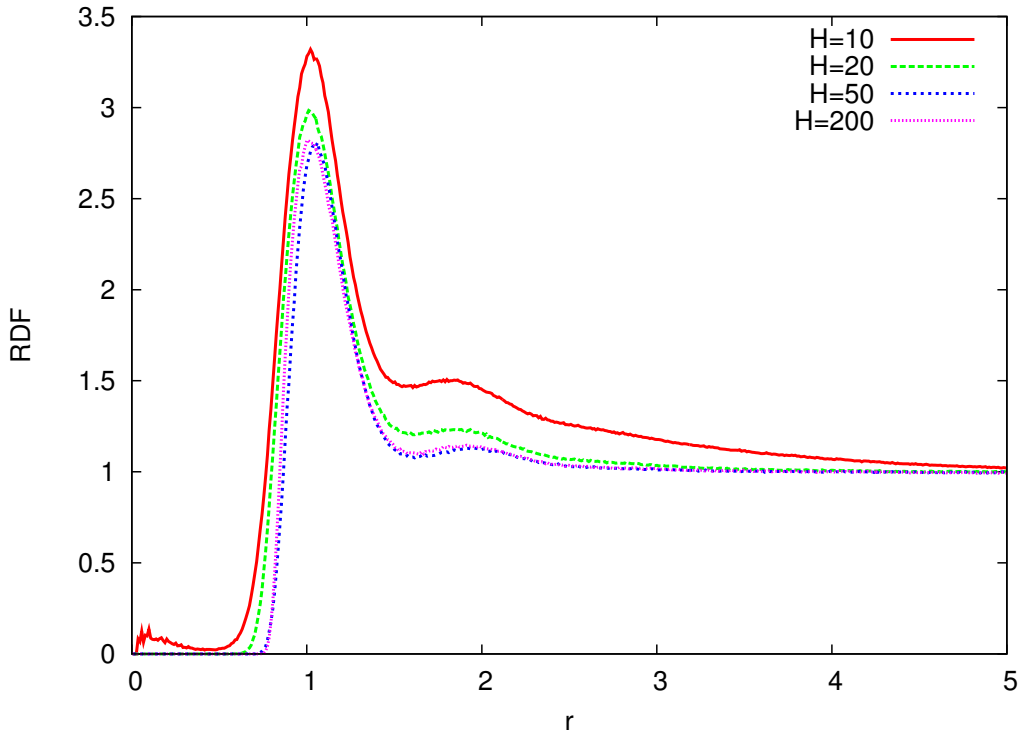

Figure 3.13 RDF of a reference MD simulation and a soft core potential with different softness parameters

3.3.3 VACF in a softcore simulation

The VACF of a simulation is influenced is influenced by the shape of the potential, and will therefore also notice the effect of a changing soft core parameter H. In Fig. 3.14 one sees that the VACF for $H = 20$ and $H = 200$ differ only marginally and are very similar to the VACF of simulation with an LJ potential (see Fig. 3.4). This difference stems probably from the different steepness of the slope of the core. Indeed, the *hardness* of the collisions is determined by the derivative of the potential.

The only inconsistency comes from $H = 5$, where the VACF deviates more from the other VACFs. During the first 1000 time steps, the VACF fluctuates wildly, whereafter it decays very slowly. This indicates that the time correlations in this simulation will be much larger and could influence the self-diffusion properties of the system. This will be confirmed in the next sections.

3.3.4 Mean squared displacement in a softcore simulation

In this section, we investigate the influence of the softcore potential on the mean squared displacement of the particles in the simulation. In Fig. 3.15 the MSD for dif-

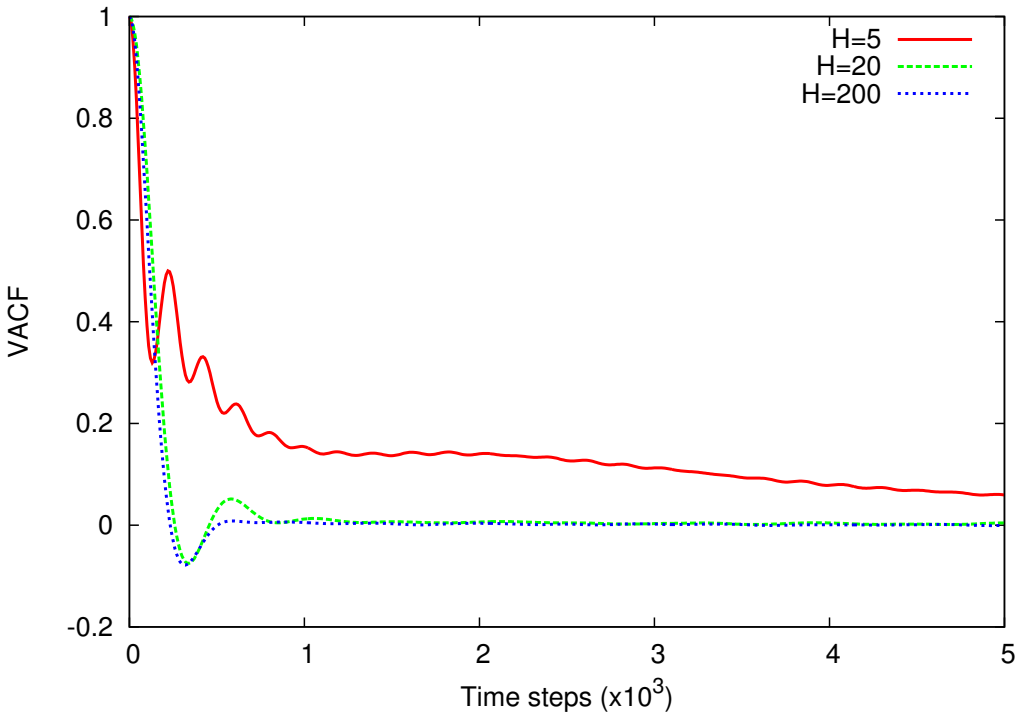

Figure 3.14 VACF of an MD simulation with different softness parameters.

ferent values of H is shown. One striking characteristic is the behaviour of the MSD for $H = 5$. Since the temperature of this simulation is never in equilibrium (Fig. 3.12), the average displacement versus time is characterized by a stronger than linear dependence. This translates in a MSD that never gets to the second stage, $\langle \Delta r^2(t) \rangle \sim t^1$, of the normal diffusion regime. The fact that this simulation is never in equilibrium is further illustrated in Fig. 3.16, where the diffusion parameter D is calculated during simulations with different softcore parameter H. For the high values of H, the diffusion parameter reaches an equilibrium value before $t = 10000$, whereas for $H = 5$ this equilibrium is still far away at $t = 100000$. Fig. 3.16 illustrates that even for high values of H, the simulation system doesn't instantaneously reach its new equilibrium temperature, and the diffusion parameter D will only be stable after equilibrium has been reached.

For large values of H, the simulation system reaches a normal diffusion regime but there remains an influence of the softcore parameter on the MSD. For softer values of H, it is easier to penetrate another particle and it is harder to deflect another particle of its present trajectory. This properties result in a larger MSD (and diffusion parameter) for smaller values of H. From Fig. 3.16 it emerges that there is some critical value for the softness parameter H below which the self-diffusion is no longer normal.

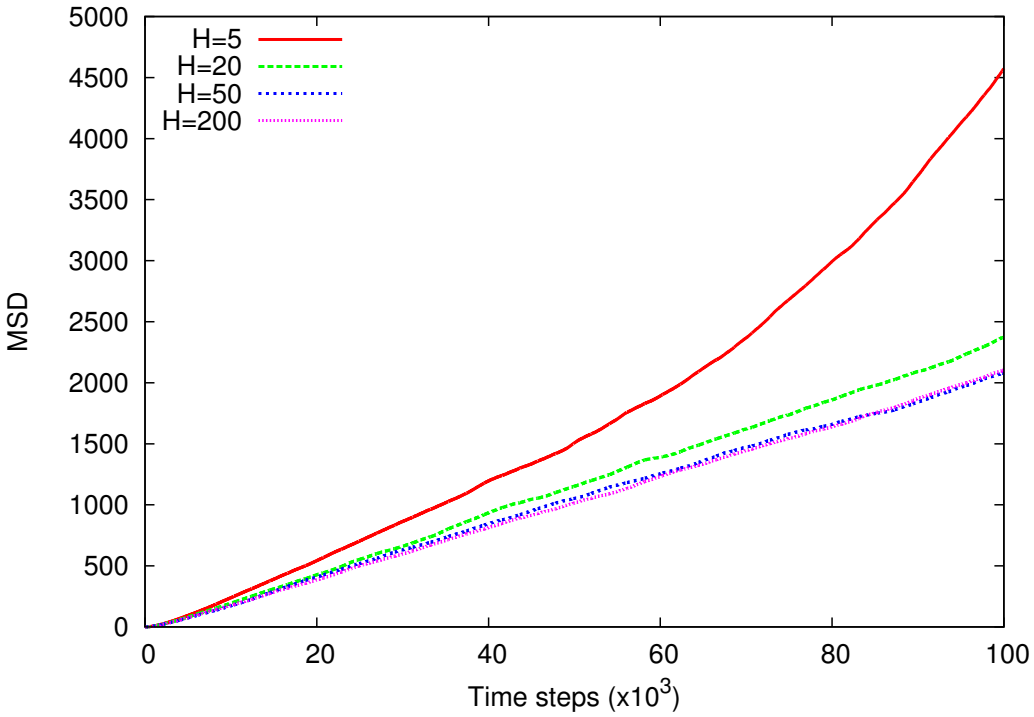

Figure 3.15 Mean squared displacement for different softness parameters

3.3.5 Single time step displacement in a softcore simulation

Since the MSD of the softcore simulations show that the normal diffusion regime is attained for large values of H, we expect to see Gaussian single time step distributions for this simulations too. In Fig. 3.17 the P($\Delta x/\sigma$) for different parameters H are shown. By comparing these distributions to the normalized LJ distribution (which was perfectly Gaussian), we can conclude that these step distributions are also normally distributed. These contradicting results (anomalous self-diffusion and normal single time step displacement distributions) can be explained by the time correlations. The displacements at every time step are normally distributed, but due to correlation in the steps, Fig. 3.14, the MSD is not normal.

Since we use the normalized distributions, the size of the standard deviation is hidden in this plot. We find that the smaller the soft core parameter H, the higher the standard deviation of $P(\Delta x)$, which results in a higher diffusion parameter D.

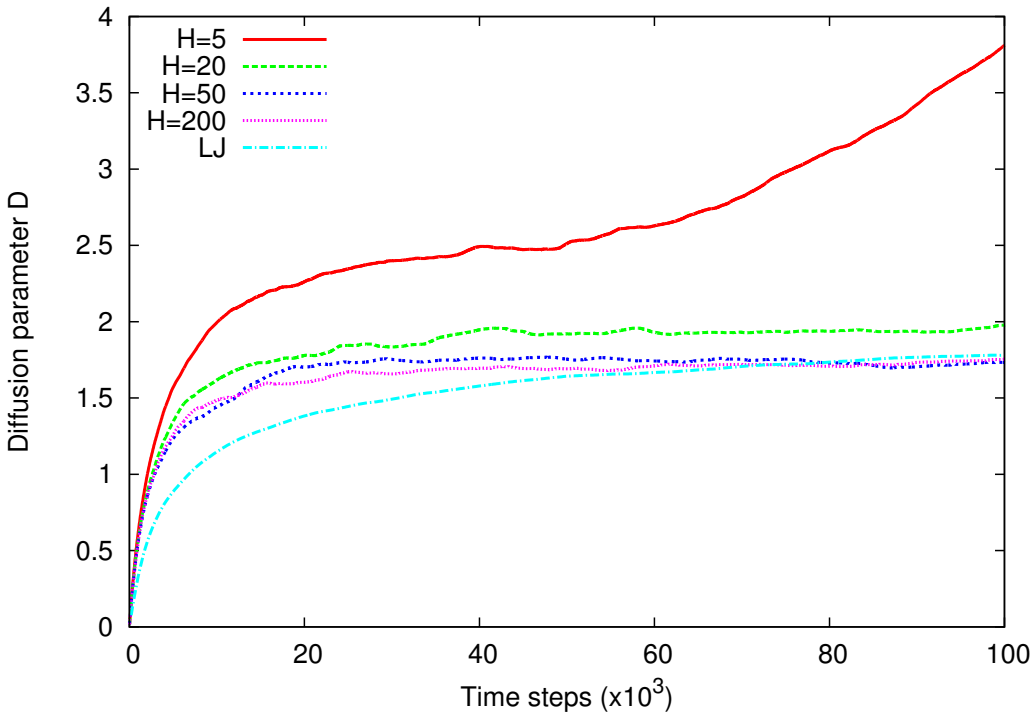

Figure 3.16 Diffusion strength in an MD simulation for different softness parameters.

3.3.6 Conclusions

To summarize, we have tested two different potentials with a soft central part that could replace the Lennard-Jones potential in a Molecular Dynamics simulation. The first (sinusoïdal) potential was discarded because it altered the simulation output to much, especially the RDF showed that there was clustering of particles at small distances. The renormalised LJ potential reproduces the original results in a qualitative way for certain values of parameters. However, the low values of the softcore parameter H result in strange and abnormal properties in the RDF, VACF, temperature and diffusion of the system. This uncontrollable behaviour is unwanted in our simulations since our search for anomalous diffusion centres around the internal (non-equilibrium) dynamics of the MD simulation and with $H = 5$ and $H = 10$ there is already anomalous self-diffusion, Fig. 3.15. Excluding these potentials means that possible anomalous self-diffusion will come from the dynamics of the system and not from a characteristic of the underlying potential.

From now on we will use as a soft core potential, the renormalised LJ potential with soft core parameter $H = 20$. This potential has a high enough ratio of the maximum to the minimum to resemble a LJ potential, but the most important aspect, however,

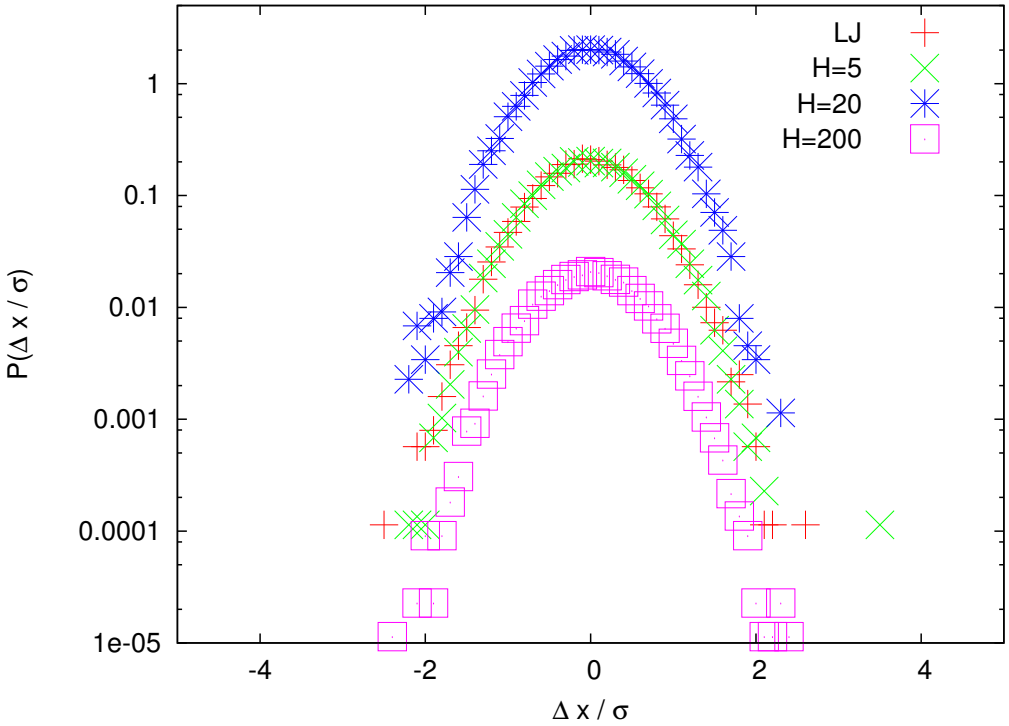

Figure 3.17 The normalized single time step distribution P($\Delta x/\sigma$) for different values of H (with $H = 20$ and $H = 200$ respectively scaled up and down by a factor 10) and for a LJ potential.

is the ubiquitous presence of the Gaussian statistics in the self-diffusion properties in simulations with this potential.

Chapter 4

Out-of-equilibrium MD

In the previous chapter we have observed that during a reference molecular dynamics simulation, with a force that has a balanced amount of short-range repulsion and medium-range attraction, normal self-diffusion is an ubiquitous feature. However, in order to link our simulation system to a financial market, we need heavy-tailed, non-Gaussian single time step distributions that are only present when the simulation system has anomalous self-diffusion regimes. These regimes are hard to find in an equilibrium MD simulation. One needs to find ways to evade the central limit theorem, which can be done using a special background, with for example traps [BG90, WGR+04, HBA02] or percolating clusters [GAA83, KNM95] or via long-range interactions [Juh08, SS06, MK99].

We turn to a method which doesn't use this background, but which centers around the concept of out-of-equilibrium simulations. The concept of out-of-equilibrium is inherent the financial system, since there is no conservation of wealth [Lux05, Fol94, Ili01] and there is a steady amount of information influx. A normal way of generating out-of-equilibrium conditions is by changing the system from a closed to an open system, but we will present a method in a closed system that doesn't alter the basics of a MD method, but still has out-of-equilibrium periods [SRC10].

4.1 Radial rescaling

We introduce non-equilibrium conditions by driving the system and modifying the inter-particle interaction. This can be achieved by rescaling the radial distances in the soft-core interaction $U_{SC}(r) \rightarrow U_{SC}(\lambda(t)r)$ with $\lambda(t) \leq 1$. This is equivalent to an effective increase in the size of the molecules. During the simulation, we adopt a stepwise change in $\lambda(t)$ at regular intervals (the length of the intervals gets determined by the variable

τ). We use the protocol

$$\lambda(t) = [\lambda(t=0)]^{\lfloor \frac{t}{\tau} \rfloor}, \tag{4.1}$$

where $\lfloor \frac{t}{\tau} \rfloor$ rounds $\frac{t}{\tau}$ towards positive integer values ($\leq \frac{t}{\tau}$). The values for τ and $\lambda(t = 0)$ are fixed at the start of the simulation. The two parameters τ and $\lambda(t = 0)$ can also be made to vary during the simulation (e.g. by drawing them from a Gaussian distribution). We have verified that this does not lead to sizeably different results and makes the subsequent analysis more convoluted. For the results shown here, we have adopted fixed values for τ and $\lambda(t = 0)$.

4.1.1 Energy evolution after a radial rescaling

We now turn to simulations in out-of-equilibrium conditions. Under equilibrium conditions, the energy is conserved and the temperature fluctuates mildly around a certain value. The forced rescaling allows the dynamics of the system to be changed dramatically, because particles that were attracting each other end up repelling each other due to the driven change in the inter-particle interaction range. As the imposed changes in the inter-particle interactions occur under conditions of constant density, the system develops regions of high energy density.

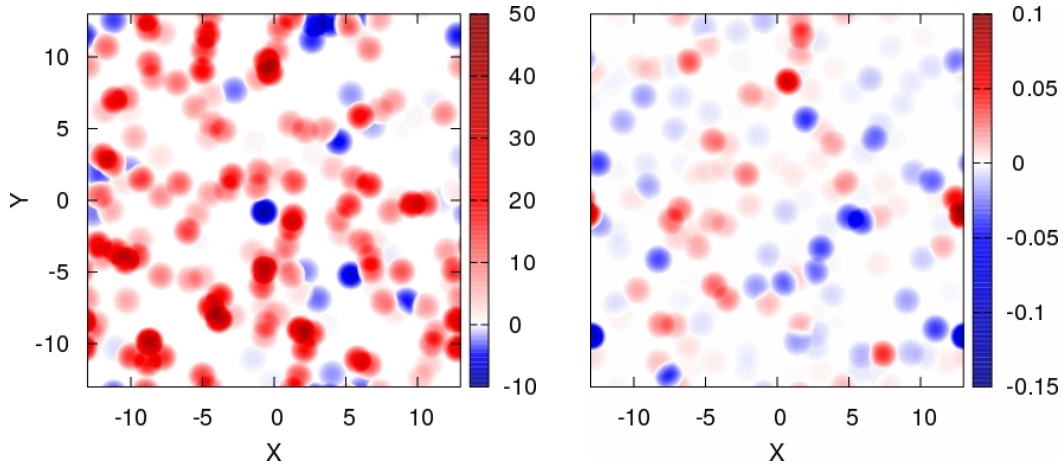

Figure 4.1 A typical spatial distribution of the potential energy changes $\Delta E_{pot}(\mathbf{r}_i)$ in one time step. We show the projection onto the xy-plane for $|z_i| \leq 0.5$ under conditions of (a) a soft-core potential just after rescaling with $\lambda(t = 0) = 0.7$, (b) a soft-core potential during equilibrium.

To illustrate the effect of the radial rescaling on the internal dynamics of the system, the potential energy fluctuation of the system during one simulation step is shown in fig. 4.1. We consider results for $U_{SC}(r)$ under typical equilibrium conditions and a situation just after a radial rescaling. For every particle the difference in potential energy

with respect to the previous configuration is shown

$$\Delta E_{pot}(\mathbf{r}_i) = \sum_{j \neq i} U\left(\mathbf{r}_{ij}\left(t + \Delta t\right)\right) - U\left(\mathbf{r}_{ij}\left(t\right)\right) \ . \tag{4.2}$$

The panels of fig. 4.1 represent a projection of a slice ($\forall i : |z_i| \leq 0.5$) onto the xy-plane. Fig. 4.1 indicates that through a sudden rescaling of the radial distances one creates regions in which the total amount of potential energy gain is much larger than the average value. Fig. 4.2 shows that the hard core of $U_{LJ}(r)$ results in values of ΔE_{pot} as high as 800, whereas this is not seen in fig. 4.1. With energy fluctuations of this size, the velocities of the particles attain values that are not compatible with a finite time step, thus eliminating the use of $U_{LJ}(r)$ in out-of-equilibrium regimes. A similar type of projection for typical equilibrium conditions is observed in both fig.s 4.1-4.2. The scale of ΔE_{pot} is clearly much smaller than in the non-equilibrium situations.

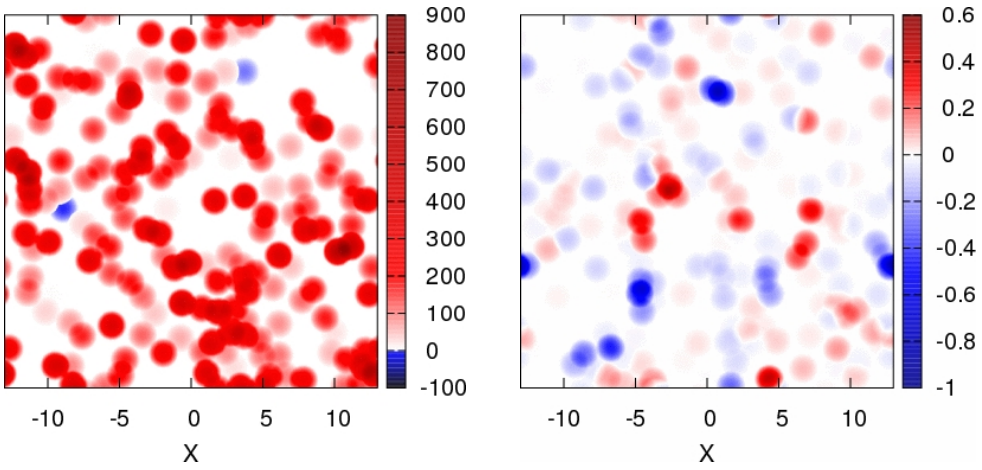

Figure 4.2 A typical spatial distribution of the potential energy changes $\Delta E_{pot}(\mathbf{r}_i)$ in one time step. We show the projection onto the xy-plane for $|z_i| \leq 0.5$ under conditions of (a) a LJ potential just after rescaling with $\lambda(t = 0) = 0.7$, (b) a LJ potential during equilibrium.

4.1.2 Temperature evolution after a radial rescaling

Through the dynamics of the system, the local energy surplus dissipates into sizeable kinetic energy and an increase in the temperature of the system is observed. Fig. 4.3 shows the evolution of the temperature with time for a simulation that undergoes a rescaling of the soft-core interaction of the particles. It is clear that the driven change in the radius of the molecules has a large effect on the temperature. After rescaling the radial distances, it takes of the order of a few hundred time steps for the temperature to reach a new equilibrium value.

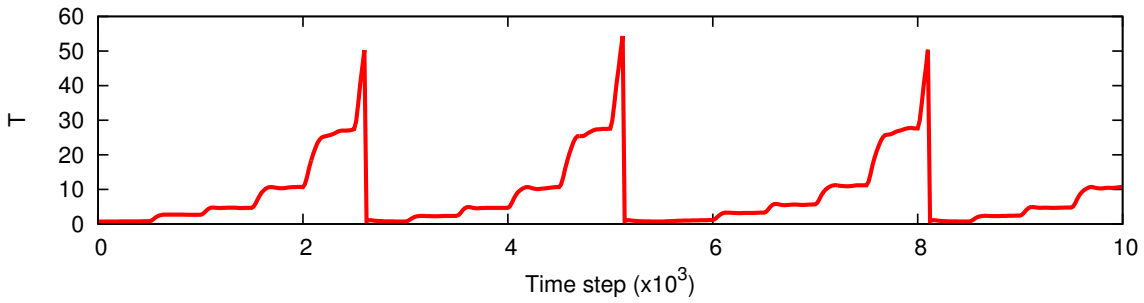

Figure 4.3 Temperature as a function of time for a simulation in which a radial rescaling with $\lambda(t=0)=0.75$ and $\tau=500$. When the temperature reaches 50, the radii and the temperature are reset to their original value ($T_{init}=0.7$).

The regular rescaling of the inter-particle distances drives the system's thermodynamic properties such as the temperature and the energy away from equilibrium, i.e. mild fluctuations around a constant value.

As repeatedly increasing the radii is not an attractive option (because of the finite size of the simulation system), after some time we reset the system's original temperature and particle radius. If the temperature exceeds a certain threshold, the radii are rescaled to their original value ($\lambda(t)=1$) and the velocities are rescaled so that the starting temperature is restored (fig. 4.3 has a threshold temperature of $T=50$). This is achieved by rescaling the velocities ($\mathbf{v}_i$) with a factor determined by the average temperature (T_{avg}) and the average kinetic energy ($E_{kin,avg}$),

$$\mathbf{v}_i \rightarrow \mathbf{v}_i \sqrt{\frac{\frac{3}{2}(N-1)k_B T_{avg}}{E_{kin,avg}}} \,. \tag{4.3}$$

Influence of λ on the temperature evolution

The value of λ has an impact on the equilibrium temperature that is eventually reached. Fig. 4.4 illustrates that a low value of λ results in a higher equilibrium temperature. A lower value of λ implies a bigger potential energy gain for particles close to each other. The resulting differences between equilibrium temperatures in Fig. 4.4 are almost equidistant on a logarithmic scale, which could stem from the fact that it is essentially the density $\rho\ \lambda^3$ that determines the new equilibrium temperature.

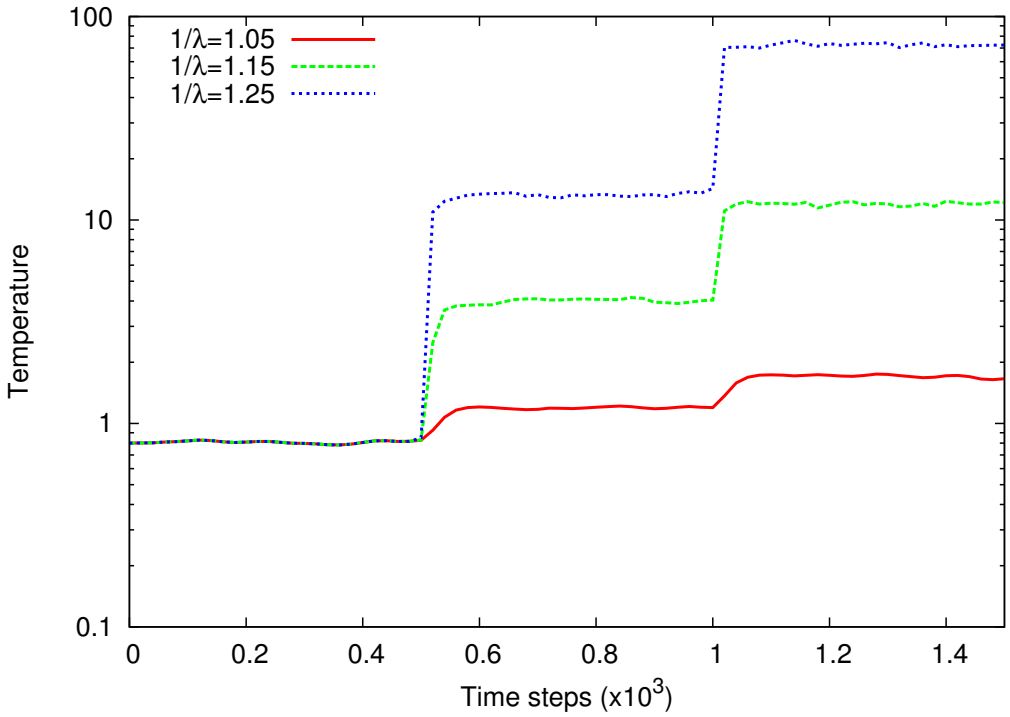

Figure 4.4 Temperature evolution of a simulation with $\tau = 500$ and different values of λ.

4.2 Correlation functions in out-of-equilibrium MD

Radial distribution function

One can expect that changing the length parameter of the simulation will affect the RDF of the system. The data for the pair distances are updated before each rescaling, so the RDFs shown here incorporate the non-equilibrium as well as equilibrium time periods after a rescaling.

In Fig. 4.5 the effect of the radial rescalings on the RDF is shown. Since a radial rescaling with $\lambda < 1$ is equal to enlarging the particle radius, the first peak in the RDF shifts to a higher value of r after every rescaling. It should be stressed that the obtained RDFS are reminiscent for a liquid.

After several rescalings, the simulation system becomes very dense and some particles can penetrate the core of other particles, thus resulting in a peak for $r < 1$ in the RDF, see Fig. 4.5 after 5 radial rescalings. For these particles, the potential energy will be much higher than average and one could expect that the dynamics of the system will eventually lead to a number of particles that could produce anomalous self-diffusion.

In [DCBC06] it was shown that soft potentials with a finite height at the origin of the coordinates can display a so-called H-instability. The H-instability was observed to

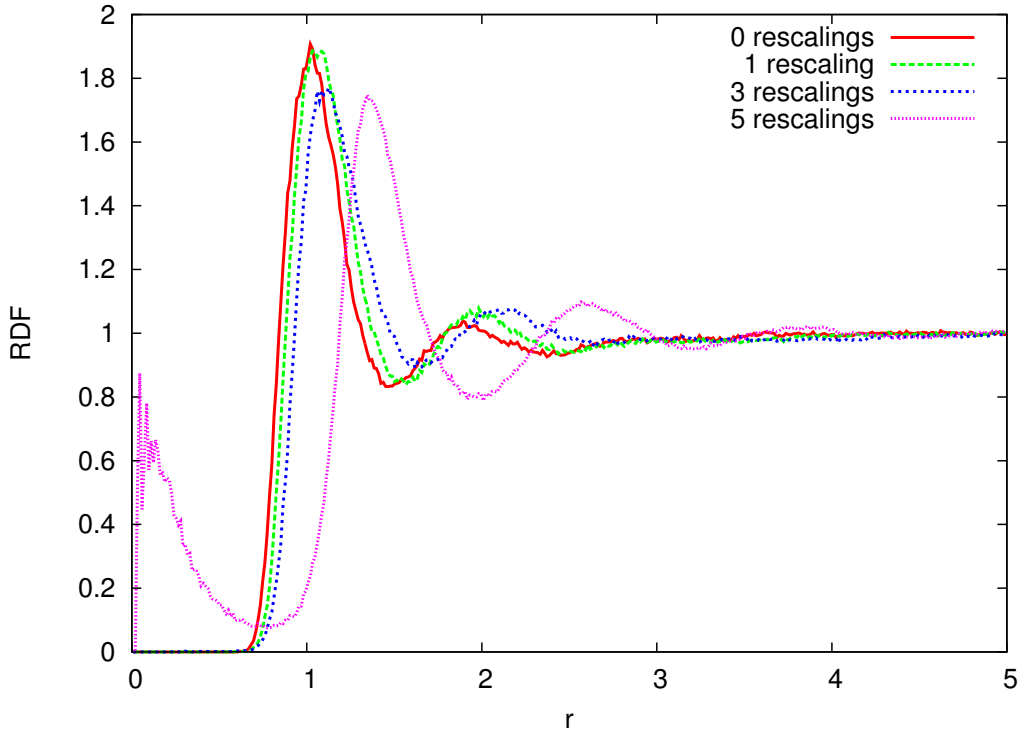

Figure 4.5 The RDF as a function of the radial distance at various time instances in a simulation with $\tau = 500$ and $\lambda(t = 0) = 0.75$. RDFs are shown for the reference simulation system (upto time step 500, red curve), and after 1 radial rescaling ($500 <$ time steps < 1000, green curve), 3 radial rescalings ($1500 <$ time steps < 2000, blue curve) and 5 radial rescalings ($2500 <$ time steps < 3000, pink curve).

occur for certain combinations of the parameters in a generalized Morse potential. Our $U_{SC}(r)$ has a balanced amount of short-range repulsion and medium-range attraction. During all stages of the simulations we have monitored the RDFs. The RDFs obtained with $U_{SC}(r)$ display all characteristics of a typical liquid and we find no signatures of a collapse as is illustrated in Fig. 4.5.

Velocity autocorrelation function

It is difficult to predict how the VACF will change under influence of the radial rescalings since the VACF specifically measures the time correlation in the system and is not related to the radial structure of the simulation system.

The VACF is usually computed using a convolution over the starting point, which will interfere with the analysis of the influence of the radial rescalings. As we recall from Chapter 3, the normal VACF at t_2 depends on the starting time t_1:

$$\text{VACF}(t_1, t_2) = \frac{1}{N v_0^2} \sum_{i=1}^{N} \langle \vec{v}_i(t_1) \cdot \vec{v}_i(t_2) \rangle \ , \tag{4.4}$$

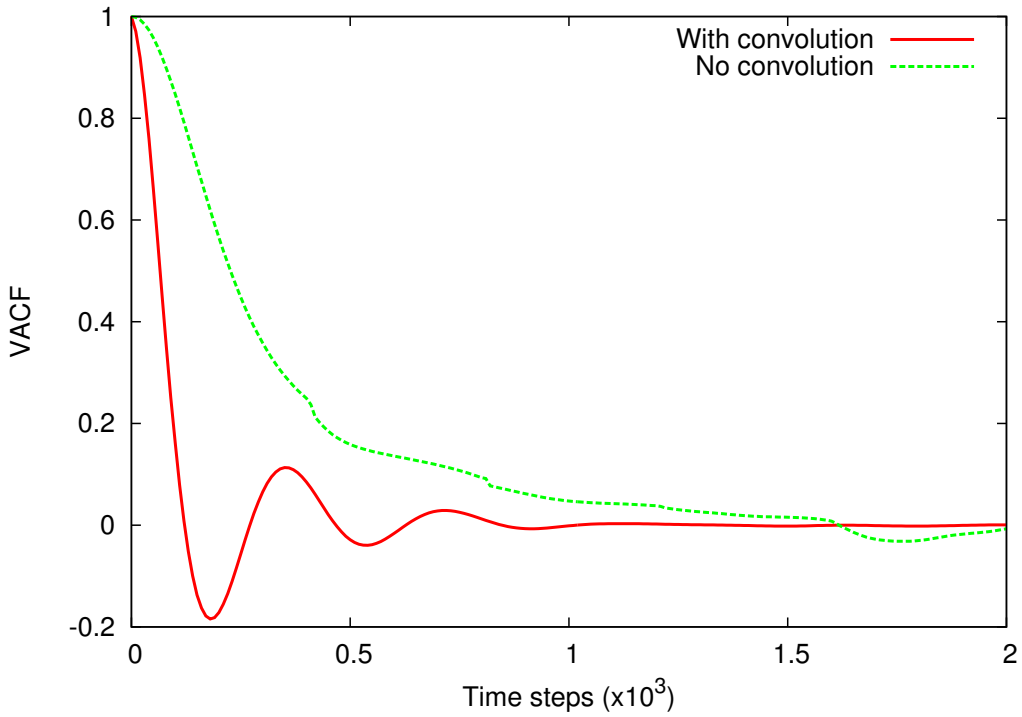

Figure 4.6 Time evolution of the VACF in a simulation with $\tau = 400$ and $\lambda = 0.75$. The VACF with convolution (Eq. 4.5) is the red curve. The VACF without convolution (Eq. 4.4), with $t_1 = 0$ is the green dotted curve.

with $v_0^2 = \frac{1}{N}\sum_{i=1}^{N} \langle \vec{v}_i(t_1) \cdot \vec{v}_i(t_1) \rangle$.

In stationary systems the VACF is only determined by the time difference $\tau = t_2 - t_1$, and the VACF can thus be averaged over the starting point:

$$\text{VACF}(\tau) = \frac{t_{max}}{2} \sum_{t_1=0}^{t_{max}/2} \text{VACF}(t_1, t_1 + \tau) \ . \tag{4.5}$$

In the non-equilibrium simulation system, there are shocks at discrete time instances, and calculating the VACF with convolution will result in averaging out these discrete shocks over time, thus hiding the influence they have. The VACF without convolution has more statistical fluctuations, but the shocks at discrete times are still present, giving an accurate influence of the shocks on the VACF.

From Fig. 4.6 the influence of the radial rescalings on the VACF can be appreciated. The VACF that is calculated using a convolution over the starting time, doesn't deviate from the VACF of the reference MD simulation in Fig. 3.4. The other VACF, that is calculated without using this convolution, diverges from this reference VACF. Every 400 time steps, a discontinuity in the VACF can be observed. At these points there is a noticeable influence of the radial rescalings. A radial rescaling results in a denser

simulation system and will therefore reduce the average correlation time of the system and produces a drop in the VACF, because larger particles result in more collisions.

In using the VACF with convolution, these drops are stretched out over the entire time range and will disappear. It is therefore desirable to use non-convoluted VACFs in analysing out-of-equilibrium systems. The VACFs of Fig. 4.6 resemble the VACF of the liquid reference MD simulation. Together with the information gathered from the RDF we can conclude that during the whole simulation time, our simulation system is in the liquid phase.

4.3 Self-diffusion in out-of-equilibrium simulations

Mean squared displacement

The higher temperature of the out-of-equilibrium conditions leads to a larger average velocity, which results in a larger MSD. This effect is shown in Fig. 4.7, where a simulation with a lower value of λ has a higher temperature and results in a larger MSD.

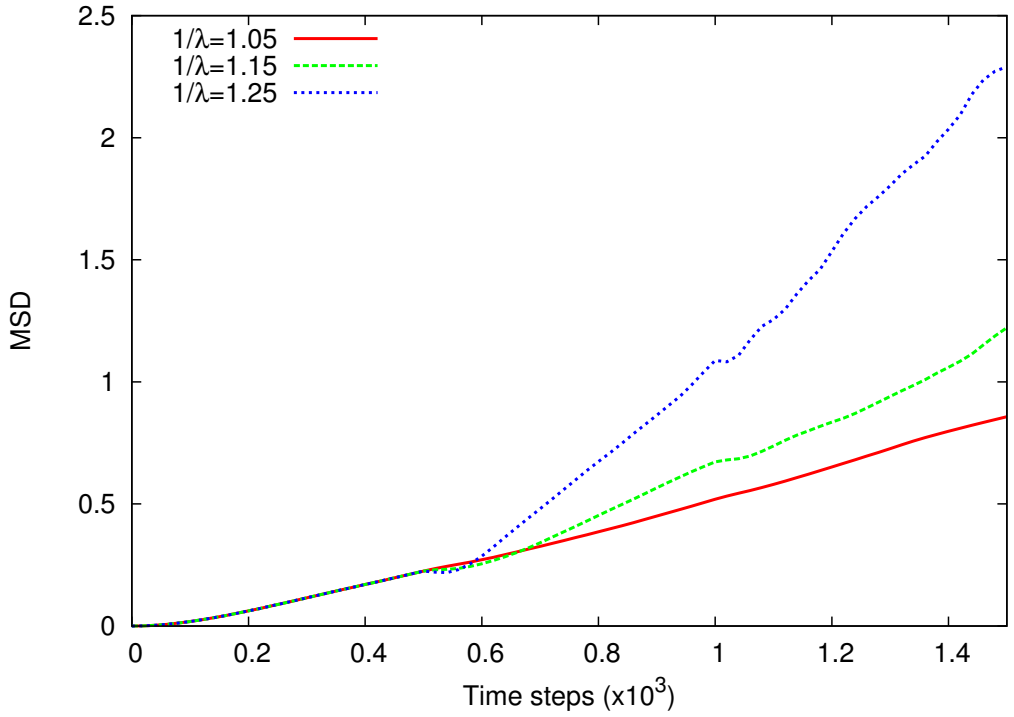

Figure 4.7 Evolution of the MSD ($\langle r^2(t)\rangle$) in a simulation with $\tau = 500$ and different values of λ.

Closer observation reveals that the MSDs deviate from $\langle \Delta r^2(t)\rangle \sim t^1$ for a very small time window, < 100 time steps. During these out-of-equilibrium periods anomalous dif-

fusion can occur, but the MSD is a function that calculates global self-diffusion characteristics, and is not suited to determine the properties during these small time windows of out-of-equilibrium behaviour.

Single time step displacement distribution

The single time step displacement distribution is much more suited to finding the properties of the out-of-equilibrium self-diffusion since it focuses on one time step. Fig. 4.8 compares $P(\Delta x/\sigma)$ for a typical equilibrium time instance with one obtained at a representative non-equilibrium time instance. Under non-equilibrium conditions, the tails of $P(\Delta x/\sigma)$ are considerably heavier than under equilibrium conditions. Moreover, a higher concentration of particles in the centre of the distribution is observed. These characteristics are typical for a leptokurtic distribution. The kurtosis of the out-of-equilibrium $P(\Delta x/\sigma)$ are larger than the typical noise level under equilibrium conditions.

We have found that after effectively enlarging the particles, anomalous characteristics can be found in the single time step displacement distributions $P(\Delta x/\sigma)$. After rescaling the interaction four times with $\lambda(t=0) = 0.75$ and $\tau = 500$, we have obtained anomalous distributions in $P(\Delta x/\sigma)$.

To establish the non-Gaussian shape of the tail of $P(\Delta x/\sigma)$ under non-equilibrium conditions, we have fitted it with an exponential because a power-law is notoriously hard to observe in a sample of finite size [GMY04], such as ours:

$$P(\frac{\Delta x}{\sigma}) = a \exp\left(-b\frac{\Delta x}{\sigma}\right), \qquad \left(\frac{\Delta x}{\sigma} > 1.5\right). \tag{4.6}$$

As can be seen in fig. 4.8, the distributions are well fitted by (4.6). This result confirms that the $P(\Delta x/\sigma)$ have heavier tails than a Gaussian distribution.

The distributions of fig. 4.8 are obtained by taking data during one time step. Summing these distributions for different time steps results in better statistics. Fig. 4.9 shows the result for P($\Delta x/\sigma$) after summation of 50 distributions during anomalous and normal (Gaussian) simulation conditions. Remark that $\frac{|\Delta x|}{\sigma} > 4$ events are one order of magnitude more likely under anomalous (non-equilibrium) conditions than under Gaussian (equilibrium) conditions. We find a fair amount of 5σ events and some rare 8σ events. The normalized cumulative distribution of fig. 4.9 clearly illustrates that the self-diffusion properties of the liquid are distinctive during the non-equilibrium and equilibrium periods of the simulation. In non-equilibrium conditions, small $\Delta x/\sigma$ are more likely, medium $\Delta x/\sigma$ less likely and large $\Delta x/\sigma$ far more likely.

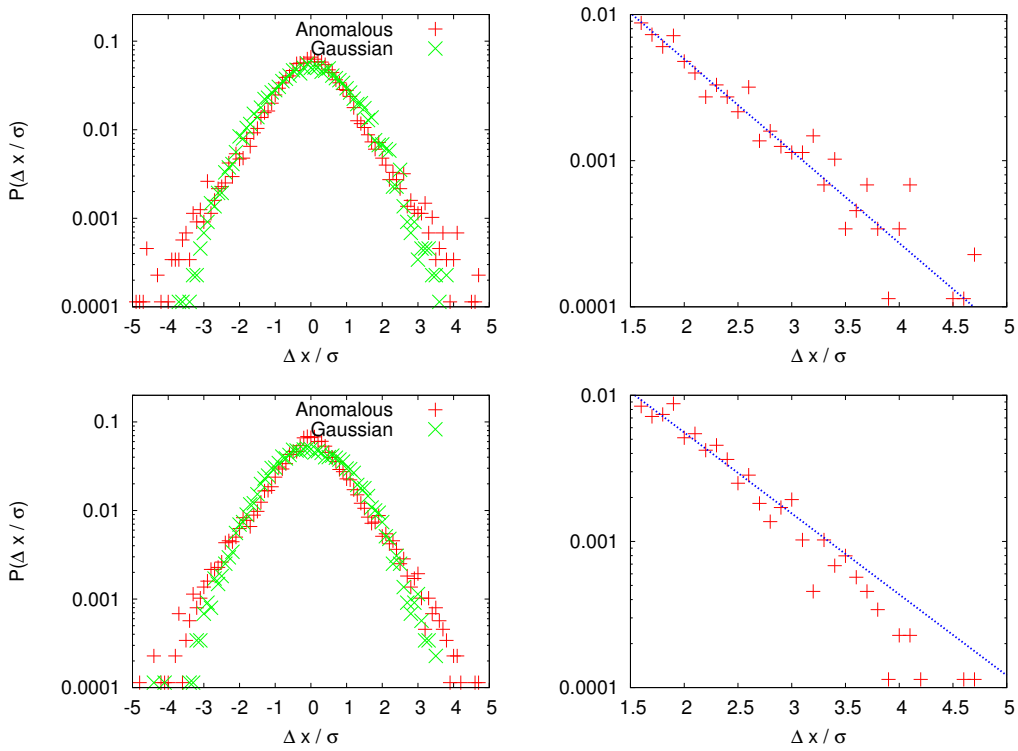

Figure 4.8 $P(\Delta x/\sigma)$ for two typical equilibrium (Gaussian) and non-equilibrium (anomalous) situations with initial density $\rho = 0.5$, temperature $T = 0.7$. The upper panels are for $\lambda(t = 0) = 0.7$ after four rescalings. The lower panels are for $\lambda(t = 0) = 0.75$ after four rescalings. The right panels are a fit of $P(\Delta x/\sigma > 1.5)$ with (4.6). The best fit parameters are $a = 0.090 \pm 0.005$ and $b = 0.14 \pm 0.01$ for the upper right panel and $a = 0.072 \pm 0.006$ and $b = 0.13 \pm 0.01$ for the lower right panel.

Trajectories of the particles

We now wish to study the trajectories of the individual particles during the complete simulation that alternates equilibrium with non-equilibrium conditions. To this end, we selected two particles: particle $\#1524$ for which $|\Delta x/\sigma|$ does not exceed 5 during the simulation (since this limit isn't attainable in a Gaussian simulation regime) and particle $\#3329$ for which this is not the case. Fig. 4.10 illustrates that the random character of the trajectories for both particles is maintained over the simulation time. The range in $\sum_t \Delta\mathbf{r}(t)/\sigma(t)$ is equivalent and doesn't discriminate between a particle that has a large peak of $|\Delta x/\sigma|$, since this peak is only present for a small time window.

Fig. 4.11 shows $\Delta x/\sigma$ as a function of time for these particles. The "anomalous" behaviour of particle $\#3329$ is confined to the time period 32000 - 33000. By contrast, no anomalous behaviour is discernible in the behaviour of particle $\#1524$. This confirms that the anomalous behaviour of the particle is too short-lived to influence the global diffusion properties of this particle of Fig. 4.10.

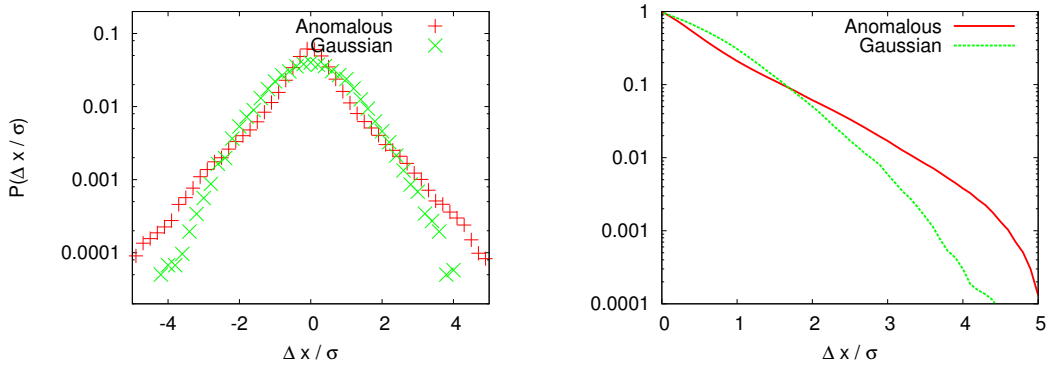

Figure 4.9 Left: Normalized summation of 50 'anomalous' and 'Gaussian' distributions of P($\Delta x/\sigma$). Right: Normalized cumulative distribution of the sum of 50 'anomalous' and 'Gaussian' distributions P($\Delta x/\sigma$).

Sensitivity to the parameters λ and τ

To establish the robustness of our technique to generate conditions of anomalous self-diffusion in a mono-atomic liquid, we have investigated its dependence on the parameters of the simulations. The non-equilibrium conditions are determined by the size of the rescaling parameter $\lambda(t=0)$ and the time intervals τ between two subsequent radial rescalings. During a simulation of 100000 time steps, the system goes through different periods of non-equilibrium conditions. The kurtosis of P($\Delta x/\sigma$) is computed for every time step and the maximal kurtosis is saved for every set of parameters. In fig. 4.12 the maximum kurtosis of the simulation is plotted as a function of $\frac{1}{\lambda(t=0)}$ and τ. The parameter τ is chosen between 100 and 1500 time steps, since equilibrium is always reached after 1500 time steps. $\lambda(t=0)$ is confined to $1 < 1/\lambda(t=0) < 1.4$, which means that the density change in one step is limited to $1 < \Delta\rho < 2.7$. Fig. 4.12 clearly shows that the anomalous character of $P(\Delta x/\sigma)$ remains present independent of the rescaling parameters. The time interval between two subsequent rescalings has only a minor influence on the maximal kurtosis (k_{max}). The adopted value of $\lambda(t=0)$, on the other hand, has a larger influence on k_{max}, but the anomalous characteristics are present in the entire $\lambda(t=0)$ interval.

The influence of the parameter $\lambda(t=0)$ on the system is further illustrated in fig. 4.13. Although $\lambda(t=0)$ has an influence on the height of the peak of the kurtosis during the non-equilibrium periods of the simulation, one can clearly see that the main characteristics of this non-equilibrium period remain roughly the same. In fig. 4.13, the non-equilibrium periods all have a period of ~ 200 time steps during which the kurtosis is equivalent to zero. This can be interpreted as the system requiring some time to convert the injected potential energy into kinetic energy. For $200 \lesssim t \lesssim 500$, the kurtosis

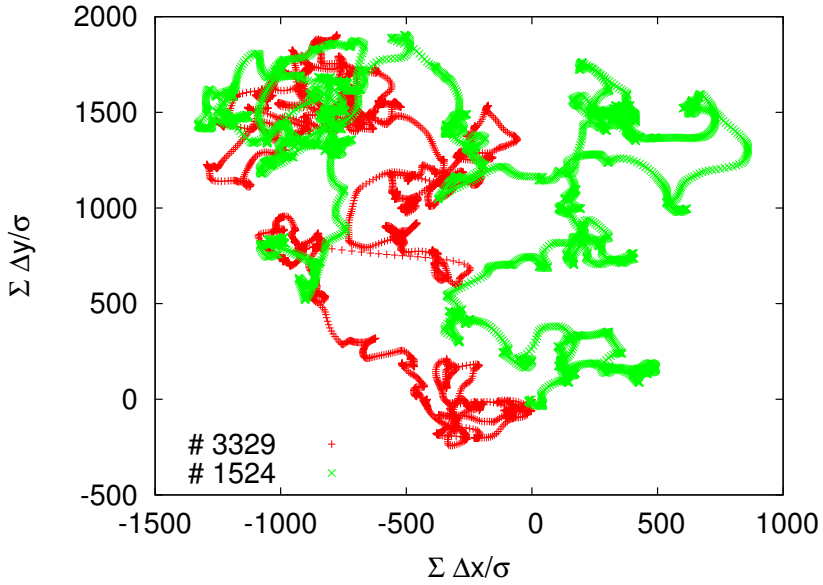

Figure 4.10 Projection on the xy-plane of $\sum_t \Delta\mathbf{r}(t)/\sigma(t)$ of particles $\#1524$ and $\#3329$ during a simulation of 100000 time steps.

features a steep ascent. For $t \gtrsim 600$, we observe a gentle decline to the equilibrium value. This reflects the fact that our simulation system has relaxed to an equilibrium situation with Gaussian self-diffusion properties.

The same robustness in the results applies to variations in the initial density and temperature of the system, provided that they generate a system in the liquid phase. The short range order and particle mobility typical for a liquid are necessary conditions. They generate the required balance between mobility and interaction, allowing the system to dissipate the potential energy surplus after being driven.

The robustness of the anomalous character of the self-diffusion properties under non-equilibrium conditions is a very useful result. It indicates that the qualitative features of the self-diffusion properties of the system are rather insensitive to the two parameters ($\lambda(t=0)$ and τ) that characterise the non-equilibrium behaviour. As a consequence, we can ascertain that it is the internal dynamics of the system that causes the non-Gaussian properties of $P(\Delta x/\sigma)$.

Robustness

We have also tested the robustness of our results to changes in the potential. To this end, we have performed simulations with the following potential: a LJ for $r_{ij} > 0.9$ and a polynomial $ar^6 + b$ for $r_{ij} < 0.9$ [TLKT00], we refer to this force as a polynomial soft core ($U_{poly}(r)$). The $U_{poly}(r)$ potential has the long-range LJ properties and a very

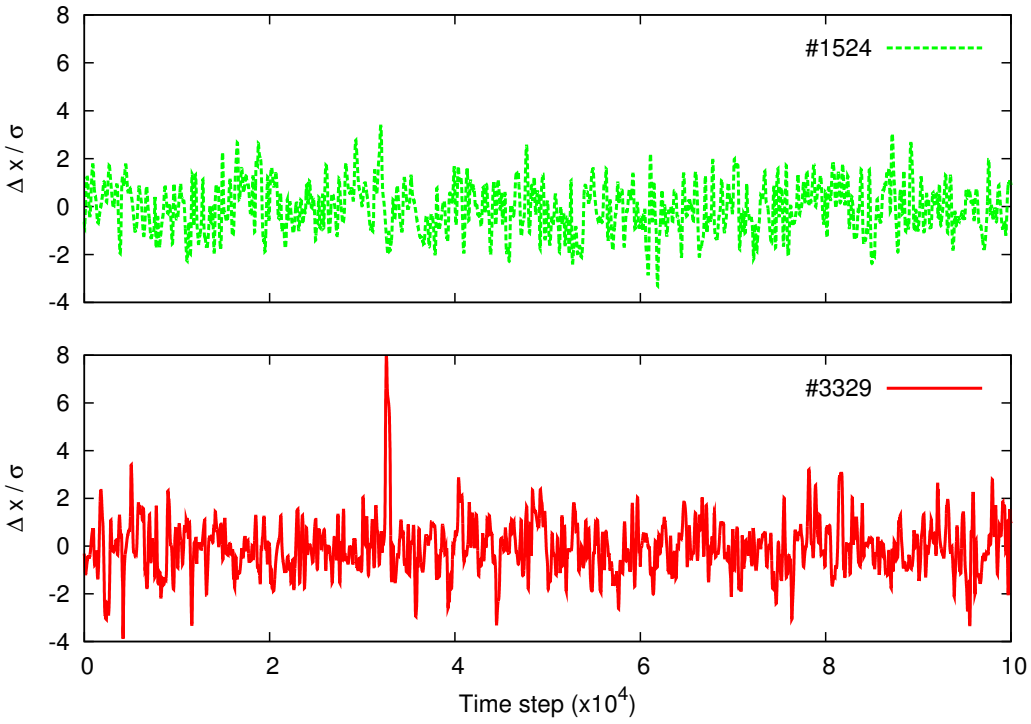

Figure 4.11 Single time step displacements ($\Delta x(t)/\sigma(t)$) of particles $\#1524$ and $\#3329$ during a simulation of 100000 time steps.

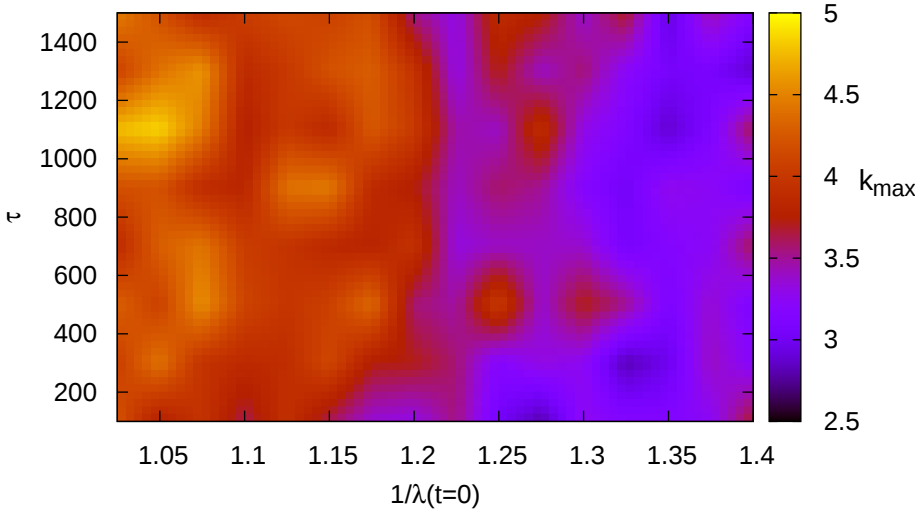

Figure 4.12 Maximal kurtosis (k_{max}) of a simulation as a function of the rescaling parameter $\frac{1}{\lambda(t=0)}$ and the time interval τ between two subsequent rescalings.

basic soft core. We have obtained non-Gaussian distributions almost identical to those obtained with $U_{SC}(r)$, see Fig. 4.14.

A further test of the robustness of our technique can be done in dimensions other than three. In two dimensions we obtain inherent anomalous self-diffusion of the sys-

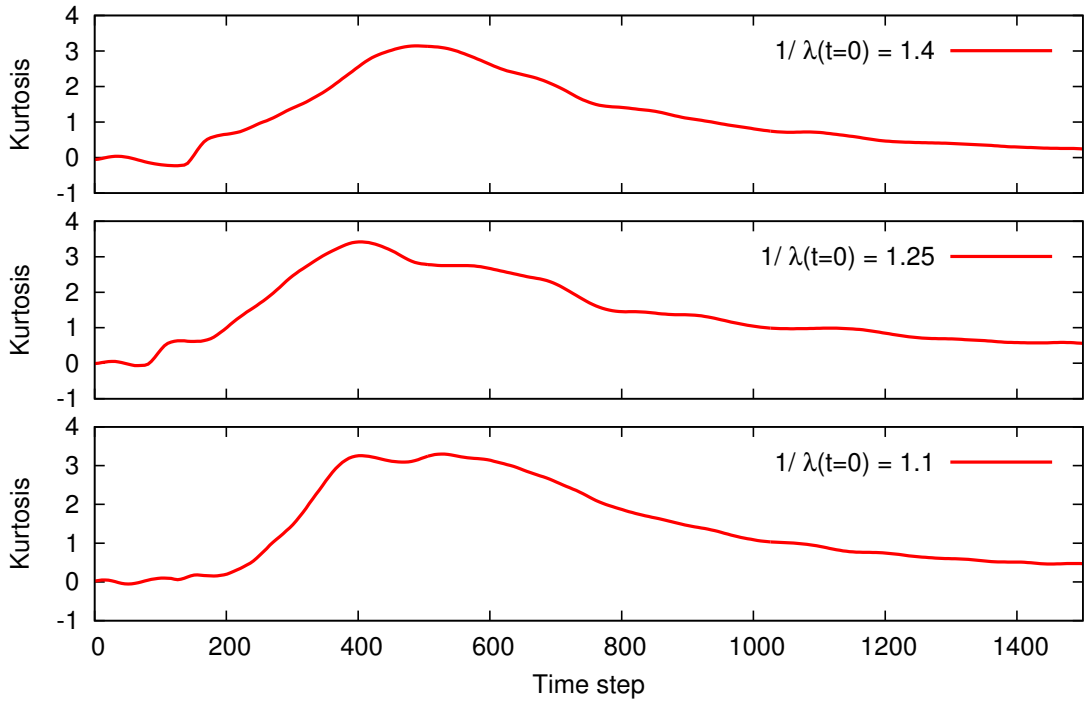

Figure 4.13 Kurtosis during a typical non-equilibrium period for three different values of $\lambda(t = 0)$, with $\tau = 1500$. Time step 0 corresponds with a driven rescaling of the size of the molecules.

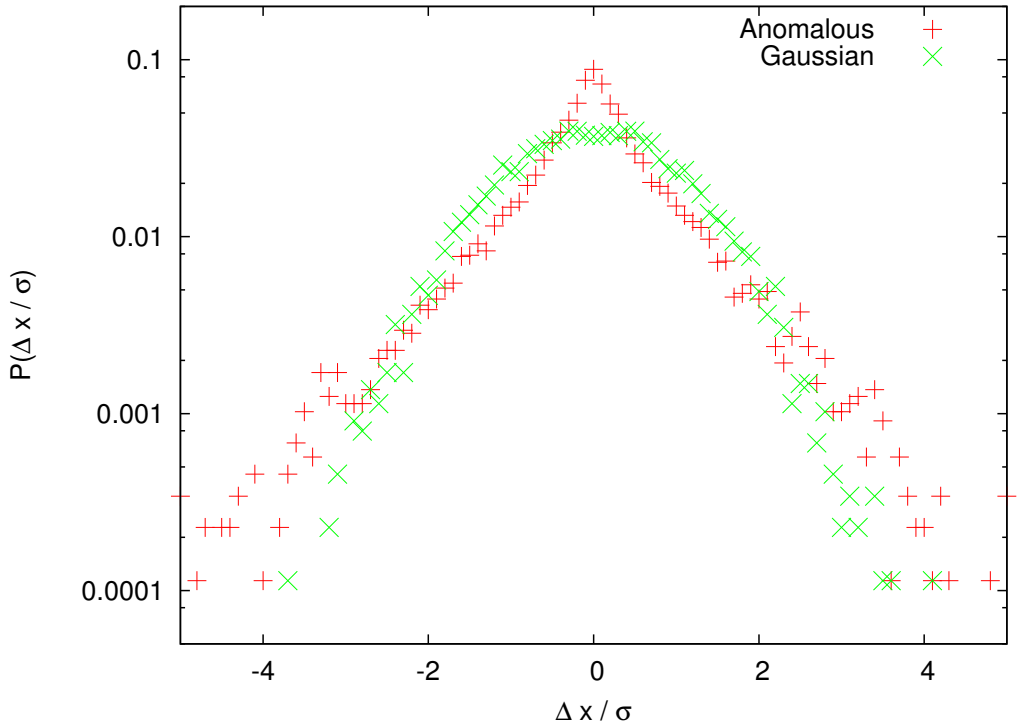

Figure 4.14 $P(\Delta x/\sigma)$ for a typical equilibrium (Gaussian) and non-equilibrium (anomalous) situations as obtained from a simulation with the polynomial soft core.

tem even in equilibrium conditions and with a LJ potential, as expected [KS05, LG07]. Fig. 4.15 shows the results of an MD simulation in two dimensions. The kurtosis of the single time step displacement $P(\Delta x/\sigma)$ is shown for the duration of the simulation. It shows that, during equilibrium time steps, there is non-Gaussian behaviour present. This is confirmed by $P(\Delta x/\sigma)$, where many particles have $\Delta x > 3\sigma$.

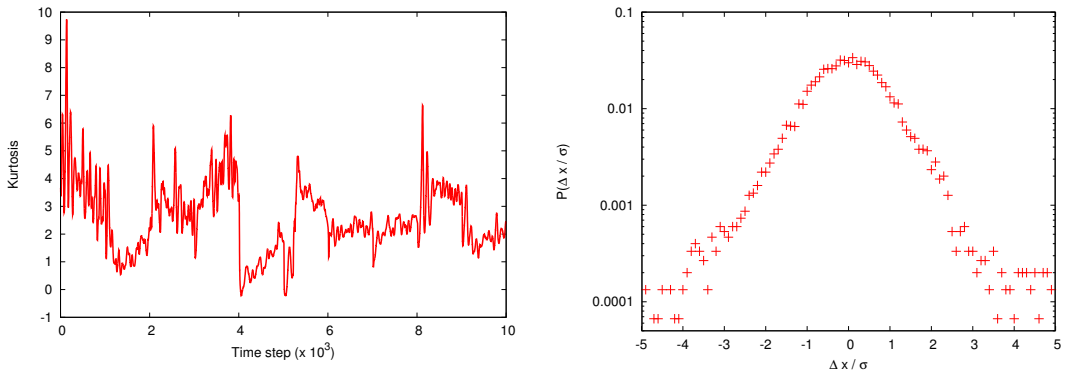

Figure 4.15 Kurtosis of the single time step displacement distribution in a reference MD simulation in two dimensions with $N = 5000$, without radial rescalings (left). Normalized $P(\Delta x/\sigma)$ for a two-dimensional simulation with 5000 particles,for a typical equilibrium (Gaussian) time step (right).

Fig. 4.16 shows the result of a simulation in four dimensions. We have used the same technique as the one adopted for the 3D results of Fig. 4.9. From fig. 4.16 it is clear that during the non-equilibrium time periods the self-diffusive properties are non-Gaussian. This provides further evidence for the robustness of the proposed technique.

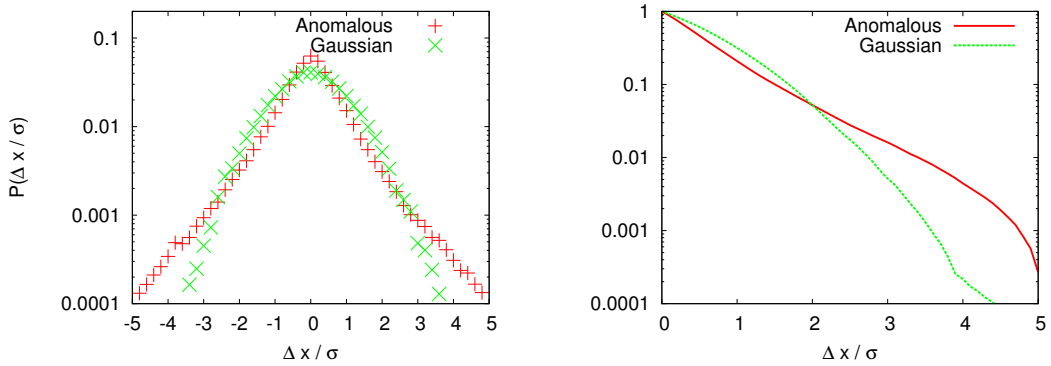

Figure 4.16 Normalized $P(\Delta x/\sigma)$ for a four-dimensional simulation with 4375 particles, summed over 350 time instances, for a typical equilibrium (Gaussian) and non-equilibrium (anomalous) situations, with $\lambda(t = 0) = 0.8$ and $\tau = 1000$.

4.4 Conclusion

In summary, we have presented a computational method, based on out-of-equilibrium MD simulations with a soft-core potential, that generates dynamical conditions of anomalous diffusion for the distribution of the one-dimensional displacements of the particles. This behaviour arises because the driving mechanism, i.e. the potential energy artificially injected into the system by increasing the radius of the particles, generates regions of increased potential energy. The dissipation of this potential energy under conditions of constant energy results in a small amount of very fast particles. For a broad range of the parameters involved, our technique generates anomalous diffusion in the simulation. In this way we have created a simple and solid method to achieve anomalous self-diffusion in an interacting system. This emergence of global behaviour that cannot be determined from local properties is also a property of self-organized criticality [CM05, Bak96], to which our model bears similarities. In the proposed simulation system equilibrium circumstances correspond to single-step displacements that are confined to a certain scale σ (Gaussian-like). Upon slowly driving the system and having it dissipate locally injected bursts of potential energy, we observe displacements Δx in a much more extended range and no characteristic size for Δx exists any more. In other words, the single-step displacement distributions $P(\Delta x/\sigma)$ obtain heavy tails. We find that this emergent feature does not require any fine tuning of the interaction parameters or of the driving protocol. Therefore, we deem that during the non-equilibrium simulation periods the system reaches a self-organized dynamical state. Available computer models that display self-organized criticality (e.g. sand-pile models [Jen98]) are typically characterized by two time scales. The external driving needs to be much slower than the typical time scale required for internal relaxation. The computer model that is described in this paper shares this property: between two subsequent (forced) swellings of the molecules we need to leave sufficient time for the system to relax. In order to observe the emergent behaviour of the heavy tails in the $P(\Delta x/\sigma)$ during the non-equilibrium periods we need to have a time evolution whereby bursts of activity are separated by relatively calm periods. Upon driving the system too fast we do not observe any general characteristic feature emerging in the $P(\Delta x/\sigma)$.

For the above-mentioned analogies, we deem that the proposed simulation system may serve as another computer method to study self-organized criticality. Whereas there is no fundamental understanding of self-organized criticality and metastable states at the very fundamental level, it is worth pursuing its study. After all, an abundant amount of phenomena in economics, earth sciences, biology and physics are characterized by

phenomena that are not confined to a certain scale.

markets.

Chapter 5

Non-equilibrium MD as an economic model?

We wish to investigate the possibility to map the non-equilibrium dynamic behaviour of classical liquids as discussed in Chapter 4 to the dynamics of markets as presented in Chapter 2. We view markets as non-equilibrium driven systems that are subject to more than average influxes of information, that are represented by the radial rescalings of the simulation system.

In Chapter 2 we have presented the geometric Brownian motion (GBM) model, on which the Black-Scholes option pricing model is based, and we have outlined the generic features of markets: the heavy tails of the return distributions, the short memory of the returns, the long memory of the volatility (or absolute returns), and the different behaviour of the return distributions at large time scales for crash or non-crash time windows.

First, we will quantify how the GBM model performs when it is tested against these generic features. We will then evaluate the generic features generated by an equilibrium molecular dynamics (MD) simulation, and discuss the advantages of this MD model when compared to GBM. We will subsequently test the generic features of the non-equilibrium MD model and compare these results with the previous models, GBM and equilibrium MD.

A second step in developing a non-equilibrium MD model consists of mapping the variables of the non-equilibrium MD simulation to those of the financial time series. In a financial time series there are essentially only two variables: value (or position) of an asset versus time. Whereas time can be expressed in terms of fixed units, the unit of value is subject to various changes like inflation, modifications in currency exchange rate, devaluation of currency, ... In the MD model, on the other hand, both time and

space can be expressed in terms of fixed units that represent physical time and space. To link both time series, a formal procedure should be established so as to match the scales of both sets of variables.

Finally, we investigate in how far non-equilibrium MD can display crash characteristics. This will be accomplished by evaluating the evolution of the simulated return (displacement) distributions at different time-scales. To confirm the presence of crash dynamics, the scale-free behaviour of the S&P 500 return distributions during crash time periods, as presented in section. 2.4.6, should also be discernible in non-equilibrium MD.

We will then discuss how this model can be used for understanding the dynamics of financial markets and the significance of volatility and information in our set-up. Different schemes are also proposed, that could make the non-equilibrium MD more realistic in its description of real financial markets. To conclude we will introduce two methods that could produce the desired crash dynamics in non-equilibrium MD.

5.1 The generic features of geometric Brownian motion

Geometric Brownian motion, as presented in section 2.2, is based on the SDE of Eq. 2.2:

$$dS = \mu S dt + \sigma S dz \ . \tag{5.1}$$

This model describes the evolution of a stock price as a multiplicative process, with a certain trend μ, and stochastic Gaussian fluctuations of size σ.

The time evolution of GBM is at first sight similar to the time series of the S&P 500, as shown in Figs. 2.2 and 2.4. The statistical properties of the GBM model are based on Gaussian dynamics whereas stock markets display size-able non-Gaussian characteristics. In order to quantify how the statistical properties of the GBM model compare to those of the S&P 500, we will generate an artificial financial time series like that of the S&P 500 and evaluate the similarities and differences in the generic features of GBM and the generic features of the S&P 500.

5.1.1 Return distributions in the GBM model

The first generic feature under study here is the presence of non-Gaussian tails in the return distributions of financial time series. To get returns in the GBM model one has to rework Eq. 5.1 so as to get returns ($d \ln S$!). This is discussed in section. 2.2 and results

in:

$$d\ln S = \left(\mu - \sigma^2/2\right) dt + \sigma\epsilon\sqrt{dt} \text{ with } \epsilon \sim N(0,1). \tag{5.2}$$

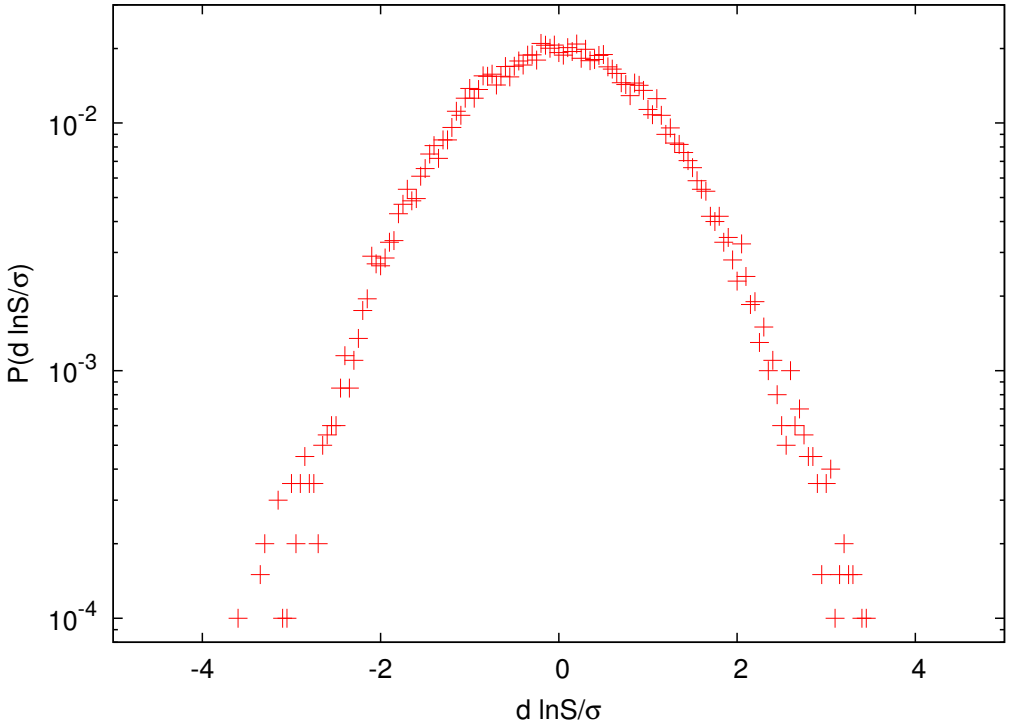

Figure 5.1 Probability distribution of the normalized (and detrended) returns $P(d\ln S/\sigma)$ in a GBM simulation with $\mu = 0.005$ and $\sigma = 0.08$.

The long-term behaviour is determined by the first term of Eq. 5.2, and is called the 'drift' term. If we neglect this term, i.e. an economic model without real growth, the returns are determined by a Brownian motion process with width σ.

A typical time series of the returns of the GBM model is plotted in Fig. 2.2. In Fig. 5.1, a distribution of the so-called detrended (i.e. without the drift term) normalized returns of the GBM model are shown. This plot readily indicates that the detrended normalized returns are, as expected, normally distributed. The first generic feature of the representative index, the S&P 500, is not reproduced by the GBM model. This major shortcoming was already mentioned in the discussion of the Black-Scholes formula in section 2.3.3. It is only substantiated by the results contained in Fig. 2.2.

This proves that the initial, visual, assessment of the GBM model is not supported by the statistical data. The similarities in the time evolution of the GBM and the S&P 500 of Figs. 2.2 and 2.4 are not reproduced in the return distributions. Using the GBM model will therefore lead to substantial deviations from reality.

5.1.2 Time correlations of the returns in the GBM model

The second generic feature of the analysis of the S&P 500 data presented in Chapter 2 is the short memory of returns. The return autocorrelation function of financial time series shows an exponential decay, and the correlation time is of the order of minutes. As discussed in section 2.4.3, this is short enough to ensure that no arbitrage opportunities arise. Here, we will turn our attention to the memory of the returns in the GBM model.

As becomes clear from Eq. 5.2 and Fig. 2.2, there is no correlation between subsequent price changes in the GBM model.

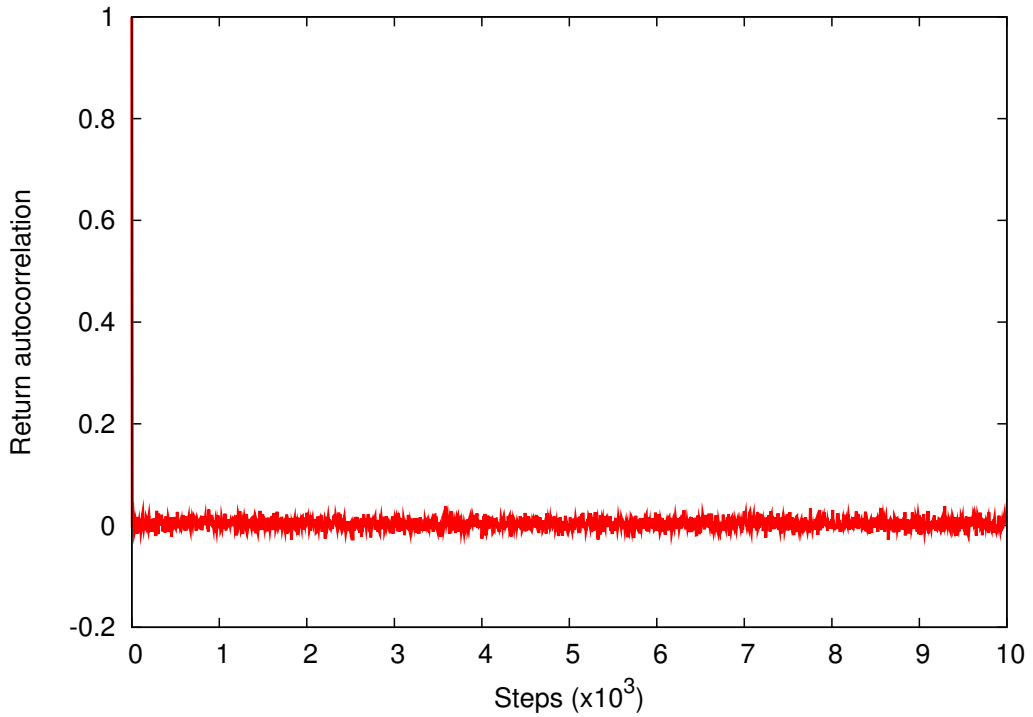

Figure 5.2 Autocorrelation function of the returns in a GBM simulation with $\mu = 0.005$ and $\sigma = 0.08$.

Fig. 5.2 shows the resulting behaviour of the autocorrelation function of the returns in the GBM model. It is clear that no time correlation exists in the GBM model. The correlation function returns immediately to the "noise level". This is not the behaviour of the generic feature of financial time series, where short time correlation exist. This provides another argument against the use of the GBM model in economic models.

Since there are no time correlations in the GBM simulation and the returns are normally distributed, we can conclude that the return distributions at all time scales will be Gaussian based on the central limit theorem. This excludes the presence of crash dynamics as defined in section 2.4.6.

5.1.3 Volatility in the GBM model

As discussed in section 2.4.4, financial markets display long time correlations in the volatility. In the GBM model, the time correlations for the fluctuations are governed by the stochastic term σdz, with σ a constant.

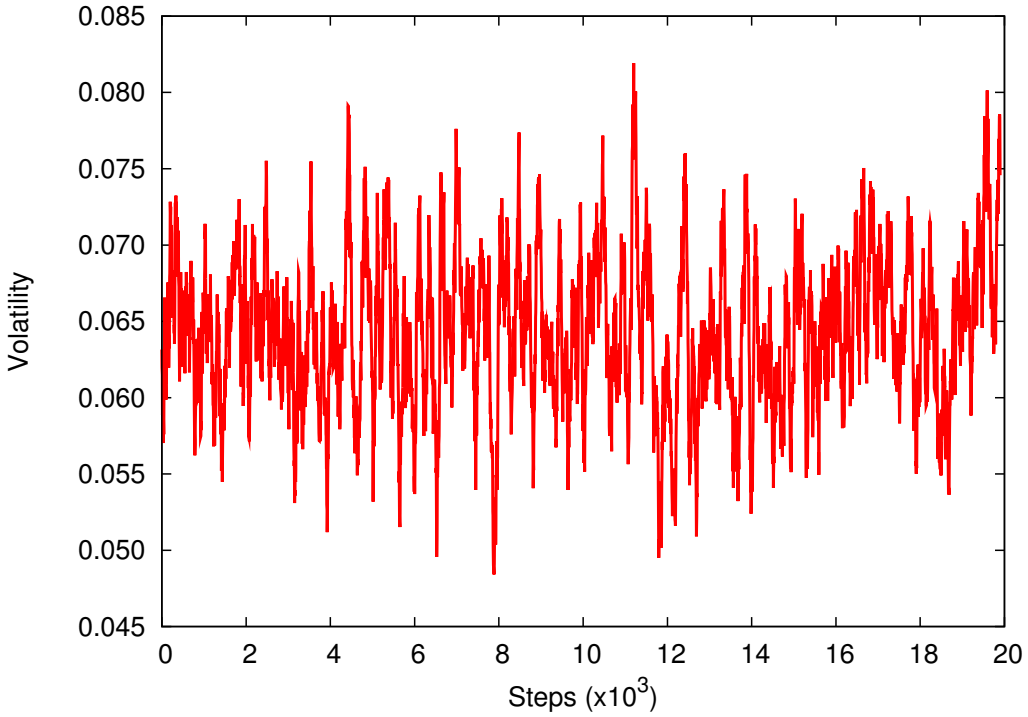

Figure 5.3 Time evolution of the volatility in a GBM simulation with $\mu = 0.005$ and $\sigma = 0.08$.

Fig. 5.3 shows the typical evolution of the volatility (of Eq. 2.34) in a GBM simulation. It is clear that the volatility fluctuates around a constant value and no periods of high and low volatility, as observed in the S&P 500 time series for example, are discernible. The constant value around which the volatility fluctuates deviates from $\sigma = 0.08$ because the volatility is calculated over 100 time steps. The time correlations in the volatility of the GBM model are infinite and the volatility autocorrelation function in the GBM model takes on a constant value. The power law, observed in the volatility autocorrelation function of the S&P 500, is not present in the GBM model.

As discussed in section 2.3.4, the GARCH-type models vary the value of σ in such a way that volatility clustering occurs. The standard GBM model is an inadequate description of the volatility of financial markets.

5.2 Generic features of equilibrium molecular dynamics

In Chapter 2 we have shown that diffusion processes have been used extensively in economics models and that one can intuitively understand that the time evolution of prices can be considered as a diffusion process. In Chapter 3 we have used the molecular dynamics technique to model self-diffusion in a liquid. In this section we will present the behaviour of the generic features of Chapter 2 in an equilibrium molecular dynamics simulation.

5.2.1 Step distribution

We have established in Chapter 3 that the self-diffusion properties of a liquid simulated in equilibrium MD are Gaussian. Accordingly it turns out to be impossible to generate the heavy tails of the return distributions in this model. The normalized single time step displacement distribution of Fig. 3.7 clearly illustrates that no improvement of the GBM model can be achieved in the return distributions of equilibrium MD.

Linking the normalized single time step displacement distributions to return distributions assumes some sort of mapping of the spatial and temporal values of both systems. This mapping is not straightforward and will be discussed in section 5.5.

5.2.2 Velocity autocorrelation function

A major improvement upon the GBM model are the time correlations in the MD simulation. As discussed in the previous section, the returns in the GBM model are not correlated, but returns in real financial time series have a short correlation time. The time correlations in the velocities of an equilibrium MD simulation of a liquid are also short as is clear from Fig. 3.4. Only in the gaseous phase does the VACF have an exponential decay. Because velocities are defined as a spatial step divided by the time step, the VACF can be considered to be the autocorrelation function of the single time step displacements. This link is not formally established, but is based on intuitive reasoning. A more firm understanding of return autocorrelation functions in MD is presented in section 5.3.2.

5.2.3 Autocorrelation function of the absolute velocities

A measure for the volatility in an equilibrium MD simulation can be the absolute velocities of the particles. High mobility of the particles corresponds to high absolute velocities and large fluctuations in the simulation system. Low absolute velocities result

in small fluctuations. In this way, absolute velocities and volatility describe equivalent properties of their systems and it is valid to use the absolute velocities to evaluate the memory of the volatility in equilibrium MD.

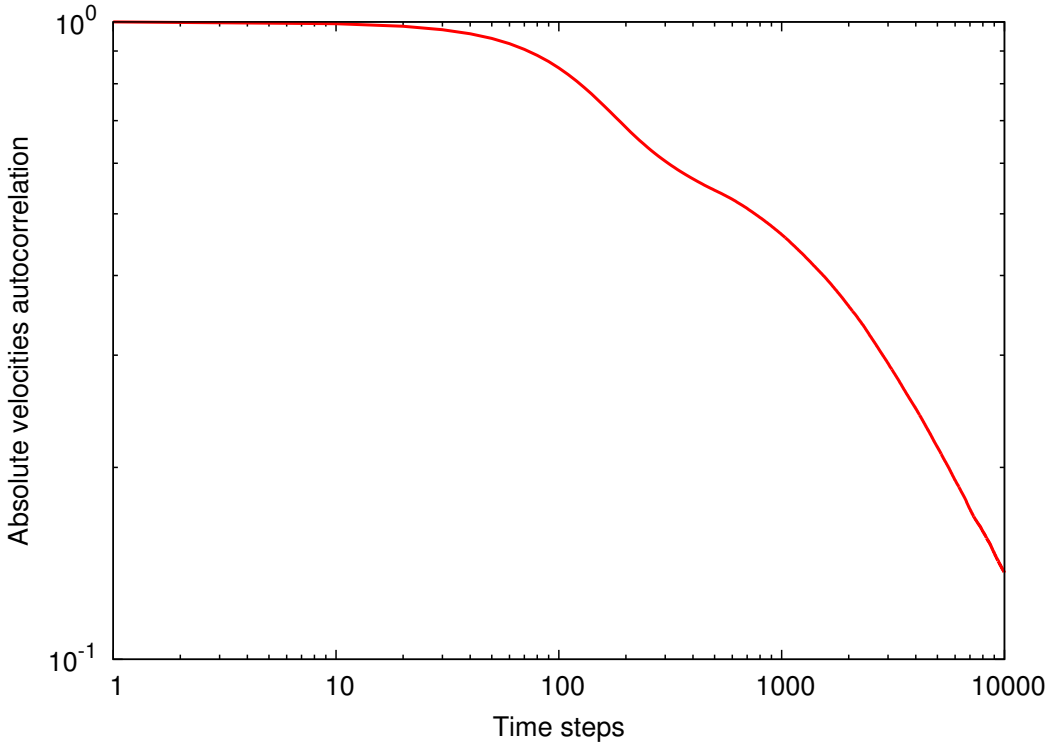

Figure 5.4 Autocorrelation function of the absolute velocities in a reference MD simulation.

Fig. 5.4 shows the autocorrelation function of the absolute velocities in an equilibrium MD simulation. It is readily observed that a long persistence in the magnitude of the velocities of the particles exists. This long-time behaviour of the equilibrium MD simulation compares well to the behaviour of the volatility in financial markets.

We can conclude from the velocity autocorrelation function and the autocorrelation function of the absolute velocities, that the equilibrium MD model emulates the time correlations of financial time series, as described in Chapter 2, much better than the GBM model.

5.3 Generic features of non-equilibrium MD

As discussed in Chapter 4, non-equilibrium MD simulations lead to conditions of non-Gaussian self-diffusion in liquids. As we have seen in the previous section, this is the only generic feature in equilibrium MD that is not qualitatively similar to the generic features of the S&P 500. This equilibrium MD model is already an improvement on

the GBM model that has no time correlations. Here, we present a rigorous comparison between the generic features of financial time series and the behaviour of the non-equilibrium MD simulations.

5.3.1 Heavy-tailed distributions

One apparent difference between equilibrium and non-equilibrium MD simulations is the presence of non-Gaussian self-diffusion. We have shown in chapter 4 that our non-equilibrium MD model produces non-Gaussian single time step displacement distributions. These distributions can be interpreted as the return distributions of our model. We refer the reader to section 5.5 for a rigorous mapping of the variables in the liquid model and those used in financial markets.

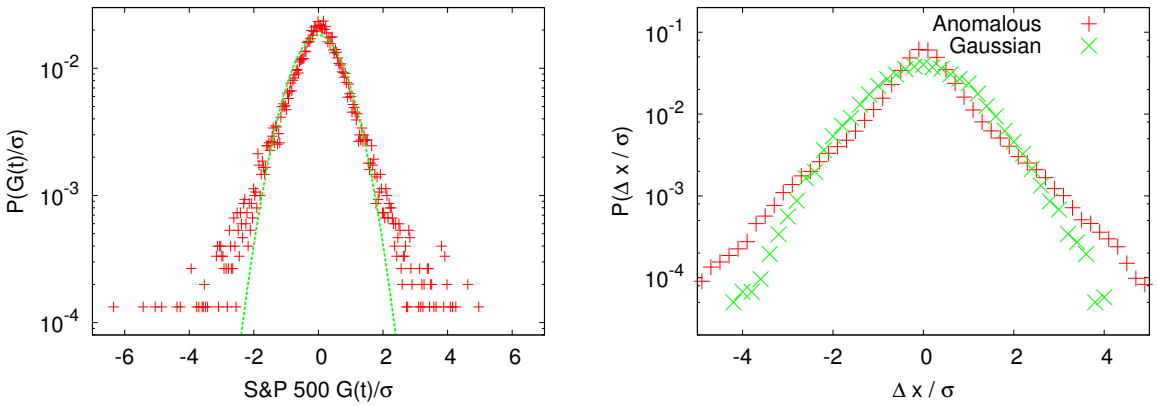

Figure 5.5 Distribution of the normalized (divided by the standard deviation σ) daily returns of the S&P 500 data from 01/03/1950 to 09/28/2009. Fit with a normal distribution: $f(x) = a\exp(-bx^2)$, with $a = 0.018 \pm 0.001$ and $b = 0.95 \pm 0.01$ (left). Normalized summation of 50 'anomalous' and 'Gaussian' distributions of P($\Delta x/\sigma$) in non-equilibrium MD (right).

It is clear from Fig. 5.5 that our model reproduces similar non-Gaussian distributions as the return distributions. Both distributions deviate from the normal distribution for returns and steps $> 3\sigma$. In section 4.3 it was pointed out that the tails of $P(\Delta x/\sigma)$ can be nicely described with an exponential function. For the description of the heavy tails in return distributions a variety of functions have been proposed: exponential [MPS05], Lèvy [Man63], truncated Lèvy flights [MS94] power law [MS99, New05], ...

5.3.2 Short memory of the returns

The MD simulations generate time correlations in the single time step displacement distributions. We have shown in the previous section that the short return correlations are

reproduced in equilibrium MD. We can expect that in non-equilibrium MD simulations the short time correlations persist.

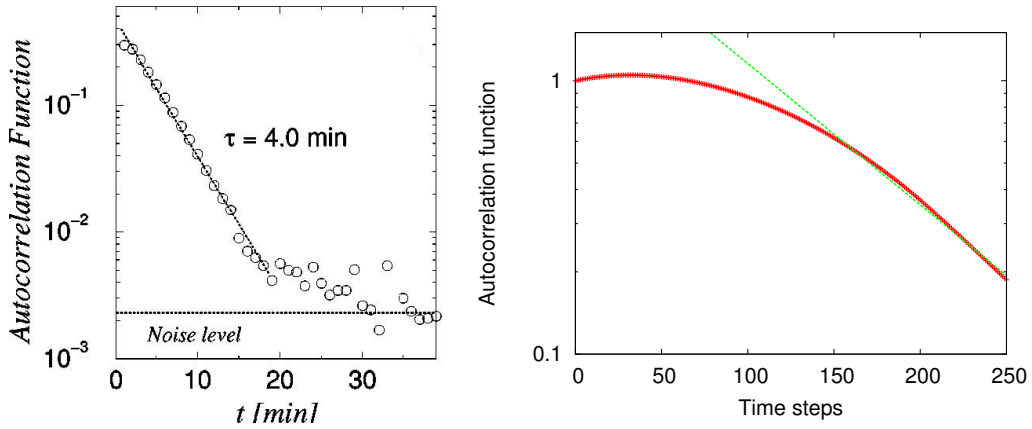

Figure 5.6 Autocorrelation function of $G(t)$ of the S&P 500 intra-minute data on a log-linear scale. Taken from [LGS99]. A fit with an exponential distribution results in a decay time of 4 min (left). Autocorrelation function of $\Delta x/\sigma$ in non-equilibrium MD (right).

In Fig. 5.6 the autocorrelation function of $\Delta x/\sigma$ is compared to the autocorrelation function of the returns. We notice that for a short time period, the autocorrelation function exponentially decays like the autocorrelation function of the returns. As will be explained in section 5.5, from the decay time of our simulation system and the decay time of the S&P 500 we will be able to link the simulation time of our model and the financial time.

5.3.3 Volatility in non-equilibrium MD

In the equilibrium MD section, we have assumed that volatility and absolute velocities describe the same characteristics of a system. To quantify the link between volatility in financial markets and volatility in MD, we have to define the volatility in MD in a way similar to the volatility of financial time series.

Before we determine the time correlations of the volatility in MD, we will determine the distribution of the volatility and compare it with the volatility distribution of the S&P 500.

Distribution of volatility

Based on [LGS99], we can compare the probability distribution of the volatility in financial markets to the probability distribution of the volatility in non-equilibrium MD. The volatility in our MD set-up can be defined as a volatility at a certain time instance

for a certain particle:

$$V_{T_M}(t,i) = \frac{1}{T_M} \sum_{t'=t}^{t+T_M-1} |\Delta x_i(t')| \ , \tag{5.3}$$

where T_M is the time window over which the volatility is calculated (in Chapter 2 the time window was 100 trading days for the plain volatility and one trading day for the autocorrelation of the volatility). We can choose the time window that resembles real financial markets. The return autocorrelation function links the time scale of our simulation to the financial time, where of the order of hundred simulation time steps are required to simulate a couple of trading minutes. Therefore, we choose a large time window, $T_M = 3600$, which represents a couple of trading hours to one trading day. This volatility should have the same characteristics as the volatility defined in [LGS99].

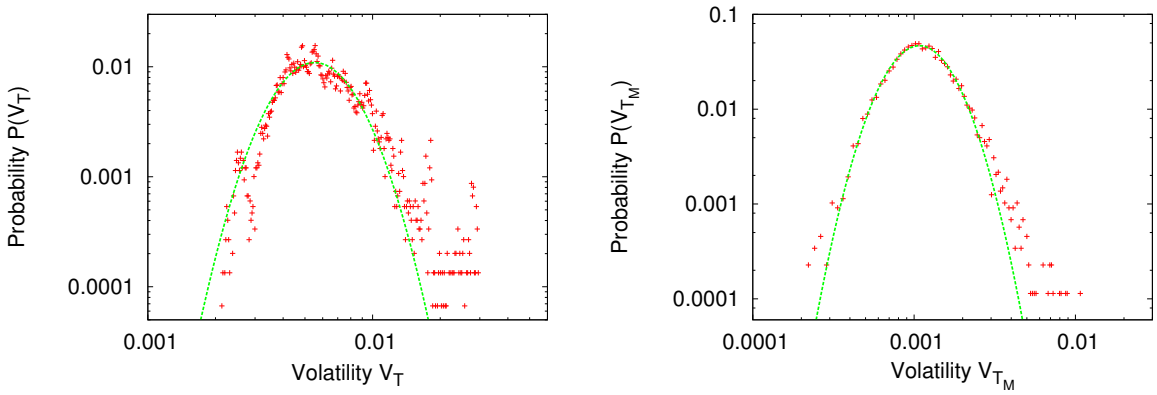

Figure 5.7 Probability density function of the volatility of the S&P 500 for a time window of 100 trading days (left). Probability density function of the volatility in non-equilibrium MD for a time window of 3600 simulation steps (right).

In Fig. 5.7 the probability density functions of the volatility are shown together with a log-normal fit in both figures. It is clear that the volatility distributions are similar in non-equilibrium MD and in the S&P 500. The order of magnitude of the average of the log-normal distributions and the width of the log-normal distributions differs, and this can be used to map the physical extension of our simulation space to the spatial variable (tick size) of financial markets.

From,

$$\frac{\left(\ln(V_T) - \mu_T\right)^2}{2\sigma_T^2} = \frac{\left(\ln(V_{T_M}) - \mu_{T_M}\right)^2}{2\sigma_{T_M}^2} \ , \tag{5.4}$$

we find a formula to match volatility in non-equilibrium MD to volatility in financial markets:

$$V_T = (V_{T_M})^{\sigma_T/\sigma_{T_M}} \times \exp\left(\mu_T - \frac{\sigma_T}{\sigma_{T_M}}\mu_{T_M}\right) \ . \tag{5.5}$$

Since volatility is expressed in unit of space, this formalism relates the spatial variables of the non-equilibrium MD simulation system to the tick size in financial markets. It is worth stressing that the rescaling relies on a power law (σ_T/σ_{T_M}), which, if applied on the absolute coordinates, would alter the single time step displacement distribution. This rescaling is therefore only applicable to relative values (Δx).

Long memory of the volatility?

The long memory of the volatility seems to be causing our model a problem. In Fig. 5.8 the volatility autocorrelation of our model doesn't decay at the same rate as the volatility autocorrelation of the S&P 500. Part of this can be explained by looking at the time-scale. The volatility autocorrelation function is at one tenth of its original value after approximately 100 trading days. One trading day is 390 minutes (there are six and a half hours of trading in the S&P 500), and minutes are linked to our system at a time-scale of hundred simulation steps. 100 days is therefore of the order of 1 million simulation steps and this length of simulation is not attainable with our current simulation and the availability of computing power.

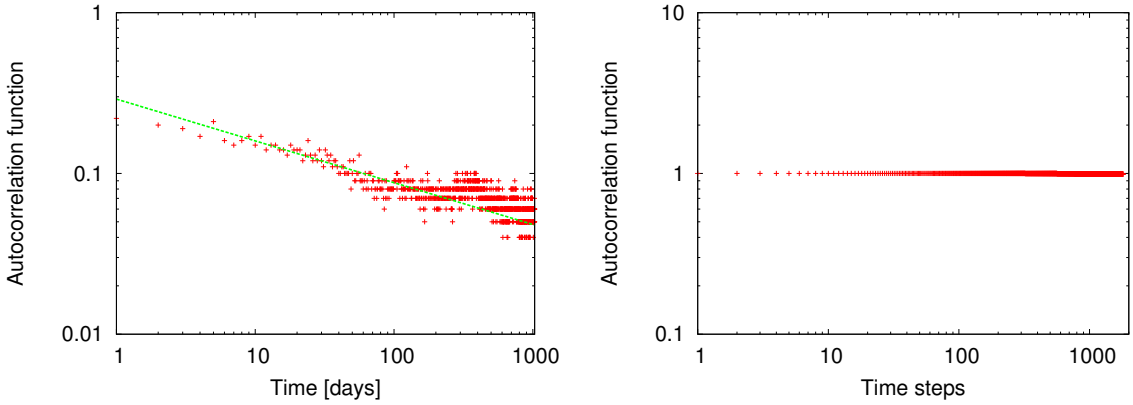

Figure 5.8 Autocorrelation function $C(t)$ of the absolute daily returns $|G(t)|$ on a logarithmic scale (left). Autocorrelation function $C(t)$ of the volatility $|G(t)|$ in non-equilibrium MD, on a logarithmic scale (right).

We have shown that in an equilibrium MD simulation, the volatility autocorrelation behaviour can be reproduced by the absolute velocity autocorrelation function of Fig. 5.4. This definition of volatility is mathematically less correct, but can be used as a measure for the fluctuations in the simulation system. The behaviour of the absolute velocity autocorrelation function is equivalent for equilibrium or non-equilibrium MD simulations. We can therefore conclude that the non-equilibrium MD simulation system produces volatility distributions and volatility autocorrelation functions that are similar

to those of financial markets.

5.4 Non-equilibrium MD and crash dynamics?

The previous sections have demonstrated that the non-equilibrium MD model of Chapter 4 displays the desired behaviour to emulate the generic features of financial time series. As discussed in section 2.4.6, it has been suggested that the non-Gaussianity of the return distributions can be used to discriminate between the "normal" and "crash" behaviour of markets.

The multi-scale analysis of [KSY06] shows that the return distributions for long time windows converge to a normal distribution during non-crash time periods of the S&P 500. The crash dynamics, on the other hand, leads to return distributions that are non-Gaussian at all time scales.

5.4.1 Kurtosis for different time windows

As discussed in section 2.4.6, in [KSY06] one uses Castaing's equation and the value of λ_s to determine the deviation of a distribution from normality. Here, we will use the kurtosis to quantify the deviations from normality. As shown in Appendix A, a large kurtosis refers to more tail events than a normal distribution, which is what we wish to express.

Fig. 5.9 displays the time evolution of the kurtosis for displacement distributions with different time windows during a typical non-equilibrium time period. The displacement of one particle is calculated by a summation of the steps of this particle over the desired time window. These displacements of all particles form the displacement distributions of Fig. 5.9.

For $T_M = 1$ the time evolution of the kurtosis is that of Fig. 4.13 for the single time step displacement distribution. The bigger the time window, the smaller the maximal kurtosis, which suggests that for large time windows the displacement distributions evolve into normal distributions, with zero kurtosis. One can also observe a shift in the position of the maximum. Since the absolute values of the displacements grow for larger time windows ($\sim \sqrt{t}$), it is harder for the anomalous steps to dominate the distributions for large time windows, which results in the shift of the position of the peak.

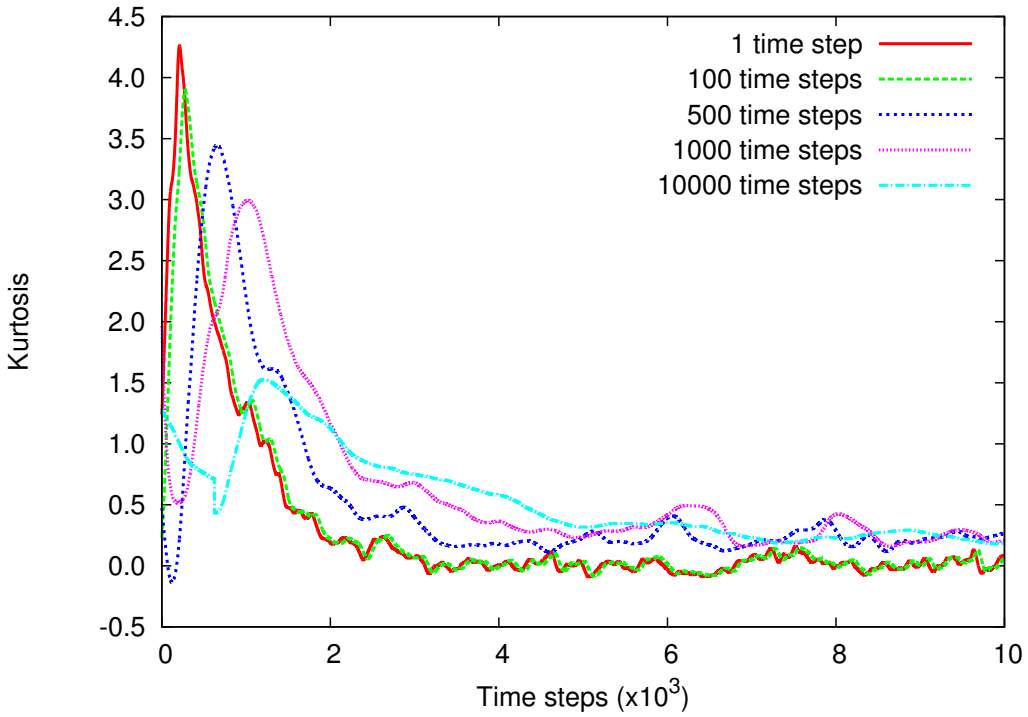

Figure 5.9 Time evolution of the kurtosis of the displacement distributions for different time windows ($1, 100, 500, 1000$ and 10000 time steps), during a typical non-equilibrium time period after a radial rescaling. The time axis is repositioned so the radial rescaling has time step 0.

5.4.2 Displacement distribution for different time windows

The displacement distributions should show that the behaviour of the kurtosis is no artifact and that they qualify as a measure for the non-Gaussianity of the distributions.

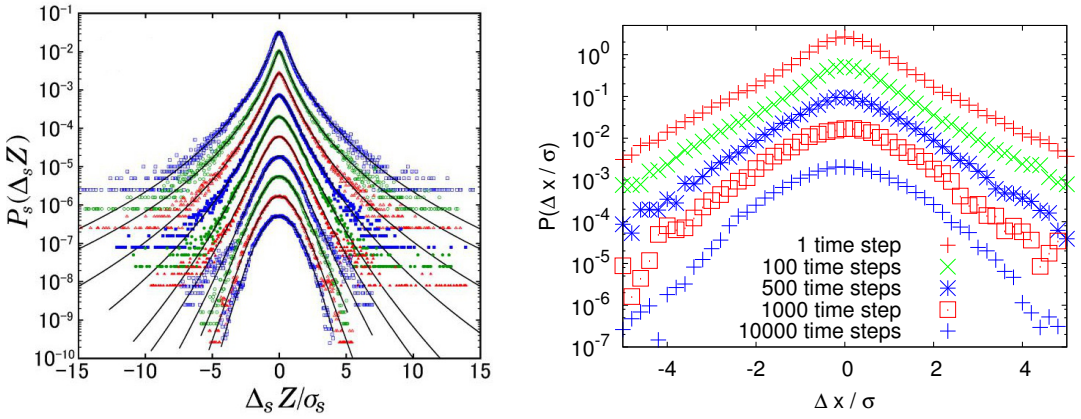

Figure 5.10 $P(\Delta x/\sigma)$ for different time scales without the 1987 crash data (left). $P(\Delta x/\sigma)$ for different time scales in non-equilibrium MD (right).

In Fig. 5.10 the evolution of the return distributions for different time windows is shown for the S&P 500 during non-crash time periods and the non-equilibrium MD

model. It is clear that the return distributions for large time windows are converging to a Gaussian distribution.

The speed of convergence in both system gives us another opportunity to establish a link between the simulation time and market time. From the size of the time windows where Gaussian distributions are observed, we are able to link our simulation time to the real financial time, see section 5.3.2.

Both figures suggest that the time correlations in the non-equilibrium MD simulation system do not lead to the crash dynamics of the S&P 500. The central limit theorem is valid for this simulation system and leads to Gaussian distributions for large time windows. We can conclude that non-equilibrium MD mimics the typical non-crash characteristics of the standard operation of the S&P 500.

5.5 Space-time structure of MD simulations and financial data

We have established that the universal non-crash characteristics of financial stock markets are present in our non-equilibrium MD set-up. In the previous sections we have also hinted at the various methods we can use to link the essential variables of time and space to the time and space (tick size) of financial markets. Here, we will clarify how this methods can be utilized in establishing a precise one-on-one relationship between the spatial and temporal variables of the financial markets and non-equilibrium MD.

5.5.1 Simulation time and financial time

In some of the generic features of Chapter 2 time and the time scales take on a central role. The autocorrelation functions display characteristic behaviour at certain short or long time scales, and the evolution of the return distributions for different time windows also possesses a strong dependence on the time scale. Both properties can be used to fix a time scale that links our simulation time with the trading time.

Autocorrelation of the returns

As shown in Figs. 2.7-2.9, the autocorrelation time of the returns in the S&P 500 is of the order of minutes. Other studies of a wide range of assets have obtained similar findings, [LGS99, Con01, VL02]. In our non-equilibrium MD set-up, the autocorrelation time of the displacements is of the order of 100 time steps (Fig. 5.6). Both estimates can differ depending on the initial conditions: in financial markets, it depends on the tick size, the

activity on the market, the time window, ... In the non-equilibrium MD set-up, the autocorrelation time of the displacements is influenced by the temperature, the number of particles and the density of the simulation system. Time in the MD simulation is linked to physical time based on the movement of Argon molecules.

As pointed out in section 5.3.2 a mapping of the time scales can be established by means of the autocorrelation times of the returns and the displacements.

One cannot use the autocorrelation of the volatility to verify this estimate because we have established that a power law should be present, Fig. 5.4. This long memory is replicated in Fig. 5.8, but no time scale can be coupled to a power law because a power law is an inherent scale free process.

Convergence to Gaussian statistics

The behaviour of the returns at different time scales, during time periods without a crash, is mirrored in the MD set-up, where the returns converge to a Gaussian distribution for large time windows. In [KSY06], the returns are calculated for time windows of $8, 16, 32, 64, 128, 256, 512, 1024, 2048, 4096$ min, shown from top to bottom in Fig. 5.10. Comparing both figures shows that for large time scales, both systems display the convergence to a Gaussian distribution that is expected from the central limit theorem, in the absence of large correlations.

The financial curves resemble a Gaussian for time windows > 512 min. In the MD simulation, only the curve with $T = 10000$ time steps resembles a Gaussian distribution, but even this distribution has a kurtosis larger than the noise level, see Fig. 5.9. A very rough estimate could be 10000 time steps $\sim 512 - 1024$ min. This estimate is in agreement with the analysis of the autocorrelation of the returns: 100 time steps in the MD simulation can be associated with a few minutes of market time for the S&P 500.

What is time in the MD system?

There are two different ways of interpreting *time* in the MD system. Starting from the non-Gaussian distributions, the displacement of every particle in the MD simulation at a fixed time step is linked with a return of the S&P 500 at a certain time step. In this way, displacements are considered to be *events* that occur at various time steps, but are not linked in time with each other. The other interpretation is perhaps a more natural interpretation, where the physical time of financial markets and the *physical* time of the MD simulation are linked. This link results in a comparison of the time scales of the systems, via the autocorrelation function of the returns and the evolution of the return

distributions for large time windows.

It is clear from the analysis of the generic features of the S&P 500 and those of non-equilibrium MD that both interpretations of time can be combined and generate the desired behaviour. In the analysis of the heavy tails and the short memory of the returns, the displacement distributions at one time step are compared to the return distributions over the complete time series. This uses both the first and second interpretation of what time is. The first interpretation is used because it treats the displacements as events. The second interpretation is used when the distributions are taken for different time windows, because it uses the time steps of the simulation as physical time.

We can conclude that the displacement of a particle at a certain time step can be interpreted as a return (*event*) at a certain time, and that the time steps of the MD set-up can be linked with the physical time of financial markets, provided that some scale transformation is performed. The fact that both methods for establishing this link result in the same order of magnitude for the ratio of the two time scales, confirms the validity of this approach.

5.5.2 Mapping the spatial variables

The other fundamental variable in both simulation systems (with time being the first), is the spatial variable. In financial markets this is expressed in terms of money (prices, tick size). We try to establish another link between both systems by matching the spatial variables onto each other. The distributions under consideration in this work are always distributions of relative variables (returns, normalized displacements), which are the natural variables of the respective systems. The absolute spatial variables (price, position), are not used in the analysis of the generic features and we will not now consider linking these variables directly.

Before attempting to establish a link between both spatial variables, we will look at a fundamental property of the relative variables. In MD, displacements obey the addition rule

$$\Delta x_i(t_1, \Delta t) + \Delta x_i(t_1 + \Delta t, \Delta t) = \Delta x_i(t_1, 2\Delta t) \ , \tag{5.6}$$

with

$$\Delta x_i(t_1, 2\Delta t) := x_i(t_1 + 2\Delta t) - x_i(t_1) \ . \tag{5.7}$$

In $\Delta x_i(t_1, 2\Delta t)$, t_1 denotes the starting time and $2\Delta t$ the time window over which the displacement is monitored and i is the number of the particle.

This addition rule is a direct consequence of our assumption of a homogeneous medium, or no background. In [BG90] it is shown that inhomogeneous systems can generate conditions of anomalous diffusion.

In financial markets, a similar addition rule applies to the returns

$$\begin{aligned} G_{\Delta t}(t+\Delta t)+G_{\Delta t}(t) &= \ln(Z(t+2\Delta t))-\ln(Z(t+\Delta t)) \\ &+ \ln(Z(t+\Delta t))-\ln(Z(t)) \\ &= \ln(Z(t+2\Delta t))-\ln(Z(t))=G_{2\Delta t}(t)\ , \end{aligned} \tag{5.8}$$

where $G_{2\Delta t}(t)$ denotes the return at time t over the time interval $2\Delta t$.

The relevant properties under observation in the probability distributions, are the normalized relative variables: $\Delta x/\sigma$ and $G(t)/\sigma(t)$. A natural way to link the positions in the MD system to the values of a financial system is consequently:

$$\frac{\Delta x_i(t_1,\Delta t)}{\sigma(t_1,\Delta t)} \equiv \frac{G(t',\Delta t')}{\sigma_f(\Delta t')}\ , \tag{5.9}$$

where $\sigma_f(\Delta t')$ is the standard deviation of the return distribution under observation over time window $\Delta t'$ and $\sigma(t_1,\Delta t)$ is the standard deviation of the displacement distribution at time t_1 over time window Δt.

A naive implementation of this link cannot account for the summation rules of Eqs. 5.6 and 5.8. Indeed, one has

$$\frac{\Delta x_i(t_1,2\Delta t)}{\sigma(t_1,2\Delta t)} \stackrel{?}{=} \frac{G(t',2\Delta t')}{\sigma_f(t',2\Delta t')} \tag{5.10}$$

$$\begin{aligned} \frac{\Delta x_i(t_1+\Delta t,\Delta t)+\Delta x_i(t_1,\Delta t)}{\sigma(t_1,2\Delta t)} &\stackrel{?}{=} \frac{G(t'+\Delta t',\Delta t')+G(t',\Delta t')}{\sigma_f(t',2\Delta t')} \\ \frac{\Delta x_i(t_1+\Delta t,\Delta t)+\Delta x_i(t_1,\Delta t)}{\sigma(t_1,2\Delta t)} &\neq \Delta x_i(t_2,\Delta t)\frac{\sigma_f(t'+\Delta t',\Delta t')}{\sigma(t_2,\Delta t)\sigma_f(t',2\Delta t')} \\ &+ \Delta x_i(t_1,\Delta t)\frac{\sigma_f(t',\Delta t')}{\sigma(t_1,\Delta t)\sigma_f(t',2\Delta t')}\ , \end{aligned} \tag{5.11}$$

with $\frac{\Delta x_i(t_1,\Delta t)}{\sigma(t_1,\Delta t)} \equiv \frac{G(t',\Delta t')}{\sigma_f(t',\Delta t')}$ and $\frac{\Delta x_i(t_2,\Delta t)}{\sigma(t_2,\Delta t)} \equiv \frac{G(t'+\Delta t',\Delta t')}{\sigma_f(t'+\Delta t',\Delta t')}$. The right hand side equals the left hand side under the following two conditions

$$\begin{aligned} \frac{\Delta x_i(t_1+\Delta t,\Delta t)}{\sigma(t_1,2\Delta t)} &\equiv \Delta x_i(t_2,\Delta t)\frac{\sigma_f(t'+\Delta t',\Delta t')}{\sigma(t_2,\Delta t)\sigma_f(t',2\Delta t')} \\ \frac{1}{\sigma(t_1,2\Delta t)} &\equiv \frac{\sigma_f(t',\Delta t')}{\sigma(t_1,\Delta t)\sigma_f(t',2\Delta t')}\ . \end{aligned} \tag{5.12}$$

These equations are not satisfied for all times and a simple linking of displacements to returns is therefore excluded. To make a rigorous link between both systems one must therefore use the absolute spatial variables, value and position.

Local coordinate transformation

A local coordinate transformation can provide a way around the problem of linking positions to prices. The suggested local transformation scales the MD simulation space with an exponential function:

$$\begin{aligned} \exp[\alpha \ln x_i(t_1)] &= x_i^\alpha(t_1) \equiv \mathcal{Z}(t') \\ \exp[\alpha \ln x_i(t_1+\Delta t)] &= x_i^\alpha(t_1+\Delta t) \equiv \mathcal{Z}(t'+\Delta t') \; . \end{aligned} \tag{5.13}$$

Converting this into returns, which are relevant for financial markets results in another equivalent relationship:

$$\begin{aligned} \ln\left(x_i^\alpha(t_1+\Delta t)\right) - \ln\left(x_i^\alpha(t_1)\right) &\equiv \ln\left(\mathcal{Z}(t'+\Delta t')\right) - \ln\left(\mathcal{Z}(t')\right) \\ \alpha \ln\left(\frac{x_i(t_1+\Delta t)}{x_i(t_1)}\right) &\equiv G(t',\Delta t') \\ \alpha \ln\left(\frac{x_i(t_1+\Delta t)-x_i(t_1)}{x_i(t_1)}+1\right) &\equiv G(t',\Delta t') \\ \approx \alpha \frac{x_i(t_1+\Delta t)-x_i(t_1)}{x_i(t_1)} &\equiv G(t',\Delta t') \\ \alpha \frac{\Delta x_i(t_1)}{x_i(t_1)} &\equiv G(t',\Delta t') \\ \Rightarrow \frac{\Delta x_i(t_1)}{\sigma(t_1)} &\propto \frac{G(t',\Delta t')}{\sigma_f(t',\Delta t')} \; . \end{aligned} \tag{5.14}$$

In this way, we can link the price and the price changes (returns) of financial markets to our observables, if we choose $\alpha := \frac{x_i(t_1)\sigma_f(t',\Delta t')}{\sigma(t_1)}$:

$$x_i^\alpha(t_1) \equiv \mathcal{Z}(t_1+t_i) \tag{5.15}$$

$$\frac{\Delta x_i(t_1)}{\sigma(t_1)} \equiv \frac{G(t',\Delta t')}{\sigma_f(t',\Delta t')} \; . \tag{5.16}$$

At this point we are in the position to link the position (space) in the MD system to the value (space) in financial markets. This link is however a cumbersome local coordinate transformation, with a complex scaling of the spatial variables by an exponent α that depends on the location ($x_i(t_1)$) and the width of the distributions of the spatial changes ($\sigma(t_1)$) and price changes ($\sigma_f(t',\Delta t')$). In Eq. 5.5 some sort of local coordinate transformation has to be performed to match the volatility behaviour in MD with the volatility of financial markets. We see that the exponent is similar to the exponent alpha derived here, but the standard deviations are those of the volatility distribution and not the displacement distribution. The transformation of Eq. 5.5 is also not dependent on the absolute position because it only involves spatial steps. In this way it resembles more a global coordinate transformation, which we will explore in depth in the next section.

Global coordinate transformation

The local transformation is rather confusing to capture and link the dynamics of the financial markets to the dynamics of our MD set-up. It does, however, provide an essential stepping stone for incorporating an essential feature of financial markets. This feature of financial markets, and its models, is the long term growth (or decline) that is visible in the global picture of the S&P 500 in Fig. 2.4. This global trend is captured by the GBM model presented in this chapter.

In this GBM model of financial markets, the following equation holds:

$$dS(t)/S(t) = \mu dt + \sigma dz(t) \ , \tag{5.17}$$

where the index value is determined by taking a weighted average of the underlying stocks. At the intial time t_0 this becomes $S(t_0)$:

$$\left\langle \sum_{i=1}^{N} \frac{\mathcal{Z}_i(t_0)}{\alpha} \right\rangle = S(t_0) \ , \tag{5.18}$$

with α the weighting factor.

The drift term is important for the overall evolution of the financial market. The short term properties of the financial markets are not dominated by this term, they are dominated by the random fluctuations of the second term. One can isolate the first term by taking a long-term average value such that the contribution from the random term vanishes. This results in an approximate expression for the cumulative return between t_0 and t

$$\left\langle \int_{t_0}^{t} \ln \frac{S(t')}{S(t_0)} dt' \right\rangle \approx (\mu - \frac{\sigma^2}{2}) \times (t - t_0) \ . \tag{5.19}$$

In our non-equilibrium MD set-up, there is no long term evolution because there are only fluctuations on the position of the centre of mass. Computing similar average (Eq. 5.18) over the positions of the particles results in eliminating these fluctuations, but no global trend:

$$\left\langle \sum_{i=1}^{N} x_i(t) \right\rangle = 0 \ , \tag{5.20}$$

because our system is symmetrical, with $-L/2 < x_i < L/2$. The above equation states that all positions are equally populated, or that the simulation system is homogeneous.

The results from the previous section and [Smo09, Ili01, Sor98b] suggest that using a global coordinate transformation, one can succeed in emulating trends of financial

markets. A first step consists of matching the initial condition of Eq. 5.18 via a translation:

$$x_i \rightarrow x_i' = x_i + L/2 \ , \tag{5.21}$$

so the system boundaries are: $0 < x_i' < L$ and all positions become positive. The average value becomes,

$$\left\langle \sum_{i=1}^{N} x_i'(t) \right\rangle = NL/2 \ . \tag{5.22}$$

This translation shows that, using the correct initial conditions, our system can be linked to the initial value of the index. A global coordinate transformation can lead us to the correct initial value of Eq. 5.18:

$$x_i \rightarrow x_i'' = x_i' \times \frac{2S(t_0)}{NL} = (x_i + L/2) \times \frac{2S(t_0)}{NL} \ , \tag{5.23}$$

which leads to the desired average position:

$$\left\langle \sum_{i=1}^{N} x_i''(t_0) \right\rangle = S(t_0) \ . \tag{5.24}$$

The averaged time evolution of a financial system is governed by Eq. 5.19 and we wish to incorporate this into our simulation set-up. This means that at every time step we have to perform a global gauge transformation:

$$x_i(t) \rightarrow x_i'''(t) = x_i''(t) \times (\mu - \frac{\sigma^2}{2}) \times (t - t_0) = (x_i(t) + L/2) \times \frac{2S(t_0)}{NL} \times (\mu - \frac{\sigma^2}{2}) \times (t - t_0) \ . \tag{5.25}$$

In this way, the desired average value (Eq. 5.19) can be achieved:

$$\left\langle \sum_{i=1}^{N} x_i'''(t) \right\rangle = (\mu - \frac{\sigma^2}{2}) \times (t - t_0) \times \left\langle \sum_{i=1}^{N} x_i''(t) \right\rangle = (\mu - \frac{\sigma^2}{2}) \times (t - t_0) S(t_0) \ . \tag{5.26}$$

The result of this rescaling is shown in Fig. 5.11, where the position of a particle is shown, together with a rescaling of this position and the total coordinate transformation of Eq. 5.25. In the first part of Fig. 5.11, the time evolution of the position of an arbitrarily selected particle during a MD simulation is shown. The location of the particle is not constrained to its original position, and the deviations from this positions are determined by random collisions and, on average, the particle will remain at its original position.

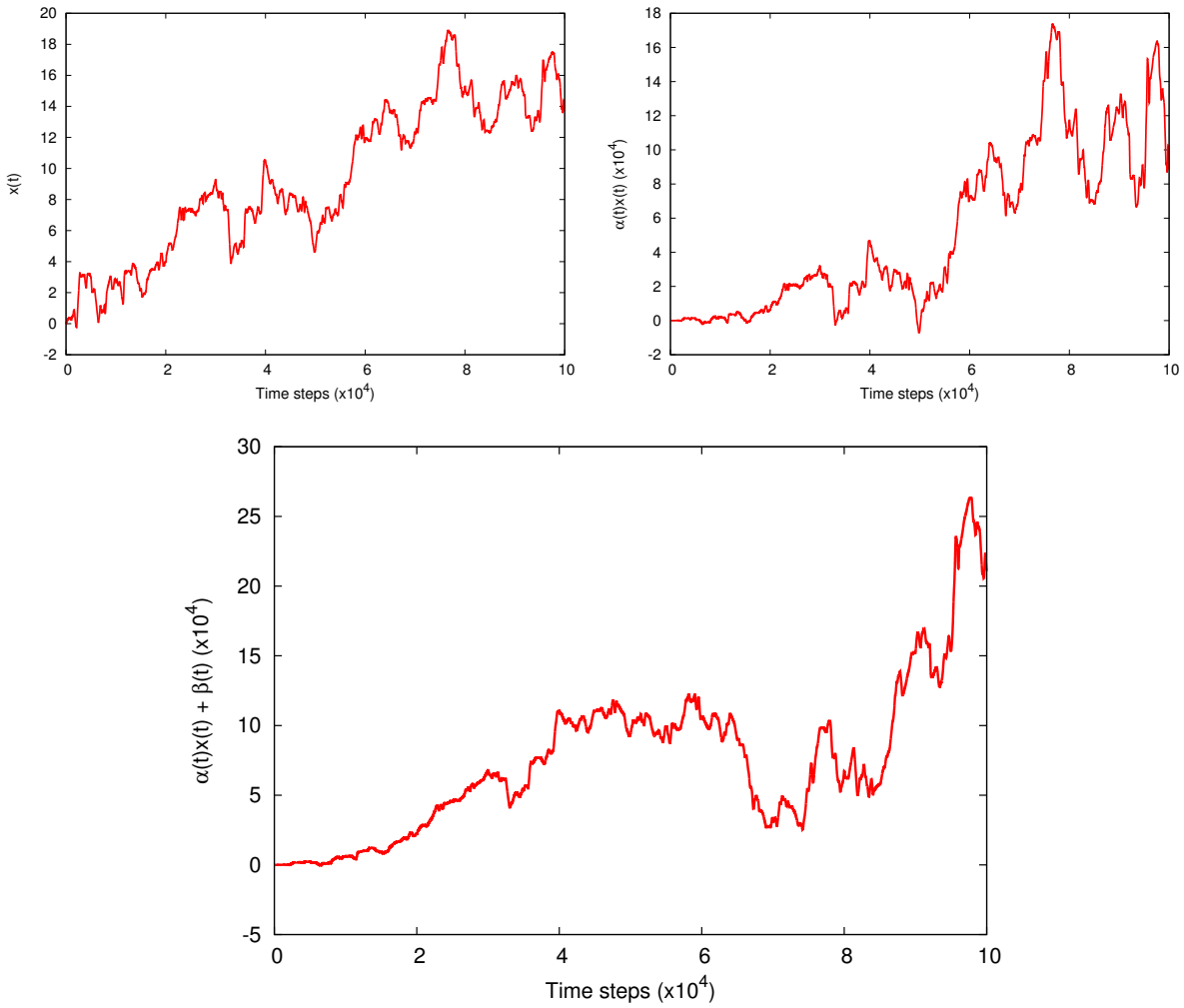

Figure 5.11 (Top left) Position ($x(t)$) of a particle as a function of time. (Top right) Modified position of a particle, with the rescaling $x_i \rightarrow x_i' = \alpha(t)x_i = \frac{2S(t_0)}{NL} \times (\mu - \frac{\sigma^2}{2}) \times (t - t_0) \times x_i$. Here, $\alpha(t) = 0.002\times$time steps was chosen. (Bottom) Modified position with added global trend: $x_i \rightarrow x_i'''(t) = \alpha(t)\times x_i + \beta(t) = (x_i(t) + L/2)\times \frac{2S(t_0)}{NL} \times (\mu - \frac{\sigma^2}{2}) \times (t - t_0)$. Here, $\alpha(t) = 0.002\times$time steps and $\beta(t) = 5\times$time steps was chosen.

We notice that the first rescaling of the second panel in Fig. 5.11 is necessary because it increases the fluctuations over time. Without this rescaling, the global trend would dominate for large time steps, and almost no fluctuations would be discernible.

The global gauge transformation derived in this section allows us to link and visualize a global trend in a financial system to a spatial stretching and translation at every time step in the MD set-up. This global gauge transformation can be executed after the simulation and therefore doesn't alter the dynamics of the simulation, but it does justify our use of $\Delta x/\sigma$. In using this normalized value, we have captured the anomalous behaviour of financial markets, but not the global trends. The global gauge transformation

fixes this shortcoming.

5.6 Applications of the non-equilibrium MD model

The above derived mapping between the non-equilibrium MD model and a financial market index makes this model a good candidate for further investigations into the dynamics of financial markets. A major advantage of this model is the way it handles the evolution of time. It has a simple algorithm, with interactions based on Newton's equation of motion, that gives the simulation a natural simulation time. This time, that can be linked to the physical time of financial time series via two different methods, allows one to evaluate the dynamics for different time scales. It also allows one to compute time correlations for both the return and volatility variables in MD. The robustness of the out-of-equilibrium dynamics ensures that various types of financial assets can be modelled with this technique.

In this section we will identify which factors of this model are suitable for explaining the behaviour of financial markets. Other improvements of the model are suggested. These suggestions mainly center around making the building blocks of the model more realistic.

5.6.1 Understanding the dynamics of financial markets

Some questions about the dynamics of financial markets can be related to the dynamics of non-equilibrium MD. The topics of concern here are the information in markets, and the volatility of financial time series. We will show that these topics are related to the following questions about non-equilibrium MD. What exactly are the shocks that drive the MD simulation out-of-equilibrium? What is temperature in the MD system and how can we relate it to a variable of financial time series?

Entropy and information of shocks

The factor that makes the MD simulation go out-of-equilibrium is the shock that is applied to the size of the particles. These shocks change the potential energy of the particles and in this way change the collisions that are taking place at this time instance. An interpretation of what these shocks represent in a financial market is essential for the interpretation of the non-equilibrium MD model in financial terms.

Up to this point, we have not yet analysed an essential variable of statistical physics: entropy. For a system in thermal equilibrium, there exists a relationship between the

energy, temperature and entropy of a system

$$T \equiv \frac{\partial E}{\partial S} \,, \tag{5.27}$$

with S, the entropy of the system.

The entropy of a system captures the underlying statistical uncertainty of disorder on the microscopic scale. A system where only one microscopic configuration is possible has zero entropy. One can rephrase the second law of thermodynamic and state that *the entropy of an isolated system can only increase in time, not decrease*. The entropy S of a MD simulation system can be defined by

$$S = -k_B P_i \ln P_i \,, \tag{5.28}$$

where k_B is the Boltzmann constant and P_i is the probability for the system to be in the i-th micro-state [AHY68].

Applying a radial rescaling to the simulation system leads to higher temperatures, or a higher average velocity. If we associate a micro-state with a particular distribution for the velocities, then a higher average velocity leads to more available micro-states for this temperature. This leads to a higher uncertainty about the exact micro state the simulation system is in and thus a higher entropy after a shock.

This higher entropy can be interpreted as an information flow in the system and in this way we can associate a shock in the MD simulation with a piece of information made available on the financial market under investigation.

If we compare this to a standard economic theory, such as the efficient market hypothesis, we find one essential difference. According to the efficien market hypothesis, every player in the market has access to all the information in the system. This can be connected with a situation whereby the entropy is a global variable. In our set-up we find local fluctuations in energy density that can be connected to entropy fluctuations, making entropy a local variable! This non-homogeneous entropy distribution means that not all players in the market receive an equal amount of information. In this way, out-of-equilibrium dynamics are essential to explain the non-Gaussian distributions.

Volatility

One could link the shocks to information flows in financial markets, but they change more than just the entropy of the system. Since the rescalings change the temperature, they also change the fluctuations in the simulation system. In the MD system, we could use the temperature as a precursor for these fluctuations.

In this way, a natural link between the volatility and the temperature could be established [RS00]. Both variables vary with time and are dependent on the initial conditions of their system. The initial density, particle number, interaction strength, ... all contribute to the initial amount of fluctuations. The volatility of financial time series, on the other hand, is influenced by the tick size, activity, liquidity, regulations, ... of the particular market [WB07]. Consequently, one could study the variations in initial conditions for both simulation systems and investigate their influence on the overall non-equilibrium behaviour.

5.6.2 To a more realistic simulation system

In Chapter 4 we have modified the standard MD simulation, based on a simulation of Argon molecules, so as to produce non-Gaussian single time step displacement distributions. This non-equilibrium MD model can be used to replicate some generic features of financial time series, but the initial configuration and interaction do not resemble the financial markets we wish to simulate. Here, we will propose some modifications to the non-equilibrium MD simulation that make it correspond more to a financial index. In this way, we could also learn more about the dynamics of these systems, and the role of the volatility in particular.

Different interactions

A big difference between the MD simulation and a financial market index is that the former system is homogeneous while the latter is a heterogeneous system, with a multitude of investors who, for instance, each utilize a different time scale for their investments. To mimic this behaviour in the MD simulation system one has the option to modify the interactions between different sorts of particles as in [Roe05b].

Fig. 5.12 shows some preliminary results of changed interactions in a reference MD simulation. We have created two types of particles (#1 and #2) and modified the ranges of the different interactions. In this example, only the interaction range of #1-#1 interactions is modified by adjusting the potential scale to a lower value. This shifts the minimum of the potential to a lower value and should result in smaller distances between #1 particles. The RDF of figures #1 from Fig. 5.12 reflects this behaviour, with a peak in the RDF at a lower value. The #2-#2 and #1-#2 RDFs remain those of a normal liquid in a reference MD model. The overall RDF, that includes all pairs of particles is modified to some extent because it is a weighted sum of all 3 previous RDFs.

Changing the interactions between groups of particles does not affect the qualita-

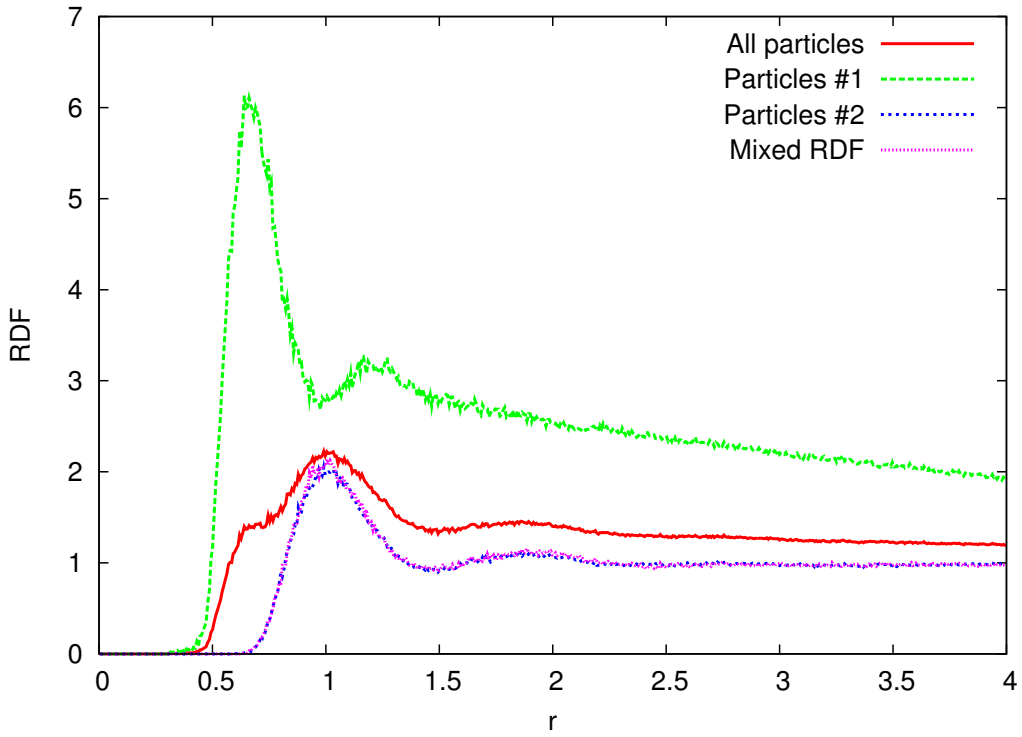

Figure 5.12 RDFs for a reference MD simulation with two different sorts of particles. Interaction length for particles #1 is smaller, the interaction length for particles #2 and mixed interactions (#1-#2) remains 1.

tive global behaviour of the simulation system. Fig. 5.13 shows that the temperature evolution and the VACF of a simulation with different interactions remain qualitatively similar to those of a reference MD simulation, chapter 3.

In this way, we could link the non-equilibrium MD system with the agent-based models of financial markets [BPS97, CMZ05, Coo05]. These models use heterogeneous investors with different strategies that trade on an artificial market to emulate the behaviour of financial time series. The two basic sort of investors are the trend-followers and the fundamentalists. The trend-followers do not analyse the firm or index in which they are investing but base their decision on the evolution of the time series and extrapolate the observed trend into the future. The fundamentalists determine a value for the stock based on an analysis of the firm and expect the value of the stock to always return to this fundamental value. They will only invest if the fluctuations drive the actual value far from their fundamental value, which (theoretically) enables them to make a profit.

Another interpretation of such a heterogeneous system is that an index is composed of different stocks and that the groups of particles that have the same interaction represent one item of this index. In this way, an index is composed of a number of small groups of particles with different characteristics. The correlations between different

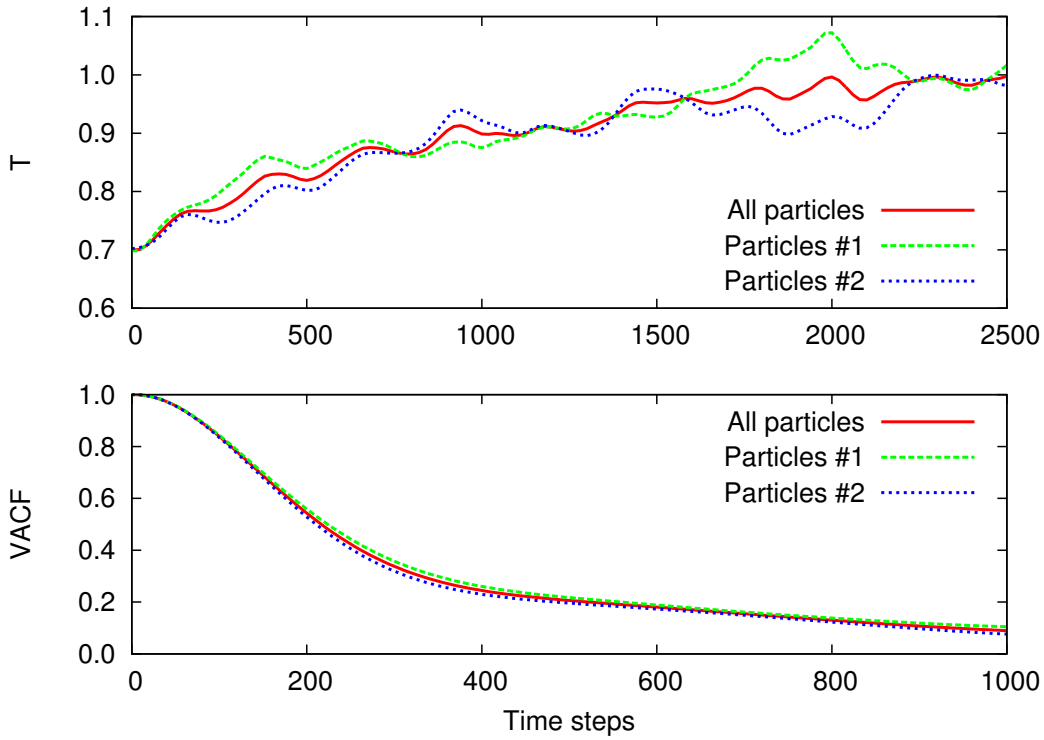

Figure 5.13 Temperature for a reference MD simulation with two different groups of particles. Overall temperature and temperature for the two different groups of particles is shown (top panel). VACFs for a reference MD simulation with two different groups of particles. Overall VACF and VACFs for the two different groups of particles are shown (bottom panel).

stocks and groups of stocks can be seen as correlations of atoms in molecules [GLO+09].

Different magnitude of the shocks

As mentioned in the previous section, the shocks can be seen as volatility indicators and it is therefore unrealistic to use a constant value for this throughout the simulation. A possible way of varying the magnitude of the shock is by using the volatility of the GARCH model. This leads to the correct volatility clustering observed in financial markets.

Another possibility is using historical volatility data as input for the simulation. In this way, the return distribution can be compared with the step distribution based on the same volatility time series. An evaluation of different volatility time series can be made to observe the effect this has on the respective distributions. If these distributions behave in the same way for different volatility time series one can conclude that the magnitude of the shocks is a good measure for the volatility of financial time series.

Different timing of the shocks

As in the variance gamma model of section 2.3.4, the time interval between the shocks, τ, could be made to vary to have a more realistic simulation of a financial index. This would again lead to more volatility clustering and a more realistic description of the financial market under observation. A random value for τ does not directly influence the single time step displacement distributions as long as τ is large enough so as to allow a return to equilibrium of the simulation system.

Varying the number of particles

If the interpretation of 'particles are investors' is upheld, it is consequently not realistic to assume a constant number of particles in the simulation system and this should be changed. It is possible to allow particles to enter the simulation system, with some restrictions on the position of the entering particle so that it doesn't superimpose another particle. Particles that disappear from the system can be chosen at random and no restrictions need to be made, but every removal of a particle will influence the dynamics of the system and violates the energy conservation of the system.

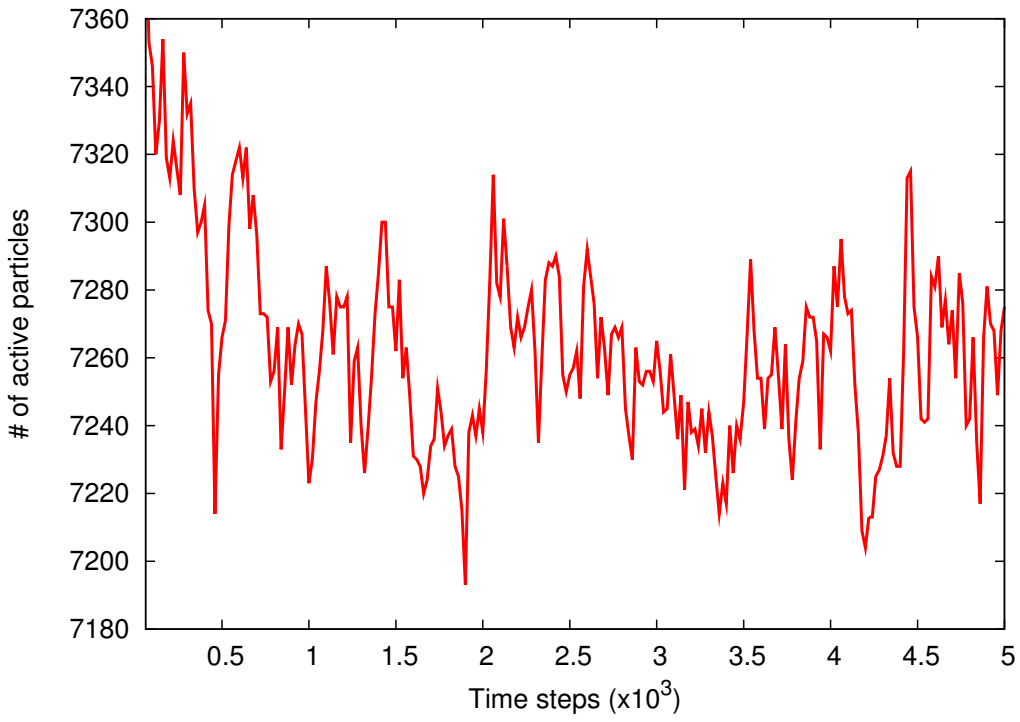

Figure 5.14 Evolution of the active number of particles in a reference MD simulation, with initially 8788 particles. The procedure for changing the (active/passive) status of particles is performed every 20 time steps.

To illustrate the feasibility of this extension, we have developed a toy model where particles are selected at random to change from active to passive particles. Passive particles remain in the simulation but do not contribute to the overall statistics such as temperature, displacement, etc. Particles are made passive when the fraction of nearest neighbours from a different type is ≤ 0.2, with two different types defined as in section 5.6.2. Passive particles are made active at random with a probability $1/20$. Fig. 5.14 displays the evolution of the active number of particles in the simulation system. It is clear that large deviations in the number of particles can be achieved by using such a set-up. This could be used as a tool to take into account the investors that enter or leave a certain stock market.

5.6.3 Crash dynamics

One generic feature of financial markets that wasn't replicated by the non-equilibrium MD simulation is the crash dynamics as observed in the S&P 500 by [KSY06]. In order to have a complete understanding of the dynamics of financial markets in terms of a non-equilibrium MD simulation system, this feature should be incorporated in this model.

Volatility time series of crash time window

As we have mentioned in the previous section, the magnitude of the shock in the MD simulation could be used as a measure for the volatility of the financial time series. The first condition that has to be met is the usage of the volatility time series as input for the magnitude of the shock as in section 5.6.2. If this results in the correct behaviour for the single time step displacement distributions during non-crash time windows, we can investigate what happens when the volatility time series of a crash period is used. In this way, we assume that volatility is the main contributor to the crash dynamics. If this method fails to reproduce these dynamics we could conclude that the volatility is not the main contributor to the crash dynamics.

Phase transition

As is clear form [KSY06], the crash dynamics of the S&P 500 behave like a different phase of the dynamics of the financial market. Because of the presence of the scale-free behaviour in the return distributions, one should look to emulate this property by making the MD simulation system scale-free.

A natural way of making a scale-free simulation system is by forcing it to make a phase transition. A phase transition from the gaseous phase to the liquid phase is rather ill-defined in the MD simulation set-up because there is no strict way to identify the different phases. The RDF of the solid phase, on the other hand, is clearly different from those of the gaseous and liquid phase is distinctly different from those of the gaseous and liquid phase. One can use this to create a liquid-solid phase transition, by controlling the density and temperature of the system. In this way, one can investigate if there is a possibility of scale-free behaviour in the displacement distributions during this phase transition.

Chapter 6

Conclusions and outlook

Now this is not the end.
It is not even the beginning of the end.
But it is, perhaps, the end of the beginning.
Sir Winston Churchill

In the previous chapters, we have tried to connect the dynamics of financial time series to the dynamics of a non-equilibrium MD set-up in the liquid phase. In doing this, we have pointed out that many processes in economics, such as the evolution of option prices, can be interpreted as a diffusion process. We have chosen to model such processes via an MD simulation in the liquid phase, which has well-known self-diffusion properties. In order to develop a MD model that could reproduce the generic features of financial time series, we had to abandon the equilibrium MD simulation system and turn to a non-equilibrium MD model. In a next step, the behaviour of the generic features of this model are examined and a possible mechanism to match the essential variables in both the financial system and the MD model is proposed. Finally, some possible extensions and refinements of the model are introduced.

6.1 Diffusion in economics

We have shown in Chapter 2 that, from the earliest attempts to model the time evolution of financial variables, diffusion processes can be used to understand the dynamics of financial markets. The first mathematical attempt to model financial time series was Bachelier's Brownian motion model, which is essentially a diffusion process of an option price. Geometric Brownian motion (GBM) is a major improvement of this model. It

uses a diffusion process for the returns (relative price changes) and not for the absolute price changes. The GBM model is a fundamental piece of input in the derivation of the Black-Scholes (B-S) formula for option pricing. Indeed, it models the time evolution of the price of the underlying stock. All further improvements of the B-S model are based on diffusion processes, be it for the evolution of the price of the underlying or the evolution of the volatility or the evolution of the interest rate. This is further illustrated in section 2.3.4.

Because of the ubiquity of diffusion processes in the modelling of financial time series, one can conjecture that models from physics which are powerful at simulating diffusion are interesting to model financial time series. One such powerful model is the molecular dynamics model, presented in Chapter 3. This technique offers a very natural way of simulating interactions between a large number of particles (or *agents*). It also has the distinct advantage of having a physical discretized time step that separates two subsequent configurations of the simulation system. Diffusion in a liquid is a typical topic that can be examined using the MD technique. In this way, it is also a candidate for simulating financial markets. Indeed, both systems are essentially a large group of agents that interact with each other and have emergent properties on the macro scale, such as crashes or phase transitions, that are not directly encoded in the interactions on the micro scale.

In order to assess the quality of performance of a model designed for financial markets, it is of the utmost importance to put forward a number of generic universal features of financial time series that can be used as a benchmark. To identify those generic features we have analyzed the time series of some well-known financial indices from different parts of the world: the S&P 500, the DAX, and the Nikkei 225. This analysis identified four well documented generic features of the time series of financial assets.

The first feature is the presence of non-Gaussian return distributions. This points towards anomalous diffusion as the underlying dynamical process that governs the time evolution of stock prices. The second feature is the short memory of the returns (of the order of minutes) which expresses the fact that no arbitrage opportunities are present in the market. The third feature is related to the observed volatility of financial markets. While there is only a short memory for the returns, a long memory (of the order of hours) is observed for the volatility.

The fourth feature touches upon an aspect in the dynamics of financial markets that is of concern to every investor and even almost every human being on this planet: market crashes. The multi-scale analysis of the S&P 500 time series by the Tokyo group [KSY06] identified two phases in the operation of the S&P 500 between 1984 and 1995.

During non-crash time periods, there is a convergence of the return distributions to normality for large time windows. No such convergence is observed for crash time periods, where the return distributions are scale-free and retain their non-Gaussian character over long time periods.

Testing an MD simulation involves testing the behaviour of the equivalent features in MD. A comparison between these properties in MD and the behaviour of the generic features in the GBM model is given at the start of Chapter 5. Both models (GBM and MD) are governed by the dynamics of normal diffusion and this results in Gaussian distributions for the returns. In the MD simulation, the single time step displacement distributions are the equivalent of the return distributions of financial time series. The MD model outperforms the GBM model on the aspect of time correlations in the system. In the GBM model, there are no correlations in the returns, and an infinite correlation (in time) in the volatility (because it is a constant value). The dynamics of MD, on the other hand, result in finite correlations in the steps and a long memory for the correlations of the absolute velocities. In this case, the absolute velocities are used to examine the behaviour of the volatility, since they have the same properties as the volatility in financial time series. Since both models already have Gaussian distributions at the shortest time scale, one cannot expect to observe the scale-free behaviour of the return distributions that is reminiscent of the crash dynamics.

6.2 The need for out-of-equilibrium MD

To improve the equilibrium MD model, we need to address the problem of the Gaussian single time step displacement (δx) distributions. In equilibrium MD, the δx are governed by Gaussian dynamics and are of a certain scale determined by the diffusion coefficient. In markets, one observes a small amount of returns that are much larger than average. This points to non-Gaussian dynamics. We wished to develop a rather simple simulation system to generate non-Gaussian self-diffusion. In this way, we could emulate the heavy tails in the return distributions of financial markets. In order to remedy this problem, we have developed a non-equilibrium MD set-up that produces anomalous single time step displacement distributions. The occurrence of these distributions results in a proper modelling of the first generic feature. An important property of this set-up is the soft-core interaction of the particles. This soft-core potential is introduced to be able to handle fast-moving particles, which is impossible with hard-core potentials. A hard-core potential (like the Lennard-Jones potential) combined with out-of-equilibrium dynamics gives rise to unstable systems.

The MD simulation system is driven out-of-equilibrium via a rescaling of the length scale of the interaction. This rescaling results in local regions of higher-than-average potential energy that dissipates partly into kinetic energy during the evolution to a new equilibrium state. The effect of this rescaling of the spatial coordinates onto the properties of the MD simulation are outlined in Chapter 4. It is shown that the method for generating anomalous self-diffusion is very robust, and produces comparable results for a broad range of the parameters that can be tuned. This robustness makes it a suitable candidate to simulate the variety of financial time series that exists worldwide.

The out-of-equilibrium MD model thus simulates the proper behaviour for three of the four benchmark features of financial time series. Examining the dynamics of the displacement distributions for larger time windows determines whether the non-equilibrium MD simulation mimics the normal operation or the crash dynamic of the S&P 500. The observed distributions display a convergence to the normal distribution for large time windows. We can consequently conclude that no crash dynamics is present in this set-up. The out-of-equilibrium MD model mirrors the normal operation (non-crash) dynamics of financial markets.

6.3 Linking MD to financial variables

We deem that reproducing the generic features of financial markets cannot be considered as a sufficient condition to establish out-of-equilibrium MD as a valid model for the underlying dynamics of financial time series. One has to establish a firm link between the variables in both systems in order to be able to learn more about the dynamics of financial markets. The two variables that are involved in the S&P 500 time series are the time and the price (value) of the index. These need to be mapped onto the time and spatial variables of the MD simulation.

The time variables can be linked via the autocorrelation functions of the returns and the displacements. Indeed, both functions have a finite autocorrelation time. The ratio of these autocorrelation times can be used to scale the MD time onto the physical time of the S&P 500 time series.

Another way to verify the mapping of the time units is via the multi-scale analysis of the return and displacement distributions. These distributions converge to a normal distribution for a certain magnitude of the time window. The sizes of the time windows, at which point this evolution is finished, can be used to construct another ratio for the time scales. The resulting ratios of both methods have the same order of magnitude and this strengthens the validity of the linking between both time scales.

Linking the spatial variables requires a more elaborate approach. Comparing the return distribution with the single time step displacement distribution (by examining the behaviour of the first generic feature) implies a mapping of the normalized returns onto the normalized displacements. This mapping is, however, not consistent on all time scales. To make such a link, one has to perform a local and time dependent coordinate transformation, that is too involved to be manageable. A maneagable mapping is proposed in the form of a global coordinate transformation. In this way, the long-term trends of financial time series can be captured in the parameters of the global coordinate transformation.

These links establish a firm connection between both simulation systems, which enables one to use the non-equilibrium MD set-up to model a preferred financial time series. This model captures the dynamics of this financial time series up-to a certain level. The presence of the three generic features, that are not dependent on some fine-tuning of parameters is a major advantage of the model. At this point, our non-equilibrium MD system cannot reproduce the peculiar features of the return distributions during typical crash periods.

6.4 Outlook

Interpreting what the radial rescalings represent in a financial context will be of utmost importance in progressing this model. The 'shocks' have profound effects on the simulation system and they correspond with more-than-average influxes of entropy or information. The magnitude of the shocks could also be linked to the magnitude of the volatility in financial markets. In this way, the simulation system can be made more realistic by varying this magnitude, as is for example done in GARCH-like models.

Another way of progressing the model is by making the basic building blocks of the model more realistic. For instance, the number of particles in the simulation system can be made to vary so as to better simulate the changing number of investors or stocks in a financial system. Different types of particles can also be introduced, which could make the simulation behave as an agent-based model. In this way, both homogeneous and heterogeneous set-ups can provide insights into the dynamics of markets.

One essential feature that is not emulated by this model is the crash dynamics. Using the volatility time series of crash periods as input for the simulation system could be instrumental in generating these dynamics. The main principle of these dynamics is the scale-free behaviour of the return distributions. Replicating this scale-free behaviour could be done by driving the simulation into a phase transition.

These different suggestions ensure that out-of-equilibrium MD simulations will remain interesting for modelling financial markets and will provide many challenges of which crash dynamics forms only a first step.

Appendix A

Diffusion in Physics

Diffusion problems are omnipresent and have a long history in physics. Here we present some basic equations and insights.

A.1 Diffusion equation

Diffusion equations date back to Fick's laws of 1855 [Fic55]. Without any prior knowledge of the structure of matter he was able to link, on a macroscopic basis, the flux $\vec{J}(\vec{r},t)$ and the density $\rho(\vec{r},t)$. This is known as Fick's first law:

$$\vec{J}(\vec{r},t) = -D\nabla\rho(\vec{r},t) \ , \tag{A.1}$$

with D the diffusion constant, $\vec{r}$ the position vector and time t.

In combination with the mass balance:

$$\frac{\partial\rho(\vec{r},t)}{\partial t} + \nabla\cdot\vec{J}(\vec{r},t) = 0 \ , \tag{A.2}$$

Fick's first law leads to Fick's second law:

$$\frac{\partial\rho(\vec{r},t)}{\partial t} = D\nabla^2\rho(\vec{r},t) + \nabla D\cdot\nabla\rho(\vec{r},t) \ . \tag{A.3}$$

This partial differential equation relates the changes in time of the density to the diffusion in space.

A solution in one dimension and for constant diffusion parameter D can be found:

$$\rho(r,t) = \frac{1}{\sqrt{4\pi Dt}}\exp\left[-\frac{r^2}{4Dt}\right] \ , \tag{A.4}$$

which is a Gaussian density function with mean zero and variance $4Dt$. Historically, this equation could for the first time establish a link between Gaussian distributions and normal diffusion.

A.2 Brownian motion

A classic example of a diffusion process is Brownian motion. Brown [Bro32] observed that large particles that are floating around in a liquid, could still move around and are not stationary by any means. It was Lord Rayleigh [Ray80] who showed that the probability of travelling a distance between R and $R + dR$ in N steps is

$$P_N(R) \sim \frac{2R}{N} e^{-\frac{R^2}{N}} , \tag{A.5}$$

but his research was not related to Brownian motion but was about sound waves in heterogeneous materials. The term random walk and Brownian motion are practically interchangeable and the first was originally proposed by Karl Pearson in 1905 [Pea05]. In his article he addressed the question how mosquito's are distributed in a forest given that they had travelled a fixed length multiple times. It was Einstein [Ein05] who made Brownian motion famous with his 1905 article. This work resulted in one of the proofs for the molecular structure of nature [Per09].

A random walk (in d dimensions) is determined by the time step Δt and the step $\vec{r}_i$. Every step is drawn from a probability distribution $p_i(\vec{r})$. The global positions after N time steps is the sum of all the steps:

$$\vec{R}_N = \vec{r}_1 + \vec{r}_2 + \ldots + \vec{r}_N . \tag{A.6}$$

If the magnitude of step $\vec{r}_i$ depends on the previous steps, the conditional probability has to be used:

$$p_i(\vec{r}|\vec{r}_{i-1}, \vec{r}_{i-2}, \ldots, \vec{r}_1) \equiv Prob(\vec{r}_i|\vec{r}_{i-1}, \vec{r}_{i-2}, \ldots, \vec{r}_1) . \tag{A.7}$$

In the case of a Markov chain, the conditional probability only depends on the previous step, and the probability of finding the particle at R after N steps becomes

$$P_N(\vec{R}) = \int p_N(\vec{r}|\vec{R} - \vec{r}) P_{N-1}(\vec{R} - \vec{r}) d^d\vec{r} . \tag{A.8}$$

If the transition probability is translationally invariant, one has $p_N(\vec{r}|\vec{R}) = p_N(\vec{r})$, which means that the step does not depend on the current position. This reduces the integral in the right hand side of Eq. A.8 to a convolution and gives us Bachelier's equation:

$$P_N(\vec{R}) = \int p_N(\vec{r}) P_{N-1}(\vec{R} - \vec{r}) d^d\vec{r} . \tag{A.9}$$

Using a Taylor expansion, it can be shown that

$$\frac{P_N(\vec{R}) - P_{N-1}(\vec{R})}{\Delta t} = \frac{\langle \vec{r}^{\,2} \rangle}{2d\Delta t} \nabla^2 P_{N-1}(\vec{R}) , \tag{A.10}$$

with d the dimension of the system. Taking the limits $N \to \infty$ and $\Delta t \to 0$, and with the density $\rho(\vec{R}, t \equiv N\Delta t) \equiv P_N(\vec{R})$, this becomes Fick's second law:

$$\frac{\partial \rho(\vec{R}, t)}{\partial t} = D\nabla^2 \rho(\vec{r}, t) \ . \tag{A.11}$$

From this equality an expression for the diffusion constant can be found:

$$D = \frac{\langle \vec{r}^2 \rangle}{2d\Delta t} \ . \tag{A.12}$$

This derivation gives another link between the random walk, normal diffusion and the Gaussian distribution. A more formal link between the random walk and the Gaussian distribution can be found via the Central Limit Theorem (CLT). After defining moments and cumulants of a distribution we will derive the CLT.

A.2.1 Moments and cumulants

To calculate the moments and cumulants one rewrites the probability distribution function (PDF),

$$P_N = P_0 * p_1 * p_2 * p_3 * \ldots * p_N \ , \tag{A.13}$$

where $*$ denotes the convolution and P_0 is the PDF of the initial position.

Convolutions are best treated in terms of Fourier transforms, where they become simple products.

$$\widehat{f * g}(\vec{k}) = \widehat{f}(\vec{k})\widehat{g}(\vec{k}) \ , \tag{A.14}$$

with $\widehat{\ }$ denoting the Fourier transform.

For a fixed initial position ($\widehat{P}_0 = 1$) the PDF after N steps $P_N(\vec{k})$ becomes

$$\widehat{P}_N(\vec{k}) = \widehat{p}_1(\vec{k})\widehat{p}_2(\vec{k}) \ldots \widehat{p}_N(\vec{k}) = \prod_{n=1}^{N} \widehat{p}_n(\vec{k}) \ . \tag{A.15}$$

If the distributions are identical for every step, i.e. in a stationary system, one can write:

$$\widehat{P}_N(\vec{k}) = \left(\widehat{p}_1(\vec{k})\right)^N \ . \tag{A.16}$$

There is one boundary condition for these PDFs,

$$\widehat{P}(\vec{0}) = \int_{-\infty}^{\infty} P(\vec{x}) d^d\vec{x} = 1 \ , \tag{A.17}$$

as $P(\vec{x})$ is normalized.

A.2.1.1 Moments

In the one-dimensional case, the moments of a random variable are defined as

$$\begin{aligned} m_1 &= \langle x \rangle \\ m_2 &= \langle x^2 \rangle \\ &\vdots \\ m_n &= \langle x^n \rangle \end{aligned} \tag{A.18}$$

In probability theory a characteristic function $\widehat{P}(\vec{k})$ is often referred to as a *moment generating function*, because the moments can be calculated by means of a Taylor expansion around the origin. For the one-dimensional situation one has:

$$\begin{aligned} \widehat{P}(\vec{k}) &= \sum_{n=0}^{\infty} \frac{(-i)^n k^n m_n}{n!} \\ &= 1 - i m_1 k - \frac{1}{2} m_2 k^2 + \dots \end{aligned} \tag{A.19}$$

with,

$$m_n = i^n \frac{\partial^n \widehat{P}}{\partial k^n}(0) \ , \tag{A.20}$$

the n-th moment of the PDF.

A.2.1.2 Cumulants

Cumulants form a very natural way of describing PDFs because they give basic information about the width and shape of the distribution. The *cumulant generating function* is defined as

$$\psi(\vec{k}) = \ln \widehat{P}(\vec{k}) \ . \tag{A.21}$$

This function is linked to the original PDF via:

$$P(\vec{x}) = \int e^{i\vec{k}\cdot\vec{x}} \widehat{P}(\vec{k}) \frac{d\vec{k}}{2\pi} = \int e^{i\vec{k}\cdot\vec{x} + \psi(\vec{k})} \frac{d\vec{k}}{2\pi} \ . \tag{A.22}$$

The cumulants c_i are given by:

$$\psi(k) = -i c_1 k - \frac{1}{2} c_2 k^2 + \dots \tag{A.23}$$

Since the moment generating function and the cumulant generating function are linked, we can also link the cumulants with the moments of the PDF. Writing $\psi(k)$ in terms of the moments results in:

$$\begin{aligned}\psi(k) &= \ln \widehat{P}(k) = \ln\left(1 - im_1k - \frac{1}{2}m_2k^2 - \frac{i}{6}m_3k^3 + \frac{1}{4}m_4k^4\right) \\ &= -im_1k + \frac{1}{2}(m_1^2 - m_2)k^2 - \frac{i}{6}\left(m_3 - 3m_1m_2 + 2m_1^3\right)k^3 \\ &+ \frac{1}{24}\left(m_4 - 4m_1m_3 - 3m_2^2 + 12m_2m_1^2 - 6m_1^4\right)k^4 + \mathcal{O}(k^5)\ , \end{aligned} \tag{A.24}$$

with,

$$\ln(1+x) = x - \frac{x^2}{2} + \frac{x^3}{3} - \frac{x^4}{4} + \mathcal{O}(x^5)\ . \tag{A.25}$$

From the above derivations it is clear that the first four cumulants are related to (m_1, m_2, m_3, m_4) by means of:

$$\begin{aligned} c_1 &= m_1 \\ c_1 &= m_2 - m_1^2 \\ c_1 &= 2m_1^3 - 3m_1m_2 + m_3 \\ c_4 &= -6m_1^4 + 12m_1^2m_2 - 3m_2^2 - 4m_1m_3 + m_4\ . \end{aligned} \tag{A.26}$$

A.2.2 Skewness and kurtosis

The third and fourth cumulant are better known in their normalized variants:

$$\lambda_3 = \frac{c_3}{c_2^{3/2}} \quad \lambda_4 = \frac{c_4}{c_2^2}\ . \tag{A.27}$$

The skewness λ_3 presents a measure for the asymmetry of the tails of the distribution, see Fig. A.2.2. If a distribution has more tail-events to the right of the peak than to the left, the skewness will be positive. A negative skewness is characteristic for a distribution with more tail-events to the left of the peak of the distribution. The kurtosis λ_4 represents the ratio of the number of tail-events to peak-events (Fig. A.2.2). For a normal distribution, the kurtosis vanishes. A leptokurtic distribution is a distribution with more tail events and less peak events than a normal distribution and has a kurtosis $\lambda_4 > 0$. A mesokurtic distribution has less tail events and more peak events than a normal distribution, $\lambda_4 < 0$.

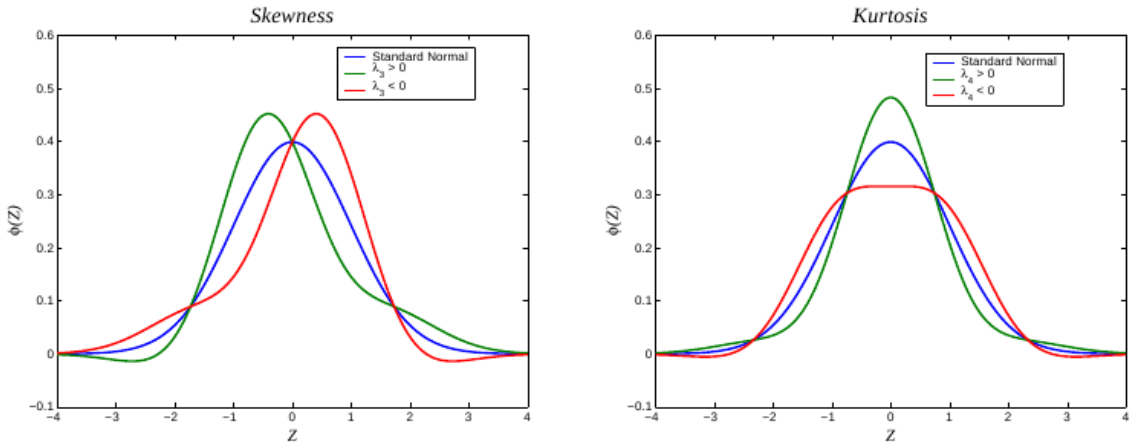

Figure A.1 Skewness ($< 0,\ 0,\ > 0$) for different distributions (left). Kurtosis ($< 0,\ 0,\ > 0$) for different distributions (right).

A.3 Central limit theorem

The CLT states that the sum of n random variables that are independent and identically distributed, converges to a normal distribution, irrespective of the shape of the underlying distribution, as long as it has a finite mean and variance. A formal statement of the theorem uses S_n, the sum of n independent and identically distributed random variables with mean μ and variance σ^2:

$$S_n = X_1 + X_2 + \cdots + X_n \ . \tag{A.28}$$

With this, a new random variable Z_n can be defined as

$$Z_n = \frac{S_n - n\mu}{\sigma\sqrt{n}} \ , \tag{A.29}$$

that can be shown to converge to a standard normal distribution:

$$Z_n \to \mathcal{N}(0,1) \ . \tag{A.30}$$

The convergence of the random variable can be expressed as

$$\lim_{n\to\infty} P(Z_n \leq z) = \Phi(z) \ , \tag{A.31}$$

with $\Phi(z)$ the cumulative distribution of $\mathcal{N}(0,1)$.

For a finite number of random variables, the CLT can be used to define a *central region* where the convergence to a normal distribution can be expected.

A.3.1 Stable functions

For distributions that don't have a finite variance, a generalized central limit theorem can be used. It states that the sum of random variables will converge to a stable distribution, with parameters that depend on the tail behaviour of the underlying distribution. A stable distribution is a distribution for which the sum of two independent variables has a distribution with an identical shape as the original distribution. The normal distribution is an example of such a stable distribution.

The most general way of describing stable functions is via the α-stable Lévy distribution ($\mathcal{L}(x)$) [Lév54]. It only has an analytical expression for its Fourier transform:

$$\varphi(k;\mu,c,\alpha,\beta) = \exp\left[\, ik\mu - |ck|^{\alpha}\,\left(1 - i\beta\,\mathrm{sgn}(k)\tan(\frac{\alpha\pi}{2})\right)\,\right]\,, \tag{A.32}$$

which uses four parameters α, β, μ, c to define its shape. The parameter that defines the behaviour of the tail is α, that is limited to the interval $]0, 2]$. The power law tails of the distribution are governed by

$$\mathcal{L}(x) \sim x^{-(\alpha+1)}\,, \text{for } x \to +\infty\,. \tag{A.33}$$

In this way, anomalous diffusion can be described by an α-stable Lévy distribution.

A.4 Anomalous diffusion in physics

Normal diffusion has the typical property that the variance of the travelled distance grows linearly with time as in Eq. A.12:

$$\sigma^2(t) = \left\langle \vec{r}^{\,2}(t) - \langle \vec{r}(t)\rangle^2 \right\rangle \sim t\,. \tag{A.34}$$

Anomalous diffusion on the other hand is characterised by a non-linear growth of the variance with time

$$\sigma^2(t) = \left\langle \vec{r}^{\,2}(t) - \langle \vec{r}(t)\rangle^2 \right\rangle \sim t^{\nu}\,, \quad \nu > 0\,, \quad \nu \neq 1\,. \tag{A.35}$$

A.4.1 Different types anomalous diffusion

Anomalous can be characterised by the coefficient ν. There exist two different categories of anomalous diffusion: subdiffusion and superdiffusion, with normal diffusion the boundary between both phenomena.

A.4.1.1 Subdiffusion

Subdiffusion occurs for $\nu < 1$. Here, the diffusion process is slower than the normal diffusion process. Subdiffusion is a process that typically takes place for diffusion in a medium with traps, in which particles are bound for a certain time. This kind of process is described by the continuous time random walk (CTRW) model [MK00, GMV07]. The CTRW can also be used to describe financial time series [MMW03, MMPW06, MS06]. Other examples include diffusion in photocopiers [SM75] and diffusion in cells [WGR+04, SRK+05].

A.4.1.2 Superdiffusion

If the coefficient ν is larger than the value for normal diffusion ($\nu > 1$), superdiffusion occurs. Again, the CTRW model can be used to describe processes that display superdiffusion [MZ07, MK00]. Typical examples include the search patterns of animals [RFMM+04, EPW+07].

Appendix B

Ito's Lemma

Ito's lemma gives a description how to compute the differential of a composite function $f(x,t)$, if x follows a stochastic differential equation (SDE).

B.1 Chain rule of calculus

In standard calculus, a differential equation is simple to write for an ordinary function $x(t)$

$$\frac{dx}{dt} = a(x,t) \ . \tag{B.1}$$

For a more involved function $f(x(t),t)$, the chain rule applies and the derivative of f becomes:

$$\frac{df(x(t),t)}{dt} = \frac{\partial f}{\partial x}\frac{dx}{dt} + \frac{\partial f}{\partial t} = f_x \frac{dx}{dt} + f_t \ , \tag{B.2}$$

with $\frac{\partial f}{\partial x} = f_x$ and $\frac{\partial f}{\partial t} = f_t$. Using Eq. B.1, the derivative becomes:

$$\frac{df(x(t),t)}{dt} = a(x,t) f_x + f_t \ . \tag{B.3}$$

This simple chain rule doesn't apply to a stochastic differential equation, such as Eq. B.5, essentially because Brownian motion (z) isn't differentiable. This results from the stochastic factor of $dz \approx \sqrt{dt}$.

B.2 Ito's Lemma for brownian motion

Ito's Lemma allows to compute the differential of a function $f(x(t),t)$, when the SDE of $x(t)$ is known.

An elegant way of deriving Ito's Lemma is by starting from the Taylor expansion of df.

$$\begin{aligned} df &= f(x(t+dt), t+dt) - f(x(t), t) \\ &= f_t dt + f_x dx + \frac{1}{2} f_{tt} (dt)^2 + \frac{1}{2} f_{xx} (dx)^2 + f_{xt} dx dt + \dots \end{aligned} \tag{B.4}$$

Using the SDE of $x(t)$:

$$dx = a(x,t)dt + b(x,t)dz \ , \tag{B.5}$$

the differential becomes

$$\begin{aligned} df &= f_t dt + f_x (a(x,t)dt + b(x,t)dz) + \frac{1}{2} f_{tt} (dt)^2 + \frac{1}{2} f_{xx} (a(x,t)dt + b(x,t)dz)^2 \\ &+ f_{xt} (a(x,t)dt + b(x,t)dz)dt + \dots \\ &= f_t dt + f_x a(x,t)dt + f_x b(x,t)dz + \frac{1}{2} f_{tt} (dt)^2 \\ &+ \frac{1}{2} f_{xx} \left(a^2(x,t)(dt)^2 + 2a(x,t)b(x,t)dtdz + b^2(x,t)(dz)^2 \right) \\ &+ f_{xt} \left(a(x,t)(dt)^2 + b(x,t)dzdt \right) + \dots \end{aligned} \tag{B.6}$$

We can now perform an essential approximation, which restricts the differential to first order in dx and dt. To do this, we need to realize that terms in dz are of the order of $dt^{1/2}$, and keep terms upto dz^2. This restricts the differential to

$$df = f_t dt + f_x a(x,t)dt + f_x b(x,t)dz + \frac{1}{2} f_{xx} b^2(x,t)(dz)^2 \ . \tag{B.7}$$

Replacing $(dz)^2 = dt$ this becomes Ito's lemma:

$$df = (f_t + f_x a(x,t) + \frac{1}{2} f_{xx} b^2(x,t))dt + f_x b(x,t)dz \ . \tag{B.8}$$

Appendix C

Black-Scholes formula

We will derive the Black-Scholes formula for a simple European call and put option using two different methods. The first methods uses techniques drawn from physics. It is based on solving a simple diffusion equation with adequate boundary conditions. The second method uses the risk-neutral interest rate r, to define the price of the stock at time T.

Once the B-S formula for a European call option is derived, we can use put-call parity to derive the corresponding formula for a European put option.

C.1 Solution using a diffusion equation

It is possible to rearrange the B-S equation so as to make it into a diffusion equation, for which standard methods exists to compute the solution. The B-S equation in its standard form is

$$c_t + rSc_S + \frac{\sigma^2 S^2}{2} c_{SS} = rc \ . \tag{C.1}$$

The payoff of a European call option is $\max(S_T - K, 0)$, with S_T the stock price at expiration date T and K the strike price. Another boundary condition is:

$$c(0,t) = 0 \ , \forall t \ , \tag{C.2}$$

which simply states that the option is worthless if the underlying is worthless. The last boundary condition states that for very large stock prices, the strike price is negligible:

$$c(S,t) \to S \text{ if } S \to \infty \ . \tag{C.3}$$

The following change in variables:

$$S = K \exp(x) \tag{C.4}$$

$$t = (T - \tau)\frac{2}{\sigma^2} \ , \tag{C.5}$$

leads to differentials of the form:

$$\frac{dS}{S} = dx \tag{C.6}$$

$$dt = -\frac{2}{\sigma^2}d\tau \ , \tag{C.7}$$

Thus Eq. C.1 can be written as a general linear parabolic equation for the function $u(x,\tau) = Kc(S,t)$:

$$\frac{\partial u}{\partial \tau} = \frac{\partial u^2}{\partial x^2} + a\frac{\partial u}{\partial x} + bu \ , \tag{C.8}$$

with $a = \frac{2r}{\sigma^2} - 1$ and $b = \frac{-2r}{\sigma^2}$. The boundary condition for the price of the derivative becomes not an end condition ($t = T$), but an initial condition $\tau = 0$:

$$u(x,0) = \max(e^x - 1, 0) \ . \tag{C.9}$$

The standard way of reducing a linear parabolic equation to a diffusion equation:

$$\frac{\partial v}{\partial \tau} = \frac{\partial^2 v}{\partial x^2} \ , \tag{C.10}$$

is by using:

$$v(x,\tau) = \exp(\alpha x + \beta\tau)u(x,\tau) \ . \tag{C.11}$$

In this case, the parameters α and β are:

$$v = u \exp\left[\frac{ax}{2}\right] \exp\left[(a^2/4 - b)\tau\right] \ . \tag{C.12}$$

The derivatives of this function are:

$$\frac{\partial v}{\partial \tau} = \left(\frac{\partial u}{\partial \tau} + (a^2/4 - b)u\right) \exp\left[\frac{ax}{2}\right] \exp\left[(a^2/4 - b)\tau\right] \tag{C.13}$$

$$\frac{\partial^2 v}{\partial x^2} = \left(\frac{\partial^2 u}{\partial x^2} + a\frac{\partial u}{\partial x} + \frac{a^2}{4}u\right) \exp\left[\frac{ax}{2}\right] \exp\left[(a^2/4 - b)\tau\right] \ . \tag{C.14}$$

And the eventual boundary condition is:

$$v(x,0) = \max\left(\exp\frac{1}{2}(k+1)x - \exp\frac{1}{2}(k-1)x, 0\right) \ . \tag{C.15}$$

The diffusion equation can now be solved via a Fourier transform:

$$v(x,\tau) = \frac{1}{2\sqrt{\pi\tau}} \int_{-\infty}^{+\infty} v(y,0) \exp\left[-\frac{(x-y)^2}{4\tau}\right] dy \ . \tag{C.16}$$

The boundary condition can than be used to limit the integration range of y (see section C.2) and the eventual result becomes:

$$c(S,t) = S_0 N(d_1) - K\exp[-r(T-t)]N(d_2)\ , \tag{C.17}$$

with

$$d_1 = \frac{1}{\sigma\sqrt{T-t}}\left(\ln\left[\frac{S_0}{K}\right] + \left[r + \frac{\sigma^2}{2}\right](T-t)\right)\ ,\ d_2 = d_1 - \sigma\sqrt{T-t}\ . \tag{C.18}$$

With,

$$N(x) = \frac{1}{\sqrt{2\pi}}\int_{-\infty}^{x}\exp[\frac{-y^2}{2}]dy\ , \tag{C.19}$$

the cumulative normal distribution.

C.2 Derivation using risk-neutral pricing

Using risk-neutral pricing means that we expect the first term of the SDE, which determines the long-term behaviour of the stock price, to be equal to the risk-neutral growth: $\mu = r$. This eliminates the need to solve the B-S equation as a diffusion problem.

The stock price under the risk-neutral condition is:

$$S_T = S_0\exp\left[(r - \frac{\sigma^2}{2})T + \sigma\sqrt{T}Y\right]\ , \tag{C.20}$$

with S_0 the stock price at the initial time and Y a gaussian random variable drawn from $N(0,1)$. Using this risk-neutral pricing, the price of the derivative is:

$$c(S,0) = e^{-rT}E\left(S_0\exp\left[(r - \frac{\sigma^2}{2})T + \sigma\sqrt{T}Y\right] - K\right)^+\ , \tag{C.21}$$

where the $+$ denotes this value if it is greater than 0 and 0 otherwise. The factor e^{-rT} reduces the amount of money at time T to an initial amount of money, via the risk-neutral return rate. The expectation value $E[\ ]$ of this function can be written as an integral over the possible values of Y:

$$c(S,0) = e^{-rT}\int_{-\infty}^{\infty}\left(S_0\exp\left[(r - \frac{\sigma^2}{2})T + \sigma\sqrt{T}x\right] - K\right)^+\frac{1}{\sqrt{2\pi}}e^{-\frac{x^2}{2}}dx\ . \tag{C.22}$$

The boundaries for x are $[-\infty,\infty]$, but this can be reduced using the condition that the integrand has to be larger than 0:

$$\begin{aligned} S_0\exp\left[(r - \frac{\sigma^2}{2})T + \sigma\sqrt{T}x\right] - K &\geq 0 \\ \Leftrightarrow \exp[\sigma\sqrt{T}x] &\geq \frac{K}{S_0}\exp[-(r - \frac{\sigma^2}{2})T] \\ \Leftrightarrow x &\geq \frac{1}{\sigma\sqrt{T}}\left(\ln\left[\frac{K}{S_0}\right] - \left[r - \frac{\sigma^2}{2}\right]T\right)\ . \end{aligned} \tag{C.23}$$

We can use this lower boundary on x: $T_1 = \frac{1}{\sigma\sqrt{T}}\left(\ln\left[\frac{K}{S_0}\right] - \left[r - \frac{\sigma^2}{2}\right]T\right)$, which reduces the integral to:

$$\begin{aligned}
c(S,0) &= e^{-rT}\int_{T_1}^{\infty}\left(S_0\exp\left[(r-\frac{\sigma^2}{2})T+\sigma\sqrt{T}x\right]-K\right)\frac{1}{\sqrt{2\pi}}e^{-\frac{x^2}{2}}dx \\
&= \frac{S_0\exp\left(-\frac{\sigma^2 T}{2}\right)}{\sqrt{2\pi}}\int_{T_1}^{\infty}\exp\left[\sigma\sqrt{T}x-\frac{x^2}{2}\right]dx - \frac{K\exp\left(-rT\right)}{\sqrt{2\pi}}\int_{T_1}^{\infty}\exp\left[-\frac{x^2}{2}\right]dx \\
&= \frac{S_0}{\sqrt{2\pi}}\int_{T_1}^{\infty}\exp\left[-\frac{1}{2}(x-\sigma\sqrt{T})^2\right]dx - K\exp[-rT](1-N(T_1)) \\
&= \frac{S_0}{\sqrt{2\pi}}\int_{T_1-\sigma\sqrt{T}}^{\infty}\exp[-y^2]dy - K\exp[-rT](1-N(T_1)) \\
&= S_0(1-N(T_1-\sigma\sqrt{T})) - K\exp[-rT](1-N(T_1))\ , \qquad \text{(C.24)}
\end{aligned}$$

with a transformation of variables: $y = x - \sigma\sqrt{T}$.

The arguments of the cumulative normal distribution can be reworked to

$$1-N(T_1-\sigma\sqrt{T}) = N(-(T_1-\sigma\sqrt{T})) = N\left(\frac{1}{\sigma\sqrt{T}}\left(\ln\left[\frac{S_0}{K}\right]+\left[r+\frac{\sigma^2}{2}\right]T\right)\right)\ , \qquad \text{(C.25)}$$

and,

$$1-N(T_1) = N(-T_1) = N\left(\frac{1}{\sigma\sqrt{T}}\left(\ln\left[\frac{S_0}{K}\right]+\left[r-\frac{\sigma^2}{2}\right]T\right)\right)\ . \qquad \text{(C.26)}$$

This eventually results in the Black-Scholes formula:

$$c(S,0) = S_0N(d_1) - K\exp[-rT]N(d_2)\ , \qquad \text{(C.27)}$$

with

$$d_1 = \frac{1}{\sigma\sqrt{T}}\left(\ln\left[\frac{S_0}{K}\right]+\left[r+\frac{\sigma^2}{2}\right]T\right)\ ,\ d_2 = d_1 - \sigma\sqrt{T}\ . \qquad \text{(C.28)}$$

C.3 Put-call parity

Put-call parity is an essential property to derive the price of a put option, using only the price of the call option.

Suppose there are two different portfolios. One has a European call option and K bonds (with maturity T, the same as the option) that each get the risk neutral (and constant) interest rate r. The other portfolio consists of a European put option and a share of the underlying stock. Each portfolio is worth the same at each time, independent of the value of the underlying stock. The value at expiration is:

$$\begin{aligned}
K \quad & \text{if } K \geq S_T \\
S_T \quad & \text{if } K \leq S_T\ . \qquad \text{(C.29)}
\end{aligned}$$

Indeed, the second portfolio's value at maturity T is $\max(K - S_T, 0) + S_T$ and the first is $\max(S_T - K, 0) + K$. During the lifetime of the portfolios there can thus be no difference in their worth, because one could otherwise make a risk-free profit.

Put-call parity thus becomes:

$$C(S,t) + e^{-r(T-t)}K = S(t) + P(S,t) \; . \tag{C.30}$$

Since the price of the stock and the call option is known at $t = 0$, the price of the put option is

$$\begin{aligned} P(S,0) &= C(S,0) + e^{-rT}K - S_0 \\ &= S_0 N(d_1) - Ke^{-rT}N(d_2) + e^{-rT}K - S_0 \\ &= Ke^{-rT}\left(1 - N(d_2)\right) - S_0\left(1 - N(d_1)\right) \\ &= Ke^{-rT}N(-d_2) - S_0 N(-d_1) \; , \end{aligned} \tag{C.31}$$

with

$$d_1 = \frac{1}{\sigma\sqrt{T}}\left(\ln\left[\frac{S_0}{K}\right] + \left[r + \frac{\sigma^2}{2}\right]T\right) \; , \; d_2 = d_1 - \sigma\sqrt{T} \; . \tag{C.32}$$

Bibliography

[ACPZ08] V. Alfi, M. Cristelli, L. Pietronero, and A. Zaccaria. Mechanisms of Self-Organization and Finite Size Effects in a Minimal Agent Based Model. *ArXiv e-prints*, November 2008.

[AHY68] BJ Alder, WG Hoover, and DA Young. Studies in Molecular Dynamics. V. High-Density Equation of State and Entropy for Hard Disks and Spheres. *The Journal of Chemical Physics*, 49:3688, 1968.

[AW70] B.J. Alder and T.E. Wainwright. Decay of the velocity autocorrelation function. *Physical Review A*, 1(1):18–21, Jan 1970.

[Baa04] B. E. Baaquie. *Quantum Finance: Path Integrals and Hamiltonians for Options and Interest Rates*. Cambridge University Press, 2004.

[Bac00] L. Bachelier. Théorie de la spéculation. École Normale Supérieure, 1900.

[Bak96] P. Bak. *How Nature Works: The Science of Self-Organized Criticality*. Copernicus, New York, 1996.

[Bal06] P. Ball. Econophysics: Culture Crash. *Nature*, 411(7094):686–688, 2006.

[BG90] J.-P. Bouchaud and A. Georges. Anomalous diffusion in disordered media: Statistical mechanisms, models and physical applications. *Physics Reports*, 195(4-5):127–293, Nov 1990.

[Bol86] T. Bollerslev. Generalized autoregressive conditional heteroskedasticity. *Journal of Econometrics*, 31(3):307–327, 1986.

[Bou05] J.-P. Bouchaud. The subtle nature of financial random walks. *Chaos: An Interdisciplinary Journal of Nonlinear Science*, 15:026104, 2005.

[BP03] J.-P. Bouchaud and M. Potters. *Theory of Financial Risk and Derivative Pricing*. Cambridge University Press, 2003.

[BPS97] P. Bak, M. Paczuski, and M. Shubik. Price variations in a stock market with many agents. *Physica A*, 246:430–453, 1997.

[Bro32] R. Brown. XXVII. A brief account of microscopical observations made in themonths of June, July and August 1827, on the particles contained in the pollen of plants; and on the general existence of active molecules in organic and inorganic bodies. *Philosophical Magazine Series 2*, 4(21):161–173, Sep 1832.

[BS73] F. Black and M. Scholes. The pricing of options and corporate liabilities. *Journal of Political Economy*, 81:637–659, 1973.

[CGH90] B. Castaing, Y. Gagne, and E. J. Hopfinger. Velocity probability density functions of high Reynolds number turbulence. *Physica D Nonlinear Phenomena*, 46:177–200, nov 1990.

[CKB+00] J.M. Courtault, Y. Kabanov, B. Bru, P. Crépel, I. Lebon, and A. Le Marchand. Louis Bachelier: on the Centenary of Théorie de la Spéculation. *Mathematical Finance*, 10(3):339–353, 2000.

[CM05] K. Christensen and N. R. Moloney. *Complexity and Criticality*. Imperial College Press, London, 2005.

[CMZ05] D. Challet, M. Marsili, and Y.-C. Zhang. *Minority Games: Interacting Agents in Financial Markets*. Oxford University Press, Oxford, NY, 2005.

[Con01] R. Cont. Empirical properties of asset returns: stylized facts and statistical issues. *Quantitative Finance*, 1(2):223–236, 2001.

[Coo05] A.C.C. Coolen. *The Mathematical Theory of Minority Games: Statistical Mechanics of Interacting Agents*. Oxford University Press, 2005.

[CRH+01] P. S. Crozier, R. L. Rowley, N. B. Holladay, D. Henderson, and D. D. Busath. Molecular Dynamics Simulation of Continuous Current Flow through a Model Biological Membrane Channel. *Physical Review Letters*, 86:2467–2470, 2001.

[CT04] R. Cont and P. Tankov. Non-parametric calibration of jump-diffusion option pricing models. *Journal of Computational Finance*, 7(3):1–50, 2004.

[Das05] J.W. Dash. *Quantitative Finance and Risk Management: A Physicist's Approach*. World Scientific, 2005.

[DCBC06] M. R. D'Orsogna, Y. L. Chuang, A. L. Bertozzi, and L. S. Chayes. Self-Propelled Particles with Soft-Core Interactions: Patterns, Stability, and Collapse. *Physical Review Letters*, 96(10):104302, Mar 2006.

[DE06] M. Davis and A. Etheridge. *Louis Bachelier's Theory of Speculation: The Origins of Modern Finance*. Princeton University Press, 2006.

[DS06] D. Darcet and D. Sornette. Emergence of human cooperation and altruism by evolutionary feedback selection. *Arxiv preprint physics/0610225*, 2006.

[Ein05] A. Einstein. Über die von der molekularkinetischen Theorie der Wärme geforderte Bewegung von in ruhenden Flüssigkeiten suspendierten Teilchen. *Annalen der Physik*, 322(8):549–560, 1905.

[EPW+07] A.M. Edwards, R.A. Phillips, N.W. Watkins, M.P. Freeman, E.J. Murphy, V. Afanasyev, S.V. Buldyrev, M.G.E. da Luz, E.P. Raposo, H.E. Stanley, et al. Revisiting Lévy flight search patterns of wandering albatrosses, bumblebees and deer. *Nature*, 449(7165):1044–1048, 2007.

[Far02] J.D. Farmer. Market force, ecology and evolution. *Industrial and Corporate Change*, 11(5):895, 2002.

[Fic55] A. Fick. Ueber Diffusion. *Annalen der Physik und Chemie*, 170(1):59–86, 1855.

[Fol94] D. K. Foley. A statistical equilibrium theory of markets. *Journal of Economic Theory*, 62(2):321–345, 1994.

[Fra07] G. Franzese. Differences between discontinuous and continuous soft-core attractive potentials: the appearance of density anomaly. *Journal of Molecular Liquids*, 136(3):267–273, 2007.

[GAA83] Yuval Gefen, Amnon Aharony, and Shlomo Alexander. Anomalous Diffusion on Percolating Clusters. *Physical Review Letters*, 50(1):77–80, Jan 1983.

[GI01] M. Gligor and M. Ignat. Econophysics: a new field for statistical physics? *Interdisciplinary Science Reviews*, 26(3):183–190, 2001.

[GKLO06] M. Gallegati, S. T. Keen, T. Lux, and P. Ormerod. Worrying trends in econophysics. *Physica A*, 370:1–6, 2006.

[GLO+09] Y.W. Goo, T.W. Lian, W.G. Ong, W.T. Choi, and S.A. Cheong. Financial Atoms and Molecules. *Quantitative Finance Papers*, 2009.

[GMV07] R. Gorenflo, F. Mainardi, and A. Vivoli. Continuous-time random walk and parametric subordination in fractional diffusion. *Chaos, Solitons & Fractals*, 34(1):87–103, 2007.

[GMY04] M.L. Goldstein, S.A. Morris, and G.G. Yen. Problems with fitting to the power-law distribution. *The European Physical Journal B*, 41(2):255–258, Sep 2004.

[HBA02] S. Havlin and D. Ben-Avraham. Diffusion in disordered media. *Advances in Physics*, 51(1):187–292, 2002.

[Ili01] K. Ilinski. *Physics of Finance: Gauge Modelling in Non-Equilibrium Pricing*. John Wiley & Sons, 2001.

[Jen98] H.J. Jensen. *Self-Organized Criticality*. Cambridge Lecture Notes in Physics, 1998.

[JJH03] N. F. Johnson, P. Jefferies, and P. M. Hui. *Financial Market Complexity: What Physicists can Tell us About Market Behaviour*. Oxford University Press, 2003.

[JLS00] A. Johansen, O. Ledoit, and D. Sornette. Crashes as critical points. *International Journal of Theoretical and Applied Finance*, 3(2):219–255, 2000.

[JSL99] A. Johansen, D. Sornette, and O. Ledoit. Predicting Financial Crashes using discrete scale invariance. *Journal of Risk*, 1(4):5–32, 1999.

[Juh08] R. Juhász. Superdiffusion in a class of networks with marginal long-range connections. *Physical Review E*, 78:066106, 2008.

[JZS+10] Z.Q. Jiang, W.X. Zhou, D. Sornette, R. Woodard, K. Bastiaensen, and P. Cauwels. Bubble Diagnosis and Prediction of the 2005-2007 and 2008-2009 Chinese stock market bubbles. *Journal of Economic Behavior & Organization*, 2010.

[KH93] G. Kresse and J. Hafner. Ab initio molecular dynamics for liquid metals. *Physical Review B*, 47:558–561, 1993.

[KNM95] M. A. Knackstedt, B. W. Ninham, and M. Monduzzi. Diffusion in Model Disordered Media. *Physical Review Letters*, 75(4):653–656, Jul 1995.

[KS05] J. Klafter and I. M. Sokolov. Anomalous diffusion spreads its wings. *Physics World*, 18:29–32, Aug 2005.

[KSY06] K. Kiyono, Z. R. Struzik, and Y. Yamamoto. Criticality and Phase Transition in Stock-Price Fluctuations. *Physical Review Letters*, 96(6):068701, Feb 2006.

[LA02] T. Lux and M. Ausloos. *The science of disasters: Climate disruptions, heart attacks, and market crashes*, chapter Market fluctuations i: Scaling, multi-scaling, and their possible origins, pages 373–409. Springer-Verlag, Berlin, 2002.

[LCX06] M. Lax, W. Cai, and M. Xu. *Random Processes in Physics and Finance*. Oxford Finance Series. Oxford University Press, 2006.

[Lév54] P. Lévy. Théorie de l'addition des variables aléatoires. Gauthier-Villars, 1954.

[LG07] B. Liu and J. Goree. Superdiffusion in two-dimensional Yukawa liquids. *Physical Review E*, 75:016405, 2007.

[LGS99] Y. Liu, P. Gopikrishnan, and H. E. Stanley. Statistical properties of the volatility of price fluctuations. *Physical Review E*, 60(2):1390–1400, Aug 1999.

[Lux05] T. Lux. Emergent Statistical Wealth Distributions in Simple Monetary Exchange Models: A Critical Review. *ArXiv Computer Science e-prints*, Jun 2005.

[Man60] B. B. Mandelbrot. The Pareto-Lévy law and the distribution of income. *International Economic Review*, 1(2):79–106, May 1960.

[Man63] B. Mandelbrot. The Variation of Certain Speculative Prices. *Journal of Business*, 36(4):394–419, October 1963.

[Man82] B. B. Mandelbrot. *The fractal geometry of nature*. San Francisco: W.H. Freeman, 1982.

[Man04] B. B. Mandelbrot. *The (Mis)Behavior of Markets*. Profile Books Ltd., London, 2004.

[McC04] J. L. McCauley. *Dynamics of Markets: Econophysics and Finance*. Cambridge University Press, Cambridge, 2004.

[McC06] J. L. McCauley. Response to "Worrying trends in Econophysics". *Physica A*, 371(2):601–609, 2006.

[MG97] M. Mondello and G. S. Grest. Viscosity calculations of n-alkanes by equilibrium molecular dynamics. *Journal of Chemical Physics*, 106:9327, 1997.

[MK99] A.J. Majda and P.R. Kramer. Simplified models for turbulent diffusion: Theory, numerical modelling and physical phenomena. *Physics Reports*, 314:237–574, 1999.

[MK00] R. Metzler and J. Klafter. The random walk's guide to anomalous diffusion: a fractional dynamics approach. *Physics Reports*, 339:1–77, 2000.

[MMPW06] J. Masoliver, M. Montero, J. Perelló, and G.H. Weiss. The continuous time random walk formalism in financial markets. *Journal of Economic Behavior & Organization*, 61(4):577–598, 2006.

[MMW03] J. Masoliver, M. Montero, and G.H. Weiss. Continuous-time random-walk model for financial distributions. *Physical Review E*, 67(2):21112, 2003.

[MPS05] Y. Malevergne, V. Pisarenko, and D. Sornette. Empirical distributions of stock returns: between the stretched exponential and the power law? *Quantitative Finance*, 5(4):379–401, 2005.

[MS94] R. N. Mantegna and H. E. Stanley. Stochastic Process with Ultraslow Convergence to a Gaussian: The Truncated Lévy Flight. *Physical Review Letters*, 73:2946–2949, 1994.

[MS95] R. N. Mantegna and H. E. Stanley. Scaling behaviour in the dynamics of an economic index. *Nature*, 376(6535):46–49, 1995.

[MS99] R. N. Mantegna and H.E. Stanley. *An Introduction to Econophysics: Correlations and Complexity in Finance*. Cambridge University Press, 1999.

[MS06] M.M. Meerschaert and E. Scalas. Coupled continuous time random walks in finance. *Physica A: Statistical Mechanics and Its Applications*, 370(1):114–118, 2006.

[MZ07] M. Marseguerra and A. Zoia. Some insights in superdiffusive transport. *Physica A: Statistical Mechanics and its Applications*, 377(1):1–14, 2007.

[New05] M.E.J. Newman. Power laws, Pareto Distributions and Zipf's law. *Contemporary Physics*, 46(5):323–351, Sep 2005.

[Par16] V. Pareto. *Trattato Di Sociologia Generale*. Harcourt, Brace and Company, New York, 1916.

[PB00] W. Paul and J. Baschnagel. *Stochastic Processes: From Physics to Finance*. Springer, 2000.

[PCB98] M. Potters, R. Cont, and J.-P. Bouchaud. Financial markets as adaptive ecosystems. *Europhysics Letters*, 41:239, 1998.

[Pea05] Karl Pearson. The Problem of the Random Walk. *Nature*, page 294, 1905.

[Per09] J. Perrin. Mouvement brownien et réalité moléculaire. In *Annales de Chimie et de Physique*, volume 18, 1909.

[Que35] A. Quetelet. *Sur l'homme et le développement de ses facultés. Essai d'une physique sociale.* Bachelier, Paris, 1835.

[Ray80] L. Rayleigh. On the resultant of a large number of vibrations of the same pitch and of arbitrary phase. *Philosophical Magazine*, 73(10), 1880.

[RFMM+04] G. Ramos-Fernandez, J.L. Mateos, O. Miramontes, G. Cocho, H. Larralde, and B. Ayala-Orozco. Lévy walk patterns in the foraging movements of spider monkeys (Ateles geoffroyi). *Behavioral Ecology and Sociobiology*, 55(3):223–230, 2004.

[Roe05a] B. M. Roehner. *Patterns of Speculation: A Study in Observational Econophysics*. Cambridge University Press, Cambridge, 2005.

[Roe05b] B.M. Roehner. A bridge between liquids and socio-economic systems: the key role of interaction strengths. *Physica A: Statistical Mechanics and its Applications*, 348:659–682, 2005.

[RS00] B.M. Roehner and D. Sornette. "thermometers" of speculative frenzy. *The European Physical Journal B*, 16(4):729–739, 2000.

[SAC+99] H.E. Stanley, L.A.N. Amarel, D. Cunning, P. Gopikrishnan, Y. Lee, and Y. Liu. Econophysics: Can Physicists contribute to the science of economics? *Physica A*, 269(1):156–169, Jul 1999.

[Sch78] T. C. Schelling. *Micromotives and Macrobehavior*. W.W. Norton and Co., 1978.

[SJ01] D. Sornette and A. Johansen. Significance of log-periodic precursors to financial crashes. *Quantitative Finance*, 1(4):452–471, 2001.

[SM75] H. Scher and E.W. Montroll. Anomalous transit-time dispersion in amorphous solids. *Physical Review B*, 12(6):2455–2477, 1975.

[Smo09] L. Smolin. Time and symmetry in models of economic markets. *ArXiv e-prints*, Feb 2009.

[Sor98a] D. Sornette. Discrete scale invariance and complex dimensions. *Physics Reports*, 297:239–270, 1998.

[Sor98b] D. Sornette. Gauge theory of Finance? *Arxiv preprint cond-mat/9804045*, 1998.

[Sor03a] D. Sornette. Critical market crashes. *Physics Reports*, 378(1):1–98, 2003.

[Sor03b] D. Sornette. *Why Stock Markets Crash: Critical Events in Complex Financial Systems*. Princeton University Press, 2003.

[SRC10] S. Standaert, J. Ryckebusch, and L. De Cruz. Creating the conditions of anomalous self-diffusion in a liquid with molecular dynamics. *Journal of Statistical Mechanics*, page P04004, 2010.

[SRK+05] K. Suzuki, K. Ritchie, E. Kajikawa, T. Fujiwara, and A. Kusumi. Rapid hop diffusion of a G-protein-coupled receptor in the plasma membrane as revealed by single-molecule techniques. *Biophysical Journal*, 88(5):3659–3680, 2005.

[SS06] M. Schmiedeberg and H. Stark. Superdiffusion in a honeycomb billiard. *Physical Review E*, 73:031113, 2006.

[Thi99] J.M. Thijssen. *Computational Physics*. Cambridge University Press, 1999.

[TLKT00] K. Tappura, M. Lahtela-Kakkonen, and O. Teleman. A new soft-core potential function for molecular dynamics applied to the prediction of protein loop conformations. *Journal of Computational Chemistry*, 21(5):388–397, 2000.

[TO96] H. Takeuchi and K. Okazaki. Dynamics of Small Molecules in a Dense Polymer Matrix: Molecular Dynamics Studies. *Molecular Simulation*, 16(1):59–74, 1996.

[Vas04] G.L. Vasconcelos. A guided walk down Wall Street: an introduction to econophysics. *Brazilian Journal of Physics*, 34:1039–1065, 2004.

[VL02] J. Voit and R. W. Lourie. The Statistical Mechanics of Financial Markets. *Physics Today*, 55(8):080000–52, August 2002.

[WB07] M. Wyart and J.P. Bouchaud. Self-referential behaviour, overreaction and conventions in financial markets. *Journal of Economic Behavior & Organization*, 63(1):1–24, 2007.

[WGR+04] I.Y. Wong, M.L. Gardel, D.R. Reichman, E.R. Weeks, M.T. Valentine, A.R. Bausch, and D.A. Weitz. Anomalous Diffusion Probes Microstructure Dynamics of Entangled F-Actin Networks. *Physical Review Letters*, 92:178101, 2004.

[YRJ09] V.M. Yakovenko and J.B. Rosser Jr. Colloquium: Statistical mechanics of money, wealth, and income. *Reviews of Modern Physics*, 81:1703, 2009.

[ZS06] W.X. Zhou and D. Sornette. Fundamental factors versus herding in the 2000-2005 US stock market and prediction. *Physica A: Statistical Mechanics and its Applications*, 360(2):459–482, 2006.

Nederlandstalige Samenvatting

De menselijke analytische geest en zijn nieuwsgierigheid is de basis van de huidige wetenschappelijke kennis. Van in het begin der tijden zijn mensen geïnteresseerd in wat zich rondom hen afspeelt in de natuur. Bliksem, regen, sterren, blauwe lucht,... waren eens onverklaarbare verschijnselen die nu perfect worden begrepen in de fysica. Vele natuurlijke fenomenen kunnen in geteste en betrouwbare wetten gegoten worden. Er is echter ook een grote uitzondering, en dat is het gedrag van de mens. Verwonderd kijkt men soms naar wat andere mensen doen en deze gedragingen kunnen niet in harde wetten gegoten worden. Sociale wetenschappers proberen hiervoor verklaringen te vinden en zoeken regelmatigheden in het gedrag van mensen.

Een onderdeel van de sociale wetenschappen is de economie. Economie, van het Griekse *oikonomia*, "beheer van een huishouden", houdt zich bezig met het bestuderen van menselijke interacties op financieel vlak, van de allerkleinste eenheid (één persoon) tot het complexe geheel van de wereld (vb. wereldhandel). In de huidige wereld spuien economieën hopen data, van de lokale verkoop van bananen in Guatemala tot de verkoop van iPhones wereldwijd.

Econofysica

Zo'n hoeveelheid data wekt niet alleen de interesse van economen, maar ook die van statistische fysici. In het begin van de jaren '90 werden er dan ook verschillende pogingen vanuit de statistische fysica ondernomen om modellen op te stellen die eigenschappen van economische data konden verklaren. Onder andere concepten geleend van percolatietheorie, zelfgeorganiseerde criticaliteit, faseovergangen,... werden gebruikt om bijvoorbeeld financiële crashes te verklaren. Dit was geen nieuw fenomeen, want door de eeuwen heen hadden wetenschappers al meerdere malen de grenzen tussen 'harde' en 'zachte' wetenschappen overgestoken. Adolph Quetelet [Que35], Louis Ba-

chelier [Bac00], Vilfredo Pareto [Par16] en Benoît Mandelbrot [Man63] zijn enkele van de meer bekende wetenschappers die fysica binnen brachten in de economie.

In 1995 werden de interdisciplinaire onderzoektechnieken gebundeld in de term 'Econofysica'. Deze term, die gekozen is door E. Stanley, bundelt alle onderzoektechnieken die methodes van de fysica toepassen op economische problemen. In tegenstelling tot mainstream economie ligt de focus bij econofysica op empirische observaties en het testen van modellen op economische data. Deze aanpak leent zich uitstekend voor gebruik in de econometrie (het verwerken van economische data via wiskundige methodes) en het analyseren van beursdata. Dit laatste is vaak te herleiden tot de analyse van tijdreeksen.

Diffusie in de economie

Een accurate beschrijving van de evolutie van beursdata is noodzakelijk voor het kwantificeren van de prijs van een optie. Een optie is een afgeleid financieel product. Het biedt de eigenaar van de optie het recht om een goed aan een vooraf bepaalde prijs te verkopen of te kopen. De prijs van deze optie wordt bepaald voordat de evolutie van de prijs van dit onderliggend goed gekend is, waardoor een statistische voorspelling noodzakelijk is om een goed inzicht te krijgen in de waarde van de optie.

De eerste persoon die op een mathematische wijze de evolutie van beursdata beschreef was Bachelier. In zijn wiskundige doctoraatsverhandeling veronderstelde hij een *random walk* voor de evolutie van de prijzen op de Franse beurs. Zijn oplossing voor dit diffusieprobleem was een Gaussische, normale distributie. Deze wiskundige beschrijving van de *random walk* of Brownse beweging vond plaats nog vóór Einstein zijn wereldberoemde afleiding neerschreef [Ein05].

Bacheliers beschrijving van beursdata had echter één grote tekortkoming. Onafhankelijk van de startprijs geeft de normale distributie altijd een kans op een negatieve prijs. Dit kan opgelost worden door geen Brownse beweging in de prijzen, maar in de returns te veronderstellen. Returns kunnen gedefinieerd worden als relatieve prijsveranderingen, wat belangrijker is voor investeerders dan de prijsveranderingen zelf. Beide beschrijvingen kunnen echter geïnterpreteerd worden als diffusievergelijkingen en kunnen dus gelinkt worden met fysische systemen. De beschrijving van diffusie in de fysica kan gevonden worden in Appendix A.

Het model waarin de returns een Brownse beweging volgen, wordt geometrische Brownse beweging (GBM, *geometric Brownian motion*) genoemd. Simulaties van markten kunnen we toetsen aan dit model. Daarbij wordt er een poging ondernomen om de

empirische eigenschappen van financiële tijdreeksen beter te beschrijven dan het GBM model.

Black-Scholes formalisme

Een belangrijke mijlpaal in de theorie van opties was het Black-Scholes formalisme. Gebaseerd op twee verschillende portfolio's die dezelfde opbrengst moeten hebben, waren zij in staat om een stochastische differentiaalvergelijking op te stellen voor de evolutie van de prijs van een optie, de Black-Scholes vergelijking. Zij vonden ook een oplossing voor deze diffusievergelijking: het Black-Scholes formalisme. Appendix C behandelt de uitwerking van dit formalisme.

De Black-Scholes vergelijking kan uitgebreid worden met een waaier van complexere processen, die dichter bij de realiteit van de beursdata liggen. De mens lijkt echter steeds in staat om complexere afgeleide producten uit te vinden, zodat de modellering hiervan vaak tekort schiet.

De complexiteit van de diffusievergelijkingen van deze modellen vindt zijn oorsprong in de moeilijke modellering van distributies met groter dan normale staarten. De aanwezigheid van deze leptokurtosische distributies in beursdata is een universeel terugkomende observatie. In plaats van de vorm van deze distributies op te leggen via een diffusievergelijking, gaan we in dit werk op zoek naar een formalisme waarbij deze distributies dynamisch gegenereerd worden.

Universele karakteristieken van beursdata

We zullen het voorgestelde formalisme toetsen aan enkele universele karakteristieken van de beursdata. De kenmerken die in aanmerking komen, zijn deze die robuust zijn, die eenvoudig af te leiden zijn uit de data en die in ongeveer elke markt voorkomen. In de afleiding van deze karakteristieken gebruiken we beursdata van `finance.yahoo.com`, en meer specifiek de 59-jarige tijdreeks van dagelijkse S&P 500 indexprijzen. Om de universaliteit aan te tonen werd een gelijkaardige analyse uitgevoerd op de tijdreeksen van de Nikkei225 en de DAX.

Het eerste universele kenmerk zijn de hierboven aangehaalde 'vette' staarten van de return-distributie. De extreemste evenementen in de staarten zijn gelinkt aan beurscrashes zoals *Black Monday*. Een ander kenmerk van returns is dat deze een verwaarloosbare tijdscorrelatie hebben. Dit houdt in dat de beste voorspelling voor toekomstige returns altijd nul is.

Tegengesteld gedrag vindt men in de tijdscorrelatie van de volatiliteit, die een maat

is voor de fluctuaties van het systeem. De eenvoudigste definitie van volatiliteit is de absolute waarde van de return. De autocorrelatiefunctie van deze volatiliteit vertoont wél een merkbare tijdscorrelatie. Voor lange tijden kan men een machtwet fitten aan deze distributie. Dit wil zeggen dat hoewel de returns ongecorreleerd zijn, er wel correlatie is in de fluctuaties, en dit is gekend als *volatility clustering*.

Een laatste kenmerk dat we hier nog aan willen toevoegen is het verschillende gedrag van beursdata in tijden mét en zonder crash. Wanneer er zich geen crash voordoet in een bepaalde tijdsspanne, dan zullen de return-distributies voor grote tijdsschalen convergeren naar een normale, niet-leptokurtische distributie. Voor tijdsspannes waarin zich een crash voordoet zal er geen convergentie zijn en is de return-distributie een schaalvrije eigenschap van de beursdata.

Anomale diffusie in moleculaire dynamica

In een poging om de universele kenmerken van beursdata te reproduceren maken we gebruik van een gekend model uit de fysica, moleculaire dynamica (MD). Het model beschrijft de dynamica van de moleculen in een gas of een vloeistof. De basis van het model ligt in de manier waarop het de interactie tussen deze moleculen bepaalt. MD lost de interactie van deeltjes op via het Verlet algoritme, en is in staat om, via periodieke randvoorwaarden, het gedrag van systemen met een groot aantal deeltjes te simuleren. Op deze manier is er een natuurlijke tijdsevolutie in het simulatiesysteem aanwezig, in tegenstelling tot bijvoorbeeld de Monte Carlo techniek, waar er niet echt sprake is van een tijdstap bij de overgang tussen opeenvolgende configuraties van het simulatiesysteem. Op deze manier kan men de tijdscorrelaties in een systeem eenvoudig berekenen in MD.

Zachte-kern potentialen

In de simulatie van een vloeistof met een Lennard-Jones (LJ) potentiaal resulteert MD traditioneel in normale diffusie-eigenschappen van deze vloeistof. Het centrale limiet theorema zorgt ervoor dat alle distributies met een eindige variantie en zonder tijdscorrelatie convergeren naar een Gaussische distributie. In een eindig simulatiesysteem zal daardoor voor lange tijdsspannes steeds een normale distributie bekomen worden in MD. Er is echter nog een onderdeel van een normale MD simulatie dat een obstakel vormt bij het genereren van leptokurtische distributies: de harde kern van de LJ potentiaal.

Simulatie van anomale diffusie resulteert in deeltjes met een extreem hoge snelheid, groter dan verwacht volgens een normale distributie. Het Verlet-algoritme kan deze hoge snelheden opvangen door de tijdstap te verkleinen, waardoor botsingen accurater worden weergegeven. Dit leidt echter tot een simulatie waar bijna alle deeltjes stil staan en alleen de meest extreme snelheden niet verdwijnen. Indien dit niet gebeurt, kunnen deze extreem snelle deeltjes de harde kern van de LJ potentiaal van andere deeltjes binnendringen en op die manier een onfysische hoeveelheid potentiële energie krijgen. Dit kan een vicieuze cirkel in werking zetten waarbij een oncontroleerbare hoeveelheid energie in het systeem gepompt wordt.

Om dit probleem te omzeilen zullen wij gebruik maken van een zachte-kern potentiaal, die een eindige waarde heeft in de oorsprong. Vergelijking van potentialen leert dat de zachte-kern potentiaal van [Fra07] een goede kandidaat is. De variabelen van deze potentiaal kunnen gefit worden aan de LJ potentiaal en simulaties met deze potentiaal resulteren in kwalitatief gelijklopende eigenschappen met een LJ simulatie.

Niet-evenwichts MD

In een standaard MD simulatie kunnen reeds enkele van de universele karakteristieken van beurzen gereproduceerd worden. Zo zijn de tijdscorrelaties van de stappen die deeltjes zetten eindig, en vertoont de correlatiefunctie dezelfde kwalitatieve vorm als de return autocorrelatiefunctie. Ook de tijdscorrelaties van de volatiliteit kunnen teruggevonden worden in een MD simulatie. In dit opzicht is MD reeds een beter model dan het eerder vermelde GBM basismodel. Om het belangrijkste universele kenmerk te kunnen simuleren moet het MD formalisme uitgebreid worden. We doen dit door het systeem uit evenwicht te dwingen. Deze stap is een natuurlijke stap in de simulatie van beurzen, aangezien dit systemen zijn waar er typisch geen evenwicht is. Er is bijvoorbeeld geen wet die stelt dat er een behoud van geld is in een economie!

Niet-evenwichts MD wordt bekomen door op bepaalde tijdstippen de deeltjes in de simulatie te vergroten. Dit geeft aanleiding tot regio's met een sterk verhoogde potentiële energie. Dit verstoort het evenwicht tussen potentiële en kinetische energie en resulteert in een omzetting van een deel van deze potentiële energie in kinetische energie. De verhoging van kinetische energie is niet dezelfde voor elk deeltje waardoor sommige deeltjes abnormaal hoge snelheden kunnen bekomen. Op deze momenten kan men anomale diffusie observeren in de stapdistributies.

Dit leidt ertoe dat niet-evenwichts MD reeds drie universele karakteristieken van beurzen reproduceert: het korte geheugen van de returns, het lange geheugen van

de volatiliteit en de niet-Gaussische return distributies. Het laatste kenmerk dat we wensen terug te vinden zijn de crashes. Hiervoor moeten we schaalvrije stap-distributies observeren, maar dit gedrag wordt niet waargenomen. Voor grote tijdsschalen zullen de stap-distributies steeds convergeren naar een Gaussische distributie.

Uit-evenwicht MD model voor de S&P 500

Om een goed model te ontwikkelen voor financiële markten is het essentieel dat tijd en prijs kunnen gelinkt worden aan de modelvariabelen.

De tijdsschalen van beurzen en MD kunnen in verband gebracht worden met elkaar via de tijdscorrelaties. Zowel in financiële tijdreeksen als in MD is er een eindige correlatie waarneembaar voor respectievelijk de returns en de stappen. Een eindige correlatietijd betekent dat na een eindig tijdsinterval de informatie over de returns of over de stappen van de deeltjes opgelost is in de rest van het systeem. De verhouding van deze correlatietijden kan gebruikt worden om de tijdsschalen van beide systemen op elkaar af te stemmen.

Een tweede methode om de tijdsschalen aan elkaar te linken is via de convergentie naar een Gaussische distributie voor grote tijdsspannes. Voor beide systemen bestaat er een grootte-orde van tijd waarbij de return/stapdistributies Gaussisch worden. Vergelijking van deze grootte-ordes resulteert opnieuw in een afschatting van de verhouding van beide tijdsschalen. Uit onze resultaten blijkt dat de schattingen van deze verhouding overeenstemmen met de schattingen die gevonden werden met de vorige methode. Deze gelijklopende schattingen versterken deze link, wat deze aanpak valideert.

Het linken van de ruimtevariabelen moet via een andere methode gebeuren. Het is niet mogelijk om de genormaliseerde returns rechtstreeks te linken aan de genormaliseerde stapgroottes omdat dit geen consistente resultaten oplevert. Dit is nochtans de meest natuurlijke manier om deze link tot stand te brengen, aangezien het deze variabelen zijn die uitgezet worden in de niet-Gaussische return- en stapdistributies. De inconsistenties komen voort uit het feit dat beide variabelen reeds afgeleid zijn uit meer fundamentele variabelen: prijs en positie. Deze kunnen wel gelinkt worden aan elkaar via een lokale coördinatentransformatie. Dit blijkt echter in de praktijk geen werkbaar resultaat op te leveren. Een afgeleid resultaat hiervan is wel dat het mogelijk is om de trends in het lange-termijn gedrag te reproduceren in niet-evenwichts MD. Hiervoor moet er na iedere tijdstap een globale coördinatentransformatie uitgevoerd worden. De resulterende tijdreeksen zijn op het zicht niet onderscheidbaar van een financiële tijdreeks.

Vooruitzichten

Op dit punt aangekomen zijn we dus in staat om de tijdreeks van een beurs te simuleren. Inderdaad, zowel de gesimuleerde tijdreeks als de typische tijdreeks in financiële markten delen drie universele karakteristieken. Het simuleren van crashes zou echter van grote waarde zijn voor het bekrachtigen van het niet-evenwichts MD model als een goed dynamisch model voor beurzen. Om dit te bereiken, kan een mogelijke uitbreiding erin bestaan om een fasetransitie te simuleren. Tijdens een fasetransitie treedt er schaalvrij gedrag op, hetgeen exact is wat er geobserveerd wordt in beursdata.

Verdere uitbreidingen van het model kunnen meer realistische veronderstellingen bijbrengen. Zo kan bijvoorbeeld het aantal deeltjes in de simulatie gevarieerd worden, zoals ook het aantal investeerders en het aantal producten in financiële markten constant varieert. Ook kunnen de herschalingen realistischer gemaakt worden door ze zowel van grootte te laten veranderen als de tijdsintervallen tussen de herschalingen te veranderen. De grote waarden van de volatiliteit kunnen dan meer gegroepeerd zitten, zoals ook het geval is in beurzen (*volatility clustering*). Mogelijke uitbreidingen kunnen ook gezocht worden op het vlak van de interacties. Zo is het mogelijk om verschillende types deeltjes te definiëren met elk hun specifieke interactieparameters. Zo een benadering sluit aan bij de *agent based modelling* techniek: modellering gebaseerd op beslissingen van individuele agents met elk hun specifieke veronderstellingen over de evolutie van de beurs. Deze manier van simuleren valt onder de categorie *heterogeneous agents*. Simulaties met slechts 1 type investeerder vallen onder de categorie *homogeneous agents*. Beide benaderingen kunnen informatie leveren over de dynamica van beurzen.

Dit alles biedt voldoende uitdagingen om te blijven werken aan niet-evenwichts MD om er zo een volwaardig financieel model van te maken.